

**NATURAL GAS STORAGE USING CLATHRATE TECHNOLOGY:
ENHANCED FORMATION AT HIGH TEMPERATURE**

Kan Jeenmuang

A Thesis Submitted in Partial Fulfillment of the Requirements
for the Degree of Master of Science
The Petroleum and Petrochemical College, Chulalongkorn University
in Academic Partnership with
The University of Michigan, The University of Oklahoma,
Case Western Reserve University, and Institut Français du Pétrole
2020

บทคัดย่อและแฟ้มข้อมูลฉบับเต็มของวิทยานิพนธ์ตั้งแต่ปีการศึกษา 2554 ที่ให้บริการในคลังปัญญาจุฬาฯ (CUIR)
เป็นแฟ้มข้อมูลของนิสิตเจ้าของวิทยานิพนธ์ที่ส่งผ่านทางบัณฑิตวิทยาลัย

The abstract and full text of theses from the academic year 2011 in Chulalongkorn University Intellectual Repository (CUIR)
are the thesis authors' files submitted through the Graduate School.



411257468

CU Theses 6173001063 thesis / recv: 25052563 12:18:23 / seq: 30



411257468

Natural Gas Storage Using Clathrate Technology: Enhanced Formation at High Temperature

Mr. Kan Jeenmuang

A Thesis Submitted in Partial Fulfillment of the Requirements
for the Degree of Master of Science in Petroleum and Energy Technology
Common Course
the Petroleum and Petrochemical College
Chulalongkorn University
Academic Year 2019
Copyright of Chulalongkorn University



411257468

CU iThesis 6173001063 thesis / recv: 25052563 12:18:23 / seq: 30

การจัดเก็บแก๊สธรรมชาติในรูปแบบของแข็งที่อุณหภูมิสูง

นายกานต์ จีนเมือง

วิทยานิพนธ์นี้เป็นส่วนหนึ่งของการศึกษาตามหลักสูตรปริญญาวิทยาศาสตรมหาบัณฑิต
สาขาวิชาเทคโนโลยีปิโตรเลียมและพลังงาน ไม่สังกัดภาควิชา/...
วิทยาลัยปิโตรเลียมและปิโตรเคมี จุฬาลงกรณ์มหาวิทยาลัย
ปีการศึกษา 2562
ลิขสิทธิ์ของจุฬาลงกรณ์มหาวิทยาลัย



411257468

CU Thesisis 6173001063 thesis / recv: 25052563 12:18:23 / seq: 30

Thesis Title Natural Gas Storage Using Clathrate Technology:
Enhanced Formation at High Temperature
By Mr. Kan Jeenmuang
Field of Study Petroleum and Energy Technology
Thesis Advisor Professor PRAMOCH RANGSUNVIGIT, Ph.D.
Thesis Co Advisor Santi Kulprathipanja, Ph.D.

Accepted by the the Petroleum and Petrochemical College, Chulalongkorn
University in Partial Fulfillment of the Requirement for the Master of Science

..... Dean of the the Petroleum and
Petrochemical College
(Professor SUWABUN CHIRACHANCHAI, Ph.D.)

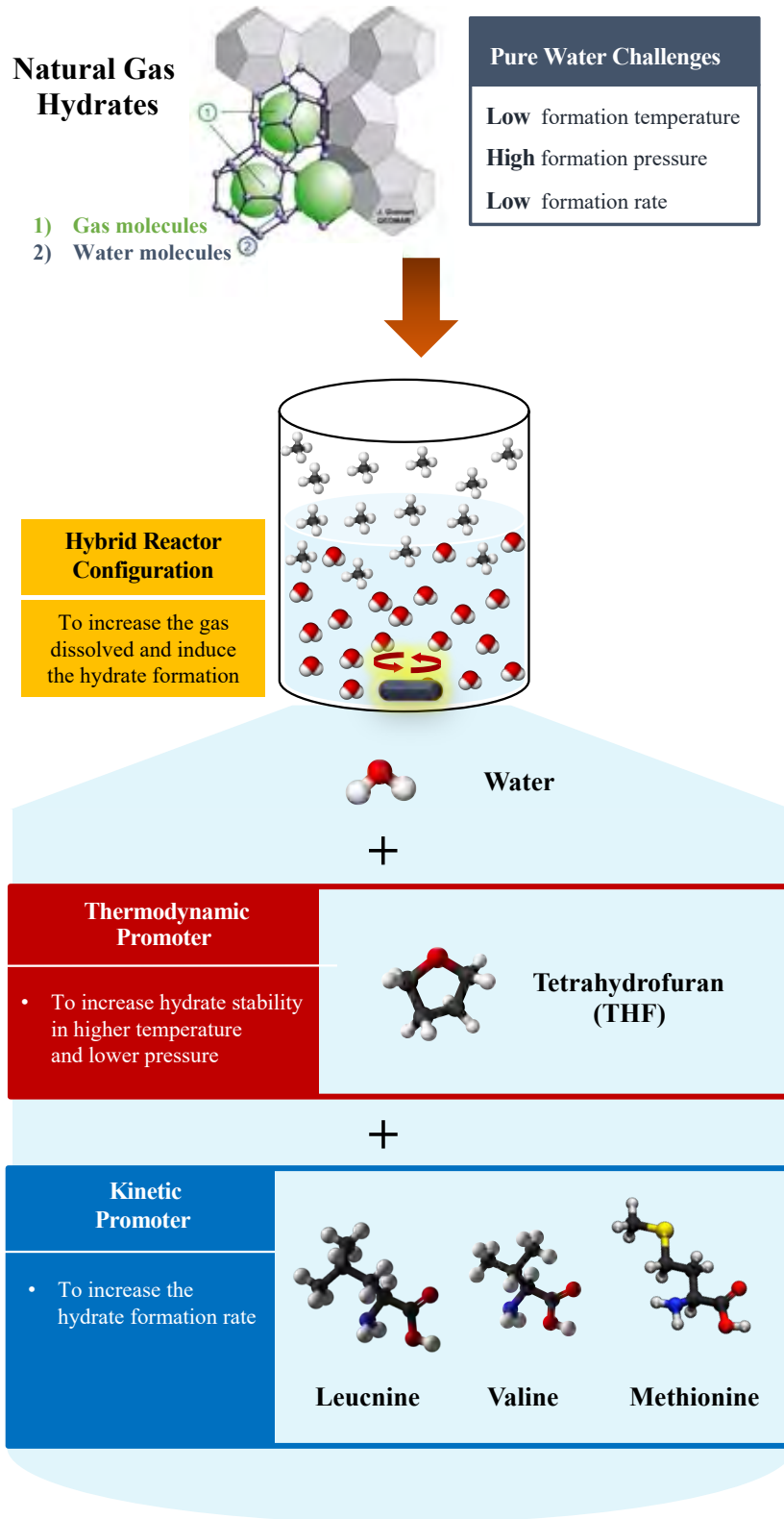
THESIS COMMITTEE *B. Kitiyanan* Chairman
.....
(Professor BOONYARACH KITIYANAN, Ph.D.)
Pramo Thesis Advisor
.....
(Professor PRAMOCH RANGSUNVIGIT, Ph.D.)
..... Thesis Co-Advisor
(Santi Kulprathipanja, Ph.D.)
T. Danuthai External Examiner
.....
(Tanate Danuthai, Ph.D.)



411257468

CD iThesis 6173001063 thesis / recv: 25052563 12:18:23 / seq: 30

GRAPHICAL ABSTRACT



411257468

CU IThesis 6173001063 thesis / rev: 25052563 12:18:23 / seq: 30

กานต์ จีนเมือง : การจัดเก็บแก๊สธรรมชาติในรูปแบบของแข็งที่อุณหภูมิสูง. (Natural Gas Storage Using Clathrate Technology: Enhanced Formation at High Temperature) อ.ที่ปรึกษาหลัก : ศ. ดร.ปราโมช รั้งสรรค้วจิตร, อ.ที่ปรึกษาร่วม : ดร.สันติ กุลประทีปปัญญา

ในปัจจุบันความต้องการใช้แก๊สธรรมชาติมีปริมาณเพิ่มสูงขึ้น ประกอบกับความยุ่งยาก และพลังงานจำนวนมากที่ใช้ในการกักเก็บและขนส่งแก๊สธรรมชาติของเทคโนโลยีปัจจุบัน ส่งผลให้เทคโนโลยีการกักเก็บแก๊สธรรมชาติในรูปแบบของแข็ง (SNG) โดยการจัดเก็บแก๊สธรรมชาติในรูปแบบแก๊สไฮเดรตได้รับความสนใจเพิ่มขึ้น อย่างไรก็ตามเพื่อให้เทคโนโลยีนี้สามารถแข่งขันกับเทคโนโลยีอื่น ๆ ได้มากขึ้น แก๊สไฮเดรตควรก่อตัวได้ที่อุณหภูมิสูง ใช้ความดันต่ำ พร้อมกับใช้เวลาก่อตัวไม่นาน ได้มีการมีเดิมตัวเร่งการก่อตัวของแก๊สไฮเดรต เช่น เตตระไฮโดรฟูแรน (tetrahydrofuran, THF) ที่มีความสามารถในการเพิ่มอุณหภูมิสำหรับการก่อตัวของแก๊สไฮเดรต และกรดอะมิโน (amino acid) ที่สามารถเพิ่มอัตราการก่อตัวของไฮเดรต ในงานวิจัยนี้ใช้ THF ที่ความเข้มข้น 5.56 เปอร์เซ็นต์โมล ร่วมกับกรดอะมิโน 3 ชนิด ได้แก่ ลิวซีน วาริน และ เมทาไทโอนีน ที่อุณหภูมิ 20 องศาเซลเซียส และ 8 เมกะปาสกาล ผลการศึกษาพบว่าการเติมกรดอะมิโนมีผลต่อจลนพลศาสตร์ของการเกิดแก๊สไฮเดรตโดยเพิ่มอัตราการก่อตัวของไฮเดรตสูงขึ้น 5 เท่า กรดอะมิโนบางชนิดสามารถลดปริมาณแก๊สมีเทนในแก๊สไฮเดรตไว้ได้สูงเช่นเดียวกับการเติมเพียง THF ผลการศึกษาลักษณะการก่อตัวของแก๊สไฮเดรตแสดงให้เห็นถึงรูปแบบการก่อตัวที่แตกต่างกันอย่างสิ้นเชิง ทั้งการก่อตัวในการเติมและไม่เติมกรดอะมิโน นอกจากนี้ลักษณะการก่อตัวยังแตกต่างกันในการเติมกรดอะมิโนแต่ละชนิด การสังเกตการสลายตัวของแก๊สไฮเดรตไม่ก่อให้เกิดโฟมเมื่อเติมกรดอะมิโนซึ่งแตกต่างจากการเติมสารลดแรงตึงผิว งานวิจัยนี้ยังได้ทำการศึกษาผลของการเพิ่มอุณหภูมิการก่อตัวที่ 25 องศาเซลเซียส ซึ่งผลลัพธ์แสดงว่าความดันที่ 8 และ 9 เมกะปาสกาลไม่สามารถให้เกิดการก่อตัวของไฮเดรตได้ เพื่อกระตุ้นให้เกิดแก๊สไฮเดรตจึงทำการติดตั้งระบบกวน ซึ่งจากผลการวิจัยแสดงให้เห็นว่ากรดอะมิโนจำเป็นในการรักษาปริมาณแก๊สในไฮเดรตให้สูงตั้งการก่อตัวที่ 20 องศาเซลเซียส นอกจากนี้การเร่งอัตราการก่อตัวของไฮเดรตที่ 25 องศาเซลเซียสเกิดจากระบบกวนไม่ใช่ผลจากการเติมกรดอะมิโน

สาขาวิชา เทคโนโลยีปิโตรเลียมและ
 พลังงาน
ปีการศึกษา 2562

ลายมือชื่อนิติ
.....
ลายมือชื่อ อ.ที่ปรึกษาหลัก
.....
ลายมือชื่อ อ.ที่ปรึกษาร่วม
.....

6173001063 : MAJOR PETROLEUM AND ENERGY TECHNOLOGY

KEYWORD Solidified Natural Gas Technology, Hydrate Promoters,

D: Tetrahydrofuran, Ambient Temperature, Nonpolar Amino Acid

Kan Jeenuang : Natural Gas Storage Using Clathrate Technology:
Enhanced Formation at High Temperature. Advisor: Prof. PRAMOCH
RANGSUNVIGIT, Ph.D. Co-advisor: Santi Kulprathipanja, Ph.D.

Solidified natural gas (SNG) by storing natural gas in the hydrate form, which is safe and easy to recover stored gas compared to other methods. However, to make this technology competitive, storing natural gas at a higher temperature, lower pressure with faster formation is needed. Tetrahydrofuran (THF) is a well-known thermodynamic promoter used to increase the hydrate formation temperature. However, increasing the hydrate formation temperature has a drawback on decreasing the formation rate. Nonpolar amino acids have been used as a secondary promoter, which increases the hydrate formation kinetics. This work used 5.56 mol% THF cooperated with different concentrations of nonpolar amino acids (leucine, valine, and methionine) at 20 °C 8 MPa in the unstirred reactor configuration. The experiment was investigated for the effects of these co-promoters in both kinetics and morphology studies. Results showed that the nonpolar amino acids affected the hydrate kinetics by increasing the hydrate formation rate up to 5 times, and certain nonpolar amino acids did not show the multi-step hydrate formation, which resulted in the low methane uptake. However, the methane uptake in the presence of leucine and methionine was as high as that 5.56 mol% THF. The morphology showed different hydrate growth patterns with the investigated solutions. The hydrate formation morphology in the 5.56 mol% THF was similar to leaflike stack up. However, that behavior was not observed when the amino acids were added for the hydrate formation. In addition, the formation morphology among the solutions with the amino acids was also different. Moreover, the presence of the amino acids did not result in the foam formation as surfactants during the hydrate dissociation. When the formation temperature was increased to 25 °C, the formation pressure at 8 MPa or even at 9 MPa was not enough to form the hydrates. To induce the hydrate formation, the hybrid reactor configuration was installed. The results showed the need of amino acid to maintain the high methane uptake and the formation kinetics was not promoted by the amino acids but rather by the hybrid reactor at this condition.

Field of Study: Petroleum and Energy
Technology

Academic 2019

Year:

Student's Signature

...*Kan Jeenuang*...

Advisor's Signature

...*Pramo Ch*...

Co-advisor's Signature

.....



411257468

CU Thesisis 6173001063 thesis / recv: 25052563 12:18:23 / seq: 30

ACKNOWLEDGEMENTS

I would like to take this chance to sincerely thanks my advisor, Prof. Pramoch Rangsunvigit, for his helpful suggestions, discussions, and supervision from the very early stage of the research. He also provided me unflinching encouragement, patience, and support in various ways throughout my graduate thesis.

I would like to offer my special thanks to my co-advisor, Dr. Santi Kulprathipanja, for his advice, guidance, and his willingness to share his bright thoughts with me, which was very helpful for sharing up my ideas and research.

I also would like to thank Prof. Boonyarach Kitiyanan and Dr. Tanate Danuthai for kindly serving on my thesis committee. Their suggestions are certainly important and helpful for the completion of this thesis.

I am grateful for the full scholarship and full funding of the thesis work provided by the Petroleum and Petrochemical College.

I wish to acknowledge the help provided by Mr. Katipot Inkong for his advice and assistance which was very helpful for my research.

I would like to thank the entire faculty and staff at The Petroleum and Petrochemical College, Chulalongkorn University for their kind assistance and cooperation.

Finally, I would like to express my sincere gratitude to thanks, my whole family, for showing me the joy of intellectual pursuit ever since I was a child, for standing by me and for understanding every single part of my mind.

Kan Jeenmuang

TABLE OF CONTENTS

	Page
ABSTRACT (THAI)	iii
ABSTRACT (ENGLISH).....	iv
ACKNOWLEDGEMENTS	v
TABLE OF CONTENTS.....	vi
LIST OF FIGURES	ix
LIST OF TABLES.....	xiii
CHAPTER 1 INTRODUCTION	1
CHAPTER 2 LITERATURE REVIEW	4
2.1 Natural Gas	4
2.2 Natural Gas Storage and Transportation.....	6
2.2.1 Compressed Natural Gas (CNG).....	7
2.2.2 Liquefied Natural Gas (LNG)	7
2.2.3 Adsorbed Natural Gas (ANG).....	7
2.3 Natural Gas Hydrates.....	8
2.3.1 Gas Hydrate Structure	9
2.3.2 Gas Hydrate Physical Properties	11
2.3.3 Physical Chemistry of Methane Hydrates	12
2.3.3.1 Thermodynamics	12
2.3.3.2 Kinetics.....	13
2.3.4 Methane Hydrates in Natural Resource.....	13
2.4 Gas Hydrate Formation.....	16
2.5 Gas Hydrate Dissociation	17
2.6 Methane Hydrate Reactor Configuration.....	18
2.7 Methane Hydrate Promoter.....	19
2.7.1 Thermodynamic Promoter.....	19

2.7.1.1 Methane + tetrahydrofuran (THF).....	20
2.7.2 Kinetic Promoter	22
2.7.2.1 Surfactants	22
2.7.2.2 Amino acids.....	24
CHAPTER 3 EXPERIMENTAL.....	27
3.1 Materials and Equipment.....	27
3.1.1 Chemicals	27
3.1.2 Equipment	27
3.2 Experimental Procedures	28
3.2.1 Experimental Apparatus	28
3.2.2 Methane Hydrate Formation	30
3.2.3 Methane Hydrate Dissociation	33
CHAPTER 4 RESULTS AND DISCUSSION.....	35
4.1 Effects of Single Promoters on Methane Hydrate Formation	35
4.1.1 Effects of 5.56 mol% THF	35
4.1.1.1 Kinetics.....	35
4.1.1.2 Morphology	38
4.1.2 Effects of Amino Acids.....	39
4.2 Effects of THF and Amino Acids on Methane Hydrate Formation	41
4.2.1 Kinetics.....	42
4.2.2 Morphology	50
4.2.3 Methane Hydrate Dissociation	55
4.3 Enhanced Methane Hydrate Formation at 25 °C with THF and Amino Acids	58
4.3.1 Methane Hydrate Formation in the Unstirred Reactor Configuration	58
4.3.2 Methane Hydrate Formation in the Hybrid Reactor Configuration	61
4.2.3 Methane Hydrate Dissociation	68
CHAPTER 5 CONCLUSIONS AND RECOMMENDATIONS	69
5.1 Conclusions.....	69
5.2 Recommendations.....	70

APPENDICES 71

 Appendix A Calculation 71

 Appendix B Supporting information 75

REFERENCES 77

VITA 85



411257468

CU IThesis 6173001063 thesis / recv: 25052563 12:18:23 / seq: 30

LIST OF FIGURES

	Page
Figure 2.1 Natural gas explained	4
Figure 2.2 Natural gas demand in overall continent (a) and in each sector (b)	5
Figure 2.3 Natural gas imports and exports trend report	6
Figure 2.4 Natural gas transport chain	7
Figure 2.5 Structure types of gas hydrates	10
Figure 2.6 A map of the discovered GHD Map showing locations where gas hydrate has been recovered	14
Figure 2.7 Schematic cross section showing gas hydrate	15
Figure 2.8 Methane bubble streams emanating from the sea floor	15
Figure 2.9 Phase diagram showing the water depths (and pressures) and temperatures for gas hydrate (purple area) stability	17
Figure 2.10 Bar plots showing the effect of stirred, unstirred, and hybrid approaches on induction time, productivity and hydrate yield	19
Figure 2.11 Methane hydrate phase equilibriums of solution mix with 1,3 dioxane, THP, acetone, and THF	20
Figure 2.12 Methane uptake in different THF concentrations	21
Figure 2.13 Methane uptake of adding and unadding 5.56 mol% THF	21
Figure 2.14 Methane uptake of different amino acid concentrations	23
Figure 2.15 Gas hydrate formation induction time (a) and the normalized rate of gas hydrate formation (NR ₃₀) of various MES concentrations	23
Figure 2.16 Solution 60 minutes after gas hydrate dissociation	24
Figure 2.17 Methane uptake of different amino acid concentrations	24
Figure 2.18 Methane uptake of different amino acid concentrations	26



411257468

CU IThesis 6173001063 thesis / rev: 25052563 12:18:23 / seq: 30

Figure 3.1 Schematic of gas hydrate system.....	28
Figure 3.2 a cross-section of a stainless steel crystallizer (a) and a cross-section of a sapphire crystallizer (b).....	29
Figure 3.3 Synergistic effect of nonpolar amino acids to 5.56mol% THF on the sII hydrate formation experimental procedures.	30
Figure 3.4 Enhanced sII methane hydrate formation temperature in 5.56 mol% THF and various nonpolar amino acid system experimental procedures.....	31
Figure 4.1 Temperature and pressure driving forces of the experiments at 20 °C and 8 MPa.....	36
Figure 4.2 Methane uptake profiles from three separate methane hydrate formation experiments in 5.56 mol% THF solution at 20 °C and 8 MPa.	37
Figure 4.3 Temperature profile of three separate methane hydrate formation experiments of 5.56mol% THF at 20 °C and 8 MPa: (a) TH1, (b) TH2, (c) TH3.	38
Figure 4.4 Morphology of methane hydrate formation in 5.56 mol% THF solution at 20 °C and 8 MPa.	39
Figure 4.5 Methane hydrate phase equilibrium in the presence of amino acids at different concentrations	40
Figure 4.6 Effects of amino acid concentrations on the 5.56 mol% THF solution interfacial tension.....	41
Figure 4.7 Normalized rate of methane hydrate formation (NR_{30}) in 5.56 mol% THF and amino acids at 20 °C and 8 MPa.	42
Figure 4.8 Effects of 5.56 mol% THF and 5.56 mol% THF with amino acids on the methane uptake and the normalized rate of methane hydrate formation (NR_{30}): (a) leucine solution, (b) valine solution, and (c) methionine solution at 20 °C and 8 MPa.	45
Figure 4.9 Methane uptake profiles from methane hydrate formation with 5.56 mol% THF and 5.56 mol% THF and amino acids at 20 °C and 8 MPa.....	46

Figure 4.10 Temperature profiles during methane hydrate formation at 20 °C and 8 MPa with (a) 5.56 mol% THF and 5.56 mol% THF with amino acids: (b) 0.25 wt% leucine (c) 0.25 wt% valine (d) 0.125 wt% methionine.	47
Figure 4.11 Comparison of (a) normalized formation rate (NR ₃₀), (b) the induction time of methane hydrate formation, and (c) the methane uptake of THF and amino acids at 20 °C and 8 MPa.....	48
Figure 4.12 Methane uptake profiles (a) and induction times (b) from methane hydrate formation with 5.56 mol% THF and 5.56 mol% THF and methyl ester sulfonate (MES) at 20 °C and 8 MPa	49
Figure 4.13 Structure of different amino acids (a) leucine, (b) valine, and (c) methionine.....	50
Figure 4.14 Morphology of methane hydrate formation in (a) 5.56 mol% THF and 5.56 mol% THF with amino acids: (b) 0.25wt% leucine, (c) 0.25wt% valine, and (d) 0.125wt% methionine at 20 °C and 8 MPa.....	52
Figure 4.15 Comparison of methane uptakes from methane hydrate formation in the sapphire crystallizer (morphology study) and the stainless-steel crystallizer (kinetic study) at 20 °C and 8 MPa.....	55
Figure 4.16 Morphology study of methane hydrate dissociation from hydrates formed in different solutions (a) 5.56 mol% THF and 5.56 mol% THF with amino acids: (b) 0.25wt% leucine, (c) 0.25wt% valine, and (d) 0.125wt% methionine monitoring from (1) the start of hydrate formation, (2) the complete of hydrate formation, (3) the start of hydrate dissociation, and (4) the complete of hydrate dissociation.	56
Figure 4.17 Methane uptakes and temperature profiles of (a) 5.56 mol% THF and (b) 5.56 mol% THF and 0.25wt% leucine at 25 °C and 8 MPa.	58
Figure 4.18 Temperature and pressure driving forces of methane hydrate formation at (a) 20 °C 8 MPa, (b) 25 °C 8 MPa and (c) 25 °C 9 MPa.....	59

Figure 4.19 Methane uptake profiles from the formation in 5.56 mol% THF and 5.56 mol% THF with amino acids at 25 °C and 9 MPa in the hybrid reactor configuration	61
Figure 4.20 Comparison of methane hydrate formation temperature profiles in different solutions (a) 5.56 mol% THF and 5.56 mol% THF with amino acids (b) 0.25wt% leucine (c) 0.25wt% valine (d) 0.125wt% methionine at different hydrate formation conditions (1) 20 °C and 8 MPa in the unstirred reactor configuration, and (2) 25 °C and 9 MPa in the hybrid reactor configuration.	63
Figure 4.21 Comparison of normalized hydrate formation rate (NR ₃₀) between different formation conditions, (pink) at 25 °C and 9 MPa and (gray) at 20 °C and 8 MPa.	64
Figure 4.22 Comparison methane uptake between different formation conditions, (pink) at 25 °C and 9 MPa and (gray) at 20 °C and 8 MPa.	65
Figure 4.23 Methane uptakes and the normalized methane hydrate formation rate (NR ₃₀) between different methionine concentrations at 25 °C and 9 MPa in the hybrid reactor configuration.	66
Figure 4.24 Methane uptake profiles from the hydrate formation with 5.56 mol% THF and methionine concentrations at 25 °C and 9 MPa in the hybrid reactor configuration.	67

LIST OF TABLES

	Page
Table 2.1 Fossil fuels emission level (Pounds/Billion Btu of energy output).....	5
Table 2.2 Geometrical parameters of the main hydrate crystal structures	10
Table 2.3 Comparison of properties of ice, sI, and sII hydrate crystal structures.....	12
Table 2.4 Average data for induction time, methane uptake, t_{90} and rate of hydrate formation for experiments conducted at 7.2 MPa and different temperatures	22
Table 2.5 Induction time, methane uptake, and rate of hydrate formation for experiments conducted using different concentrations of leucine amino acid	25
Table 4.1 Methane hydrate formation in the 5.56 mol% THF solution at 20 °C and 8 MPa.....	36
Table 4.2 Methane hydrate formation in THF and amino acids at 20 °C and 8 MPa.....	44
Table 4.3 Morphology study methane hydrate formation inside sapphire crystallizer at 20 °C and 8 MPa	54
Table 4.4 Comparison of the methane consumed, the methane release, and the methane recovery from the methane hydrate formation with 5.56 mol% THF and 5.56 mol% THF with amino acids at 20 °C and 8 MPa.....	57
Table 4.5 Methane hydrate formation at 25 °C and 8 MPa in the unstirred reactor configuration	60
Table 4.6 Methane hydrate formation at 25 °C and 9 MPa in the unstirred reactor configuration	60
Table 4.7 Methane hydrate formation in 5.56 mol% THF and 5.56 mol% THF with amino acids at 25 °C and 9 MPa in the hybrid reactor configuration.....	62
Table 4.8 Methane hydrate formation in 5.56 mol% THF and 5.56 mol% THF with methionine concentrations at 25 °C and 9 MPa in the hybrid reactor configuration	67



411257468

CD IThesis 6173001063 thesis / rev: 25052563 12:18:23 / seq: 30

Table 4.9 Methane hydrate dissociation of the hydrates formed with 5.56 mol% THF and 5.56 mol% THF with amino acids at 25 °C and 9 MPa in the hybrid reactor configuration	68
---	----



411257468

CU IThesis 6173001063 thesis / recv: 25052563 12:18:23 / seq: 30

CHAPTER 1

INTRODUCTION

Using natural gas as alternative energy has been increasing. BP energy outlook (2019) reported that natural gas demand and production grow at an average rate of 1.7% per annum and increased nearly 50% from 2017 to 2040 because of its availability, cost, and low CO₂ emission. However, its properties like the boiling point, -162 °C under 0.1 MPa, make it challenging to store and transport. The conventional natural gas storage includes compressed natural gas (CNG), liquefied natural gas (LNG), and adsorbed natural gas (ANG). For CNG, natural gas is pressurized at a high pressure with a small storage scale. The disadvantage of CNG is a low volumetric energy store compared to gasoline (Wang *et al.*, 2010). For LNG, natural gas is cooled to a cryogenic liquid (-160 °C) and pressurized inheriting expensive pressurization and cooling system and boil-off gas during the transpiration of gas to a receiver tank, which changes the quality of LNG (Lozano-Castelló *et al.*, 2002). ANG uses porous adsorbent materials to lower the pressure of the system compared to CNG. However, ANG is still in the research stage due to this method requires the low cost of an adsorbent (Afework *et al.*, 2018). Recently, the discovery of a method to store natural gas in the solid form or solidified natural gas (SNG) has prompted a viable alternative for natural gas storage. SNG is a technology that stores natural gas in the hydrate form, which uses lower pressure and higher temperature compared to the conventional methods (Veluswamy *et al.*, 2017b). SNG has higher volumetric energy storage in the compact mode, operates at moderate temperature and pressure conditions, almost completes recovery of stored natural gas with minimal energy requirement, and is the safest mode of natural gas storage (Veluswamy *et al.*, 2018)

Hydrates or clathrate hydrates are an ice-like solid, which contains small gas molecules, such as methane, ethane, propane, etc., in the cage of water molecules. The physical interaction (Van der Waals forces) of small gas molecules and water molecules (cage) results in the gas molecules retained inside the cage structures (Sloan and Koh, 2008). There are three common types of the hydrate structures,



411257468

CU IThesis 6173001063 thesis / rev: 25052563 12:18:23 / seq: 30

which are structure I (sI, primitive cubic), structure II (sII, face-centered cubic), and structure H (sH, hexagonal) (Englezos and Lee, 2005; Jager *et al.*, 1999; Khokhar *et al.*, 1998; Sloan and Koh, 2008). The different structure comes from the different sizes of the guest molecule and the formation condition (Khurana *et al.*, 2017). At STP, the gas molecules in one cubic of hydrates can store natural gas around 163 cubics of natural gas (Veluswamy *et al.*, 2016b). This characteristic of the natural gas hydrates is the key factor for this application. Moreover, hydrate technology can be applied to many applications, i.e., gas separation (Babu *et al.*, 2013a; Partoon *et al.*, 2018; Sun *et al.*, 2014), energy storage (Siažik and Malcho, 2017; Veluswamy and Linga, 2013), CO₂ capture (Babu *et al.*, 2014; Babu *et al.*, 2013a; Dashti *et al.*, 2015), and desalination applications (Babu *et al.*, 2018; Kang *et al.*, 2014; Seo *et al.*, 2019).

The process to form natural gas hydrates is similar to the crystallization, which includes two major steps, nucleation phase and growth phase (Khurana *et al.*, 2017). However, the hydrate nucleation must have specific condition, and the rate of hydrate formation is very slow together with the requirement of low temperature for formation and storage, which causes high refrigeration cost (Gudmundsson *et al.*, 1994; Lang *et al.*, 2010). The two hurdles can be overcome by increasing the mass transfer between the gas phase and liquid phase during the hydrate formation process (Du *et al.*, 2014; Zhang *et al.*, 2007). That can be achieved by using a stirred reactor (Mech *et al.*, 2016; Verrett *et al.*, 2012; Zhong *et al.*, 2015), a spray reactor (Englezos and Lee, 2005; Tang *et al.*, 2006), or a gas bubble reactor (Luo *et al.*, 2007; Vysniauskas and Bishnoi, 1983). However, this technique requires significant energy during the formation, which results in the cost issue (Shi *et al.*, 2017). Promoters were reported to enhance both the kinetics and the gas capacity of hydrates. Promoters can be divided into thermodynamic and kinetic promoters. For the thermodynamic promoters, which shift the hydrate equilibrium. Tetrahydrofuran (THF) is a common promoter used to shift the hydrate equilibrium to lower pressure and higher temperature, and thus enables hydrate formation at moderate conditions (Khurana and Veluswamy, 2019; Lee *et al.*, 2012; Seo *et al.*, 2001). Lin *et al.* (2018) and Beheshtimaal and Haghtalab (2018) reported that using 5.56 mole% THF (stoichiometric) in the hydrate formation gave the highest methane uptake due to maximum capacity. Veluswamy *et al.* (2016c) reported that adding 5.56 mole% THF

at 283.2 K and 7 MPa increased the rate of methane hydrate formation and methane uptake 11.66 times compared to pure methane at 9.5 MPa and 272.K. Veluswamy *et al.* (2016b) also showed that there was no significant difference of methane uptake at different temperatures (283.2 K, 288.2 K, and 293.2 K). In addition, the increase in the temperature decreased the rate of formation, so they suggested using a kinetic promoter to solve the problem. Surfactants are commonly used kinetic promoters. They lower the solution interfacial tension, which increases the mass transfer between the two phases; hence, increasing the rate of formation step and also the methane uptake of the system (Chaturvedi *et al.*, 2018). However, surfactants generate foam during hydrate dissociation, which results in gas and solution lost. To prevent this, amino acids, which have surfactant like properties with no foam created become more reasonable. Amino acids can also increase the hydrate formation rate (Bavoh *et al.*, 2018b) and reduce the induction time of the methane hydrate formation (Kumar *et al.*, 2019). Veluswamy *et al.* (2016a) studied the effects of amino acid concentration. They showed that when the amino acid concentration was higher than 0.3 wt%, the amino acid acted as a kinetic promoter but at concentration lower than 0.3 wt%, there was no action from the amino acid.

There has been no report on the effects of THF and amino acids as a co-promoter for methane hydrate formation. Thus, the purpose of this work was to investigate roles of both promoters on the formation temperature, the rate of formation and also the hydrate growth pattern of the methane hydrate formation. The stoichiometric ratio of THF concentration, 5.56 mol%, was used with amino acids (leucine, valine, and methionine).



CHAPTER 2

LITERATURE REVIEW

2.1 Natural Gas

Natural gas is a fossil energy source formed under Earth's surface. Natural gas contains mainly methane (CH₄) and some other gases. Natural gas also contains small amounts of natural gas liquids (NGL; which are heavy hydrocarbon compound) and non-hydrocarbon gases such as carbon dioxide. Over long periods of time, the remains of plants and animals (such as diatoms) accumulated under earth's surface and ocean floors. Pressure and heat changed some of these carbons and hydrogen-rich materials into coal, some into oil (petroleum) and some into natural gas as show on Figure 2.1 (EIA, 2018).

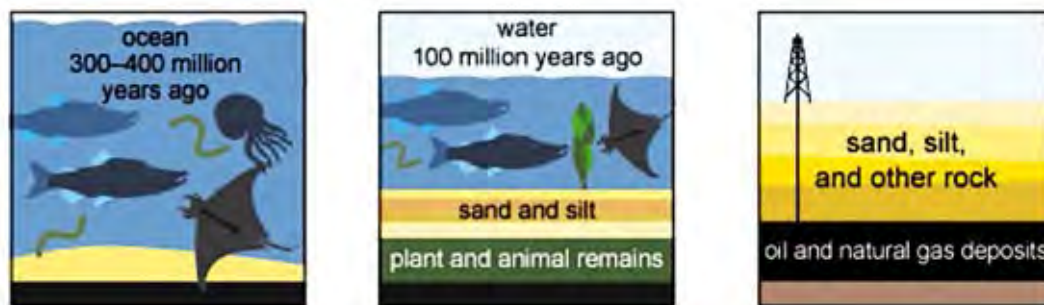


Figure 2.1 Natural gas explained (U.S. Energy Information Administration).

Natural gas can also move into large spaces between layers of source rock. Natural gas found in these types of formations is sometimes called conventional natural gas. In other places, natural gas occurs in the tiny pores (spaces) within some formations of shale, sandstone, and other types of sedimentary rock. This natural gas is referred to as shale gas or tight gas, and it is sometimes called unconventional natural gas. Natural gas also occurs with deposits of crude oil, and this natural gas is called associated natural gas. Natural gas deposits are found on land and some are offshore and deep under the ocean floor. A type of natural gas found in coal deposits is called coalbed methane (EIA, 2018).

From all fossil fuels, natural gas is the cleanest with less toxic mixture. The emission gases are almost carbon dioxide and lower particle emission compared to other fossil fuels, as shown in Table 2.1 (EIA, 2018). This makes natural gas demand increased. BP (2019) reported the increase in the natural gas demand of every continent. In 2040, it will be increased to almost 5500 billion cubic meters (BCM) (Figure 2.2a). The demand is increasing in every human sector, which is led by industry and power sectors. The increase in the industry sector is for the country economic, and the increase in the power sector is driven by the overall growth of power demand (Figure 2.2b).

Table 2.1 Fossil fuels emission level (Pounds/Billion Btu of energy output) (EIA, 2018)

Pollutant	Natural Gas	Oil	Coal
Carbon Dioxide	117,000	164,000	208,000
Carbon Monoxide	40	33	208
Nitrogen Oxides	92	448	457
Sulfur Dioxide	1	1,122	2,591
Particulates	7	84	2,744
Mercury	0.000	0.007	0.016

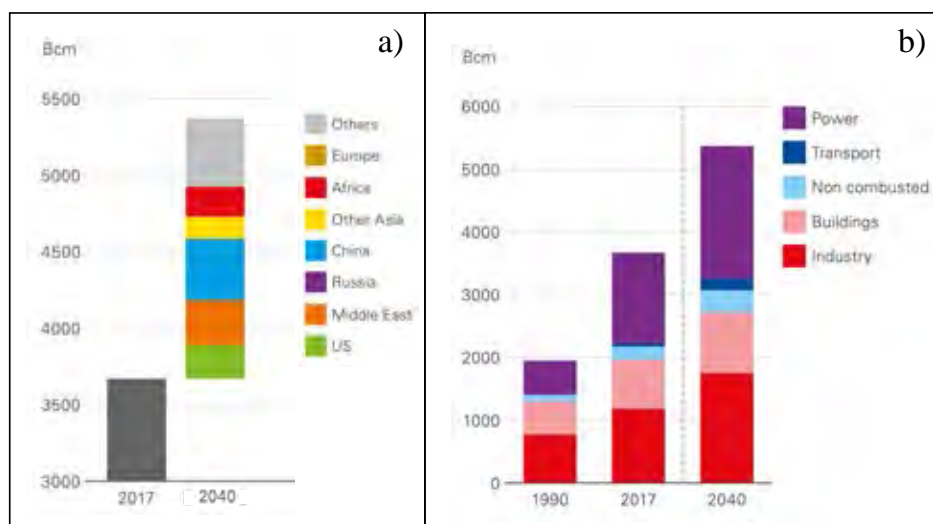


Figure 2.2 Natural gas demand in overall continent (a) and in each sector (b) (BP, 2019).

2.2 Natural Gas Storage and Transportation

The demand for energy is growing every day. Using coal and oil still worsen the environment, so the world tries to find new sources of energy that are cleaner and less toxic. Within the fossil fuel family, the greenest energy is natural gas. For the same amount of heat energy, burning natural gas produces about half as much carbon dioxide, the main cause of global warming, as burning coal. Indeed, natural gas is used every day in cooking, vehicle, and a source for electrical generation. Its high natural gas consumption could help to battle global warming. There are sources of natural gas located far away from end users that requires transportation and storage natural gas (EIA, 2018). BP (2019) reported the increasing trend of import and export of natural gas across the continent. It will be almost two times increase in 2040, as shown in Figure 2.3. This requires a good transport technology and transport chain, shown in Figure 2.4.

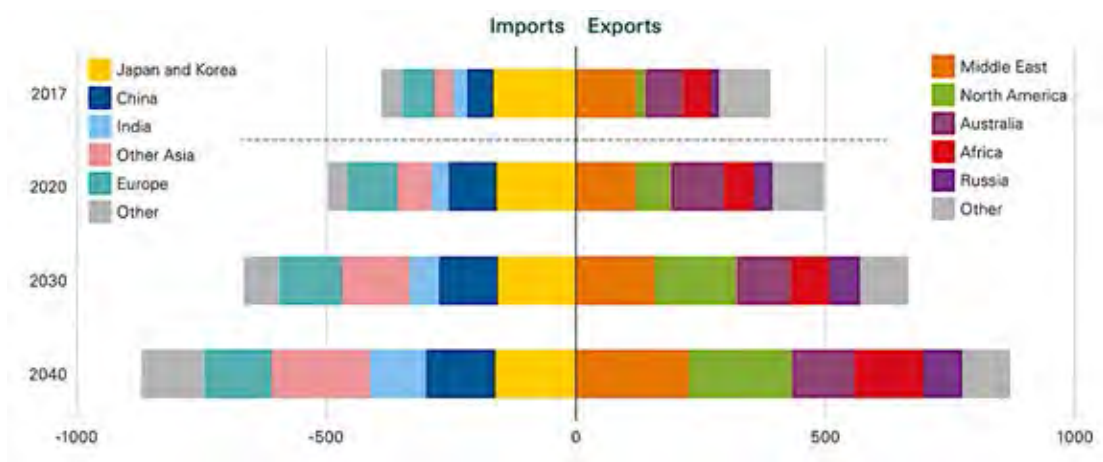


Figure 2.3 Natural gas imports and exports trend report (BP, 2019).

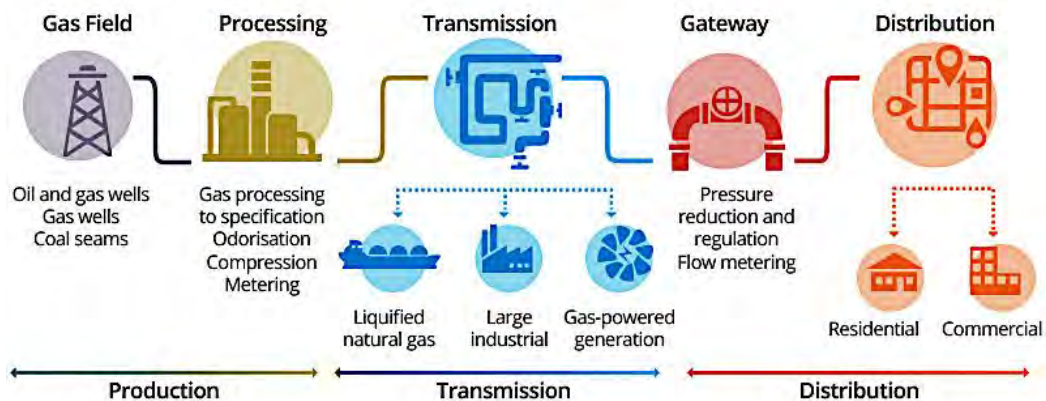


Figure 2.4 Natural gas transport chain (DTE Energy, 2019).

2.2.1 Compressed Natural Gas (CNG)

Compressed natural gas or CNG is simply natural gas mainly comprised of methane that is stored under high pressures (while remaining in its gaseous form) in thick-walled tanks made of aluminum, steel, or some composite. These high-pressure tanks are kept at pressures around 20-25 MPa (200-250 bar or 3000-3600 psi) The disadvantage of CNG is a low volumetric energy store compared with gasoline (Wang *et al.*, 2010).

2.2.2 Liquefied Natural Gas (LNG)

Liquefied natural gas or LNG is a colorless and odorless liquid that contains 85-95% methane with some amounts of ethane, propane, butane, and nitrogen. Liquefied natural gas is made by cooling natural gas to $-162\text{ }^{\circ}\text{C}$ ($-259\text{ }^{\circ}\text{F}$) at 1 atm. This process of going from gas to liquid makes the volume taken up by the fluid decrease considerably, up to 600 times smaller. This reduced volume makes it easier to store and transport natural gas to markets that are lack of natural gas reserves. However, there is a problem due to boil-off gas, which changes the quantity of LNG over time (Veluswamy *et al.*, 2018).

2.2.3 Adsorbed Natural Gas (ANG)

Adsorbent natural gas (ANG) is a new technology that is similar to CNG, except ANG uses porous adsorbent materials to adsorb natural gas at lower

pressures compared to CNG (500 to 600 psig). Because of the lower pressure, costs required to pump and store natural gas in ANG are lower than CNG. ANG can store half to two-thirds the amount of gas at one-sixth of the pressure of CNG. The adsorbent materials are carbon derived and highly disordered. However, the biggest disadvantage is the readsorption that is not complete and 15% to 30% of natural gas in adsorbent is unused (Afework *et al.*, 2018).

Recently, a method to store the natural gas in the solid form called solidified natural gas or SNG was discovered. SNG is a technology that imitates natural phenomena by storing natural gas in the hydrate form with the addition of additive for the formation at lower pressure and higher temperature compared to conventional methods (Veluswamy *et al.*, 2017b). Hydrate structure is stabilized by the interactions between water and gas molecules and a volume of hydrate contains 150- 180 volumes of gas. Gas storage in hydrate form also becomes especially efficient at relatively low pressures where substantially more gas per unit volume is contained in the hydrates than in the three states or in CNG when the pressure has dropped. The choice of these technologies depends on many factors such as the scale of development and distance from markets. On the other hand, natural gas transportation by pipelines is economically suitable for short distances. For medium or small-scale natural gas fields, storage and transportation by gas hydrate technology could be an appropriate and safe alternative.

2.3 Natural Gas Hydrates

Gas hydrates are a naturally occurring, ice-like substance that forms when water and natural gas surrounded by water cage molecules under high pressure and at moderate temperatures. Most naturally occurring gas hydrates contain methane but can also contain other gases like ethane, carbon dioxide, and hydrogen sulfide. In the past, studies of gas hydrates originally focused on ensuring the flow of oil and gas in pipelines, which often clogged with gas hydrates. However, natural gas hydrates become more significant. After the deep-sea exploration, scientist discovered a huge amount of natural gas hydrates in the deep-sea, where one cubic meter of natural gas hydrates can release 160 cubic meters of natural gas (Lenz and Ojamae, 2011).



411257468

CU IThesis 6173001063 thesis / revv: 25052563 12:18:23 / seq: 30

2.3.1 Gas Hydrate Structure

With the help of x-ray diffraction methods, von Stackelberg provided the information of the detailed structure of gas hydrates. The method gave us three different types of methane hydrate structures known as sI, sII, and sH hydrates. All the three-hydrate structure has a cage of water molecule enclosing methane known as pentagonal dodecahedron (Gabitto and Tsouris, 2010).

1. Structure I or sI, a body-centered cubic structure, contains 46 water molecules with 8 potential gas sites (Lonero, 2008). This structure encases small diameter molecules (0.40 - 0.55 nm) such as methane or ethane gas but not bigger than propane, is the most commonly encountered naturally. sI hydrates are found in situ in deep oceans with biogenic gases containing mostly methane, carbon dioxide, and hydrogen sulfide.

2. Structure II or sII, a diamond lattice within a cubic framework, contains 136 water molecules with 24 potential gas sites. Gas hydrates can maintain relatively large molecules (0.6–0.7 nm). This hydrate structure accommodates larger guest molecules, typically propane or iso-butane or combinations of methane gas (Harrison, 2010).

3. Structure H or sH contains 34 water molecules with 6 potential gas sites. It only contains mixtures of large and small molecules (0.8-0.9 nm) such as methyl cyclohexane and methane (Sloan, 2003). It contains 3 small (5^{12}), 2 medium-sized ($4^35^66^3$) and 1 exceptionally large ($5^{12}6^8$) cages (Bohrmann and Torres, 2006). The formation of Type H requires the cooperation of two guest gases (large and small) to make sH stable.

Figure 2.5 depicts the three-unit cells and different pathways each structure must follow to form its respective geometry and guest molecules. The symbol $5^{12}6^2$ specifies a water cage composed of twelve pentagonal and two hexagonal faces. This figure also shows number of water and gas molecules, for example the structure I unit crystal is composed of contain 46 water molecules per 8 gas molecules consisting of 2 small and 6 large cages (Sloan, 2003). Other structures are summaries in Table 2.2 (Gabitto and Tsouris, 2010).

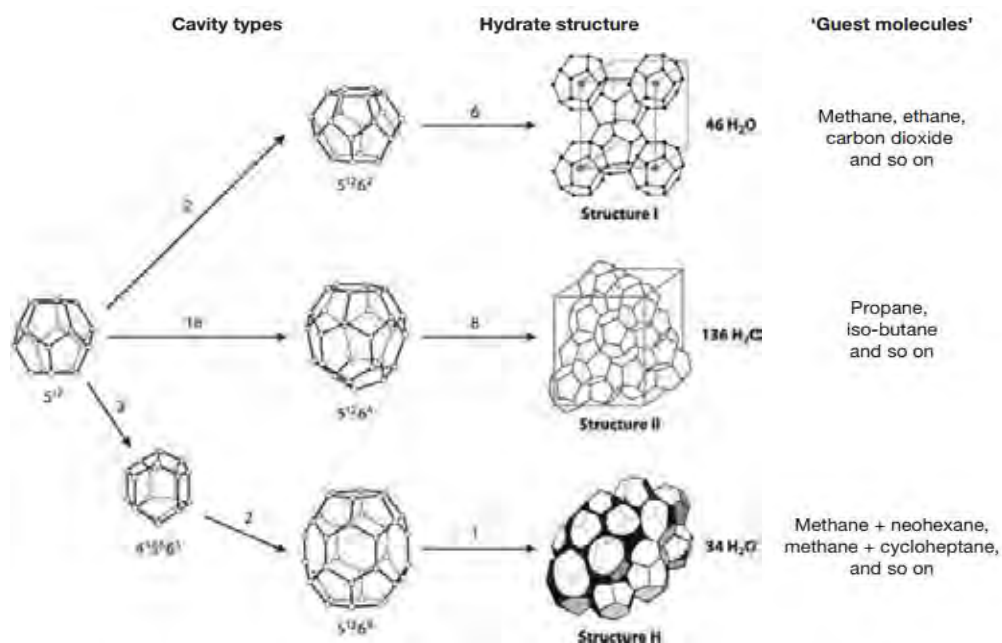


Figure 2.5 Structure types of gas hydrates (Sloan, 2003).

Table 2.2 Geometrical parameters of the main hydrate crystal structures (Gabitto and Tsouris, 2010)

	Structure I		Structure II		Structure H		
Cavity	small	large	small	large	small	medium	large
Description	5^{12}	$5^{12}6^2$	5^{12}	$5^{12}6^4$	5^{12}	$4^35^66^3$	$5^{12}6^8$
Cavities/unit cell	2	6	16	8	3	2	1
Average cavity radius, nm	0.395	0.433	0.391	0.473	0.391	0.406	0.571
Coordination number	20	24	20	28	20	20	36
Water molecules per unit cell	46		136		34		
Lattice type	Cubic		Face-centered cubic		Hexagonal		
Unit cell parameters, nm	$a = 1.2$		$a = 1.7$		$a = 1.21, c = 1.01$		
Density, kg m ⁻³	912		940		1952		

2.3.2 Gas Hydrate Physical Properties

Water molecules are linked through hydrogen bonding and create cavities (host lattice) that can enclose a large variety of molecules (guests). No chemical bonding takes place between the host water molecules and the enclosed guest molecule (Gabitto and Tsouris, 2010). As stated in the hydrate model, the water molecules form a well-defined crystal lattice (the host lattice) containing cavities into which small gas molecules (guests) may be adsorbed; under appropriate conditions the adsorption energy may reduce the free energy of the hydrate sufficiently to make the hydrate phase stable than either pure water or ice (Rodger, 1989). The mechanical properties of the three hydrate structures should be similar to those of ice. The mechanical properties of the three hydrate structures are shown in Table 2.3.

The molecular structures are determined by properties of structure I (sI) and structure II (sII), described by three heuristics: (i) Mechanical properties approximate those of ice, yet each volume of hydrate may contain large volumes of the hydrate forming species at standard temperature and pressure conditions (STP). (ii) Phase equilibrium is set by the size ratio of guest molecules within host cages, and three phase (liquid water hydrate vapor; Lw-H-V) equilibrium pressure depends exponentially upon temperature. (iii) Heats of formation are set by the hydrogen bonded crystals and are reasonably constant within a range of guest sizes.

The physical properties of gas hydrates trapped in sediments are very important in detecting the presence of these compounds, estimating the amount of gas hydrates trapped in the sediments, and developing processes to exploit this resource (Gabitto and Tsouris, 2010). The phase transition that occurs at higher temperatures causes concern when structures are placed in the vicinity of hydrates.

In laboratory, analytical investigation of the interaction between hydrates and the host sediment at the grain level has been highlighted and shown that hydrates are not restricted to forming in a unique way in the pore space. Methane hydrates have a porous nature. The presence of hydrates, which replaces water in pore space, strongly alters the physical properties of the sediments, in which it occurs. The bulk densities of methane hydrates range from 0.35 to 0.75 kg/L and are inversely correlated with the pore volume, which ranges from 10 to 70% by volume. In present, the researchers have had only peripheral interest in hydrate mechanical properties.



411257468

CU Theses 6173001063 thesis / recv: 25052563 12:18:23 / seq: 30

Table 2.3 Comparison of properties of ice, sI, and sII hydrate crystal structures (Gabitto and Tsouris, 2010)

Property	Ice (I_h)	Structure I	Structure II
Water molecules number	4	46	136
Lattice parameters at 273 K, nm	$a = 0.452, c = 0.736$	1.20	1.73
Dielectric constant at 273 K	94	~58	58
Water diffusion correlation time, μs	220	240	25
Water diffusion activation energy, kJ/m	58.1	50	50
Isothermal Young's modulus at 268 K, 10^9 Pa	9.5	8.4 (est.)	8.2 (est.)
Poisson's ratio	0.33	~0.33	~0.33
Bulk modulus (272 K)	8.8	5.6	NA
Shear modulus (272 K)	3.9	2.4	NA
Compressional velocity (V_p), m/s	3870.1	3778.0	3821.8
Shear velocity (V_s), m/s	1949	1963.6	2001.1
Velocity ratio (comp./shear)	1.99	1.92	1.91
Linear thermal expn., at 200 K, K^{-1}	$56 \cdot 10^{-6}$	$77 \cdot 10^{-6}$	$52 \cdot 10^{-6}$
Adiab. bulk compress. (273 K), 10^{-11} Pa	12	14 (est.)	14 (est.)
Heat Capacity, $\text{J kg}^{-1} \text{K}^{-1}$	3800	3300	3600
Thermal conductivity (263 K), $\text{W m}^{-1} \text{K}^{-1}$	2.23	0.49 ± 0.02	0.51 ± 0.02
Refractive index, 638 nm, -3°C	1.3082	1.3460	1.350
Density, kg m^{-3}	916	912	940

2.3.3 Physical Chemistry of Methane Hydrates

2.3.3.1 Thermodynamics

Natural gas hydrates are usually found distributed within the pores of sediments and the thermodynamic parameters of methane hydrate are affected by size of the pores, in which the hydrates form. Studies of gas hydrate thermodynamics have concentrated upon measuring the pressure-temperature conditions, at which three phases, water, hydrate, and gas, are all in equilibrium. The stability of hydrates, which is determined by temperature and availability of methane and the partial pressure of methane is determined by total fluid pressure. Therefore, the hydrates are not stable as the Earth surface temperature and atmospheric pressure. At water depths of 100 m, hydrates would form at about -20°C , while at 500 m depth, the melting temperature approaches in situ temperatures (Archer, 2007).

2.3.3.2 Kinetics

Hydrates can persist metastable. In general, kinetic effects are probably of secondary importance for predicting the hydrate response to anthropogenic climate change because the thermal forcing takes place on such long-time scales. Lab experiments show that hydrates can nucleate from the pure aqueous phase, with no bubbles required, helping the creation of hydrates from advective or biogenic methane. Several studies predict inhibition of hydrate formation in fine-grained sediment caused by the high activation energy. This can explain the characteristic textures of hydrates: as pore-filling cement in coarse grained sediment, but as irregularly shaped masses of pure hydrates in fine-grained sediment and predicts that hydrates should form first or predominantly in sandy sediments (Archer, 2007).

2.3.4 Methane Hydrates in Natural Resource

At present time, we know that a huge potential resource of hydrated gas exists on our planet, and it has been estimated in over 15×10^{12} TOE. If we will produce only 15 to 17% from this resource, it can be a sufficient supply of energy for 200 years. Gas hydrate deposits exist on land in the polar region, and offshore around the globe. Over 220 Gas Hydrate Deposits (GHD) have been found in the world. A map where gas hydrates are inferred to be present on the basis of seismic data, and where gas hydrate drilling expeditions have been completed in permafrost or deep marine environments, also leading to recovery of gas hydrates is shown in Figure 2.6. The production of hydrated gas could be used to contribute not only to the sustained economic development of the individual countries, but also to the political stability in the world (Makogon, 2007).



411257468

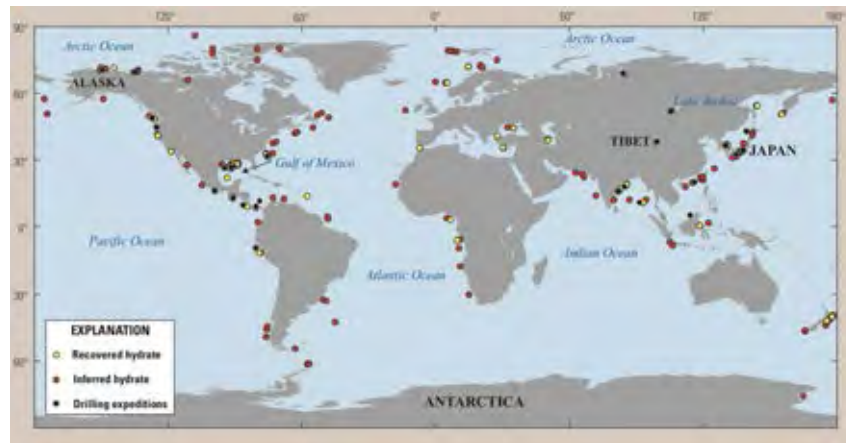


Figure 2.6 A map of the discovered GHD Map showing locations where gas hydrate has been recovered (U.S. Geological Survey).

In nature, the sediments of deep marine continental margins host nearly 99 percent of the world's gas hydrates, typically at water depth of 500 m (approximately 1,640 ft) and greater. The sediments on continental margins often contain substantial concentrations of organic carbon, which is used by microbes to produce methane. This methane, as well as older microbial methane or even methane that migrates upward from deep conventional gas reservoirs, can combine with sediment pore waters to form gas hydrates beneath the sea floor. Gas hydrates also sometimes form directly on the sea floor, where fluids leak into the ocean at seep sites, but such deposits are not considered an important component of the global gas hydrate inventory.

In continental margin sediments, the natural pressure and temperature conditions mean that the gas hydrate zone thins upslope and thickens downslope, reaching hundreds of meters of thickness as water depth increases. In many locations, field studies show that only a small fraction (less than 5 percent) of the sediments host gas hydrates, which is sometimes concentrated in specific layers or in fractures.

Figure 2.7 shows schematic cross section showing gas hydrates within and beneath permafrost (left side) and in deep water marine sediments (right side). The locations described in orange are the most susceptible to climate processes that can affect the stability of methane hydrate deposits. Oxidation can destroy methane in the sediments, in the water column, and in the atmosphere.

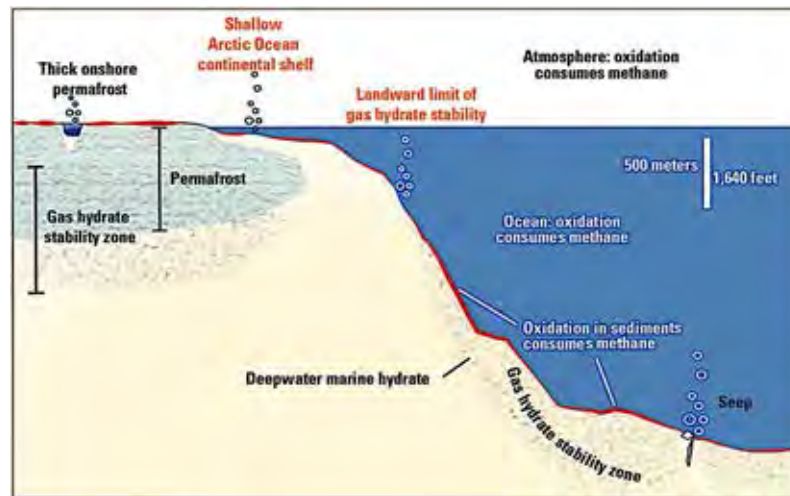


Figure 2.7 Schematic cross section showing gas hydrate (U.S. Geological Survey).

Gas hydrates are stable only within specific ranges of temperature and pressure. As average atmospheric and ocean temperatures increase, gas hydrates in permafrost and deep marine settings may break down and release the trapped methane. Much of the liberated methane is likely to remain in the sediments. Methane that escapes from the sea floor into the ocean (Figure 2.8) is typically converted to carbon dioxide by micro-organisms, a process that increases the acidity of ocean waters. In Figure 2.8 a photograph taken by Oceanering Inc. using the Global Explorer remotely operated vehicle shows methane bubble streams emanating from the sea floor.

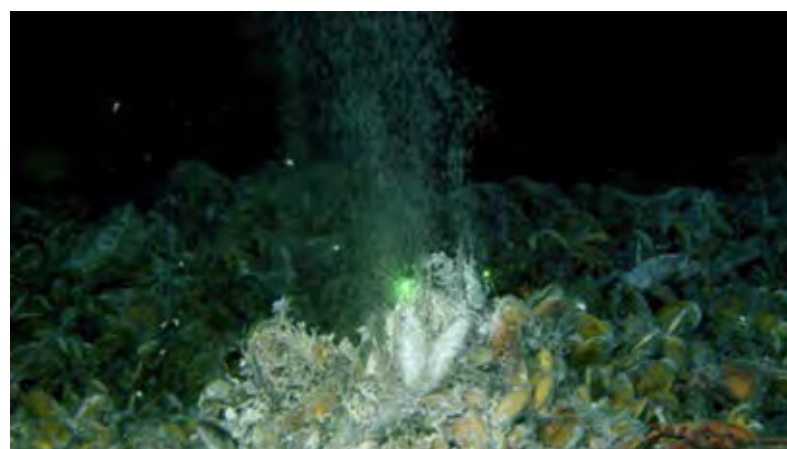


Figure 2.8 Methane bubble streams emanating from the sea floor (U.S. Geological Survey).

2.4 Gas Hydrate Formation

As natural gas hydrates or clathrate hydrates are an ice-like solid, which can contain gas molecule, occupied in the cage of a water molecule. This characteristic of the natural gas hydrates is the key factor for natural gas storage in the hydrate form. Moreover, hydrate technology can apply to many applications; i.e., gas separation (Babu *et al.*, 2013a; Partoon *et al.*, 2018; Sun *et al.*, 2014), energy storage (Siažik and Malcho, 2017; Veluswamy and Linga, 2013), CO₂ capture (Babu *et al.*, 2014; Babu *et al.*, 2013a; Dashti *et al.*, 2015), and desalination applications (Babu *et al.*, 2018; Kang *et al.*, 2014; Seo *et al.*, 2019).

The process to form the natural gas hydrates is similar to the crystallization consisting of two major steps, a nucleation phase and a growth phase. Upon successful hydrate nucleation, a thin hydrate film forms on the water–gas interface, which grows further in a mass transfer limited regime. It has been identified that other than utilizing better reactor designs, higher solubility of hydrate forming guests in water, and a larger contact area between the hydrate formers and water can reduce the mass transfer resistance and ensure faster hydrate growth (Kumar *et al.*, 2015).

Methane hydrates only occur naturally in subsurface deposits, where temperature and pressure conditions are favorable for its formation. These conditions are illustrated in Figure 2.9, which shows the depth and pressure on the y axis and the temperature on the x axis. The dashed lines separate stability fields of gas, gas hydrates, water, and water ice. The line labeled “hydrate to gas transition” is the important one because the conditions for the formation of methane hydrate occur below this line. On the other hand, above this line, the methane hydrate will not form. The red line traces a geotherm (the change of temperature with depth at a specific location). As depth increases, the geotherm crosses the hydrate to gas transition line. This means that gas hydrate in sediments usually overlies free gas.



411257468

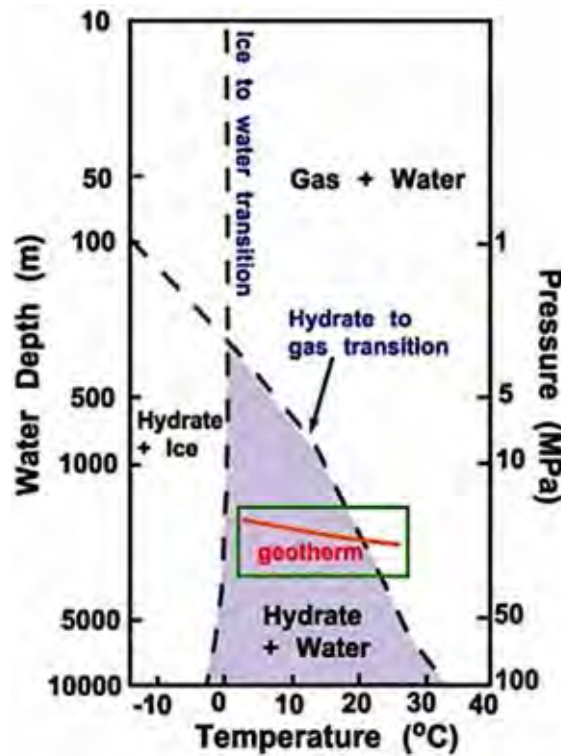


Figure 2.9 Phase diagram showing the water depths (and pressures) and temperatures for gas hydrate (purple area) stability (<https://oceanexplorer.noaa.gov>).

2.5 Gas Hydrate Dissociation

Gas hydrate dissociation is the process, which provides heat to break the hydrogen bonds between water molecules and the van der Waals interaction forces between guest molecule and water molecule of the hydrate lattice. When the process completes, the products of hydrate dissociation are water molecules (host molecules) and gas molecules (guest molecules).

Several conventional methods have been proposed for the production of natural gas from hydrate reservoir, including depressurization, thermal stimulation, chemical inhibitor injection, or a combination of these methods. Depressurization is the most popular method including decreasing the pressure to below the hydrate stability zone. The second method is thermal stimulation, which requires increasing the temperature above the natural gas hydrate equilibrium temperature at the prevailing pressure. The third method is chemical inhibitor injection, which can be

differentiated into two different types: thermodynamic inhibitor and kinetic inhibitor injection (Yin *et al.*, 2016). This method uses some chemical inhibitors to inhibit hydrate formation by using chemicals like methanol or glycols and act by shifting the water/hydrocarbon/ hydrate three-phase equilibrium line.

Intrinsic decomposition rate of methane hydrate is controlled by temperature, pressure, interfacial area, and the intrinsic rate constant. It affects the heat transfer rate from surrounding to hydrate core due to the endothermic characteristics of the reaction.

2.6 Methane Hydrate Reactor Configuration

To overcome the slow hydrate nucleation and rate of hydrate formation, mass transfer between the gas phase and liquid phase during the hydrate formation process must be improved (Du *et al.*, 2014; Zhang *et al.*, 2007). Mechanical means were used to improve the gas/liquid interphase, e.g. stirred reactor (Mech *et al.*, 2016; Verrett *et al.*, 2012; Zhong *et al.*, 2015), spray reactor (Englezos and Lee, 2005; Tang *et al.*, 2006), or gas bubble reactor (Luo *et al.*, 2007; Vysniauskas and Bishnoi, 1983).

Veluswamy *et al.* (2017a) studied the methane hydrate formation in a stirred system with amino acids. The result shows that the stirred system enhanced the methane hydrate nucleation time (induction time) 150 times faster than the unstirred system (Figure 2.10a). However, due to the water circulated inside, it reduced the hydrate formation rate and also the gas uptake compared to the unstirred reactor configuration, as shown in Figure 2.10b, c, respectively. Another reactor configuration was introduced by combining the advantages of stirred and unstirred systems, called the hybrid system. In the system, stirring started at the beginning until the first nucleation. The result showed short induction times of hydrate formation as same as the stirred system, and high hydrate formation rate and also high methane uptake as same as the unstirred system. (Figure 2.10a, b, c).



411257468

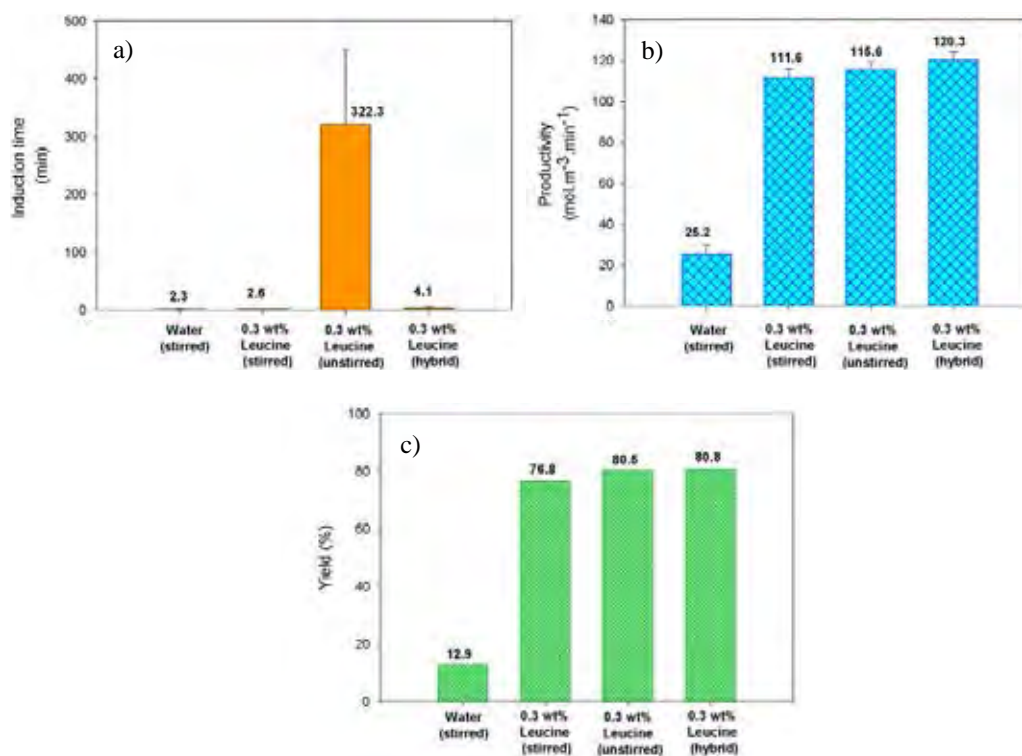


Figure 2.10 Bar plots showing the effect of stirred, unstirred, and hybrid approaches on induction time, productivity and hydrate yield (Veluswamy *et al.*, 2017a).

2.7 Methane Hydrate Promoter

To overcome the slow hydrate nucleation and rate of hydrate formation, mass transfer between the gas phase and liquid phase can be increased not only by improving the reactor configuration, promoters can also be used to enhance both the kinetics and the gas capacity. Promoters are mostly divided into thermodynamic and kinetic promoters.

2.7.1 Thermodynamic Promoter

There are many chemicals used as a gas hydrate thermodynamic promoter. Lee *et al.* (2012), de Deugd *et al.* (2001), and Mainusch *et al.* (1997) reported the methane hydrate phase equilibriums of solution mixed with 1,3 dioxane, tetrahydropyran (THP), acetone, and tetrahydrofuran (THF). The results in Figure 2.11 show that THF shifted the hydrate phase equilibrium to the lowest pressure and highest temperature.

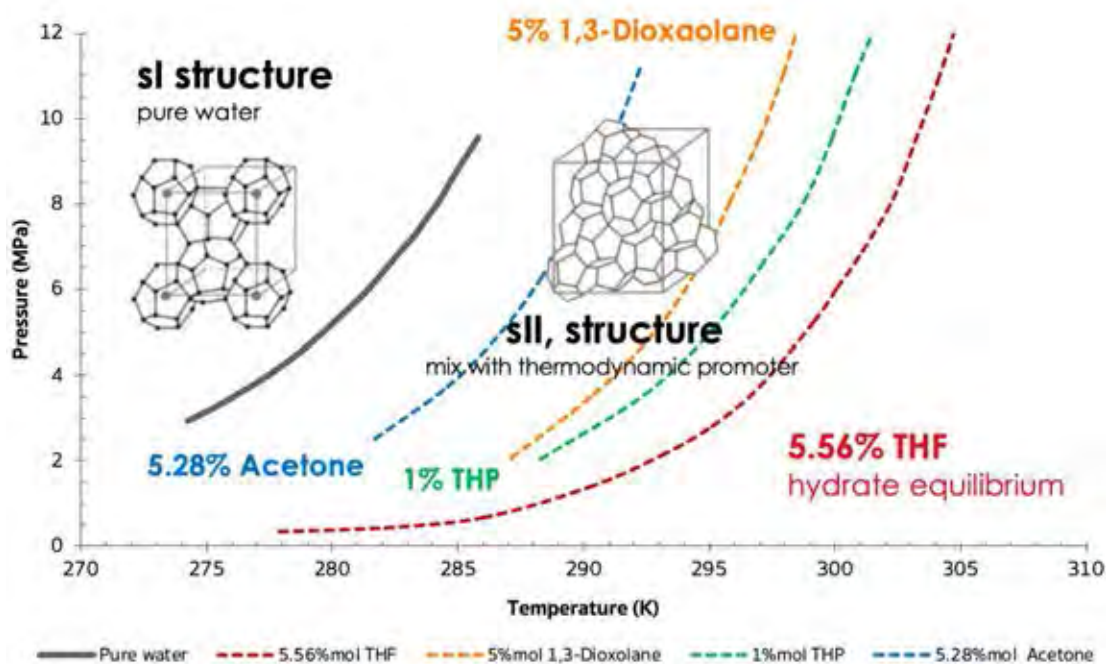


Figure 2.11 Methane hydrate phase equilibria of solution mix with 1,3 dioxane, THP, acetone, and THF (de Deugd *et al.*, 2001; Lee *et al.*, 2012; Mainusch *et al.*, 1997).

2.7.1.1 Methane + tetrahydrofuran (THF)

Lin *et al.* (2018) and Beheshtimaal and Haghtalab (2018) reported that 5.56 mole% THF (stoichiometric) gave the highest methane uptake. Figure 2.12 shows the bar plots of methane uptake and the rate of hydrate formation with and without a thermodynamic promoter under the same experimental conditions of 5 MPa and 283.2 K. It has to be noted that slight variation in THF concentration did not significantly affect the thermodynamics of mixed methane THF hydrate formation but the methane uptake of THF concentrations (4.5 and 5 mol %) was lower than that at 5.56 mol % as the amount of THF available for mixed hydrate formation was lower.

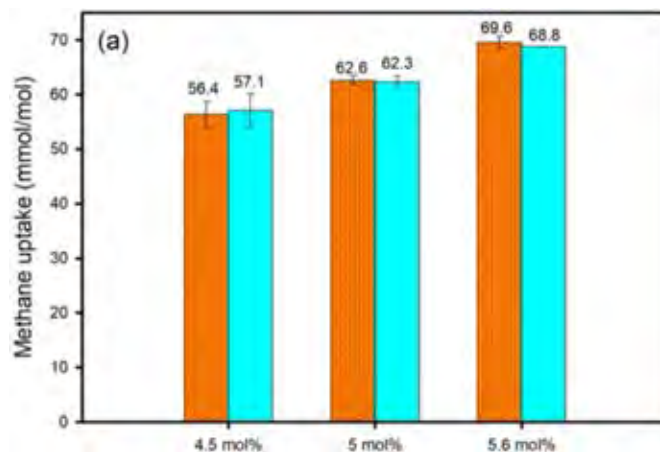


Figure 2.12 Methane uptake in different THF concentrations (Lin *et al.*, 2018).

Veluswamy *et al.* (2016c) investigated the effects of 5.56 mole% THF as a thermodynamic promoter. Figure 2.13 shows that adding 5.56 mole% THF at 283.2 K and 7 MPa resulted in the increased rate of hydrate formation, and the methane uptake increased 11.66 times compared to pure methane at 9.5 MPa and 274.2 K. Therefore, the presence of promoter like THF mixed with methane in the process of hydrate formation can enhance both thermodynamic and kinetic performance, which enables the development of a low cost and energy efficient of solid natural gas technology via clathrate hydrates for natural gas storage.

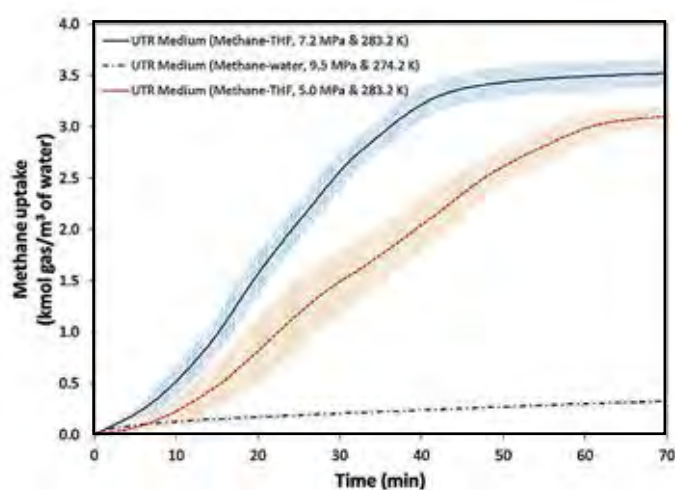


Figure 2.13 Methane uptake of adding and unadding 5.56 mol% THF (Veluswamy *et al.*, 2016c).

Veluswamy *et al.* (2016b) studied the effect of temperature on methane/5.56 mol% THF hydrate formation kinetics by using 3 different temperatures (283.2 K, 288.2 K, and 293.2 K). At the chosen experimental temperatures and pressure, it is possible to form sII hydrates only, and there exists no chance for the formation of pure sI methane hydrates. The report shows that no significant difference of methane uptake in different temperatures (283.2 K, 288.2 K, and 293.2 K), as shown in Table 2.4. This result also shows that increasing the temperature decreased the rate of formation.

Table 2.4 Average data for induction time, methane uptake, t_{90} and rate of hydrate formation for experiments conducted at 7.2 MPa and different temperatures (Veluswamy *et al.*, 2016b)

Experiment no.	Experimental temperature (K)	Induction time, IT (min)	Time taken for 90% completion, t_{90} (min)	Methane uptake ^a (kmol/mol)	Rate of methane uptake, NR_{3h} (kmol m ⁻² h ⁻¹)		
					Stage 1 ^b	Stage 2 ^b	Stage 3 ^b
A1	283.2	5.55 (± 0.05)	46.22 (± 1.39)	3.82 (± 0.166)	5.500	-	-
A2					(± 0.208)	-	-
A3					-	-	-
B1	288.2	1.11 (± 0.70)	112.44 (± 3.15)	3.68 (± 0.166)	1.840	2.098	-
B2					(± 0.276)	(± 0.144)	-
B3					-	-	-
C1	293.2	25.80 (± 17.72)	401.05 (± 96.25)	3.81 (± 0.082)	0.204	0.510	1.005
C2					(± 0.077)	(± 0.093)	(± 0.155)
C3					-	-	-
C4					-	-	-
C5					-	-	-

^a Methane uptake for experiments A1-A3 and B1-B3 reported at 3 h of hydrate growth while gas uptake for C1-C5 reported at 8 h of hydrate growth.

^b The average variation (R^2) for stage 1, 2 and 3 are 0.8890 (± 0.0105), 0.9951 (± 0.0025) and 0.9933 (± 0.0048) respectively.

2.7.2 Kinetic Promoter

2.7.2.1 Surfactants

Surfactant is one of the well-known chemicals used to increase the gas hydrate formation kinetics. Anionic surfactants were reported as the highest kinetic enhancement surfactant. Zhao *et al.* (2015) investigated the effect of sodium dodecyl sulfate (SDS) at 277.25 K and 6 MPa condition. It was found that the rate of hydrate formation in the 300 ppm SDS solutions increased compared with pure water, as shown in Figure 2.14. From this figure, the final methane uptake was also increased.

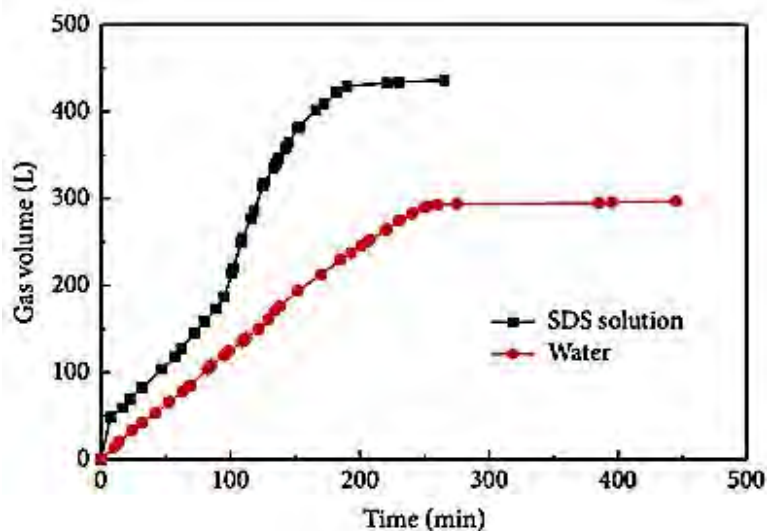


Figure 2.14 Methane uptake of different amino acid concentrations (Zhao *et al.*, 2015).

Methyl ester sulfonate (MES) is a bio-based anionic surfactant. Inkong *et al.* (2019b) reported that increasing the MES concentration from 1 mM to 8 mM at 277.2 K and 8 MPa decreased the gas hydrate formation induction times and increased the gas hydrate formation rate, as shown in Figure 2.15a, b, respectively. Even MES has low toxicity and is environmentally friendly, it still generates foam during gas hydrate dissociation, as shown in Figure 2.16. This is the main cause of gas loss and a single use solution.

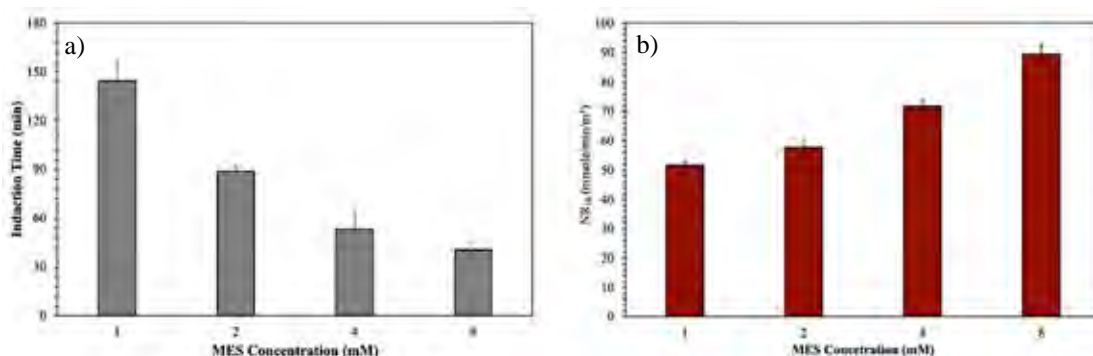


Figure 2.15 Gas hydrate formation induction time (a) and the normalized rate of gas hydrate formation (NR_{30}) of various MES concentrations (Inkong *et al.*, 2019b).

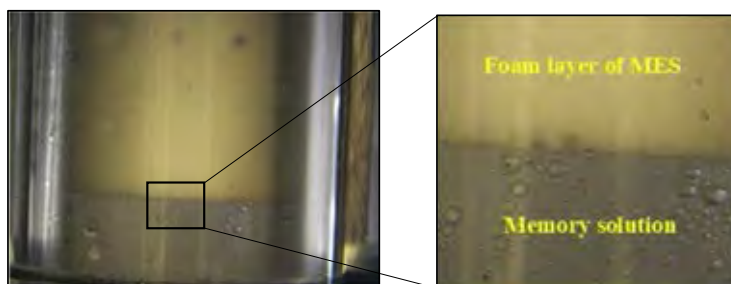


Figure 2.16 Solution 60 minutes after gas hydrate dissociation (Inkong *et al.*, 2019b).

2.7.2.2 Amino acids

Due to the environmental toxicity and the foam generated after hydrate dissociation, a surfactant or even bio-based surfactant has to be replaced. Amino acids with surfactant-like ability were selected as an alternative for gas hydrate enhancement. (Veluswamy *et al.*, 2016a) studied the effect of amino acid concentrations between 0.1 and 0.5 wt%. Figure 2.17 presents the methane uptake curves determined with different concentrations of leucine. The characteristic observation for leucine is that a certain deflection point exists, beyond which the rate of hydrate formation drastically improves compared to the rate initially exhibited from the nucleation.

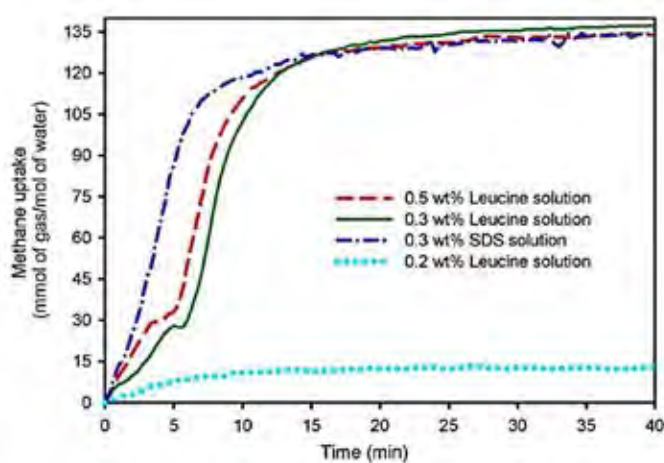


Figure 2.17 Methane uptake of different amino acid concentrations (Veluswamy *et al.*, 2016a).

Table 2.5 shows kinetic data for one fresh and one memory trial (two runs) at each experimental condition by providing detailed information on the methane uptake, nucleation time, and rate of hydrate formation observed after 5 min from nucleation for different experimental trials.

Table 2.5 Induction time, methane uptake, and rate of hydrate formation for experiments conducted using different concentrations of leucine amino acid (Veluswamy *et al.*, 2016a)

exp. no.	solution volume (mL)	solution nature	conc. (% wt)	induction time (min)	methane uptake (mmol/mol water)	deflection time [D _f] (min)	rate of hydrate formation (mmol m ⁻² s ⁻¹)	
							Stage 1 ^a	Stage 2 ^b
X1	1.5	fresh	0.5	27.0	129.9	8	236.83	702.33
X2		memory		6.7	134.3	8	253.83	673.67
Y1		fresh	0.3	18.3	133.8	10	202.17	722.67
Y2		memory		0.3	112.3	10	191.00	670.00
A1	1.0	fresh	0.5	0.3	133.5	5	371.17	889.83
A2		memory		0.3	154.6	5	380.17	923.50
B1		fresh	0.4	9.8	135.0	5	293.50	984.50
B2		memory		1.0	131.2	5	261.67	850.67
C1		fresh	0.3	3.0	157.4	6	305.33	1036.33
C2		memory		67.0	159.1	6	285.67	930.33
C3		memory		208.0	136.5	6	481.67	392.50
D1 ^d		fresh	0.2	322.0	27.17			
D2 ^d		memory		34.0	23.14			
E1 ^d		fresh	0.1	602.0	28.29			
E2 ^d		memory		0.3	28.70			

^aAll experiments were conducted at a starting pressure of 10 MPa and 275 K ($\Delta T = 11$ K). ^bRate of hydrate formation calculated after 5 min from induction. ^cRate of hydrate formation calculated 5 min after deflection point. ^dLow concentration amino acid experiments (0.1 and 0.2 wt %) resulted in a hydrate "skin" at the interface with no promotion effect observed.

Both data show that, at 0.1 and 0.2 wt% leucine concentrations, there was no promotion effect observed; thereby, no characteristic deflection point and the rate was not calculated. The time delay (deflection time) increased with the decrease in the concentration of leucine, and it increased with the increase in the overall volume of the solution. Furthermore, the second growth stage with leucine had a significantly higher rate (about 3–4 times) in comparison to the rate observed in the first stage. The result can be concluded that at concentrations higher than 0.3 wt%, there was a rapid methane hydrate growth resulting in faster kinetics. At concentrations lower than 0.3 wt%, there was no promotion effect exhibited by the amino acid.

Liu *et al.* (2015) studied the effect of amino acid (leucine) concentration on the methane hydrate formation at 273 K with a starting pressure of 7.5 MPa. They confirmed that amino acid concentrations below 0.3 wt% were not enough to enhance methane hydrate formation. The result in Figure 2.18 also shows that the rate of methane hydrate formation and the methane uptake of the leucine concentration higher than 0.3 wt% are not significantly different.

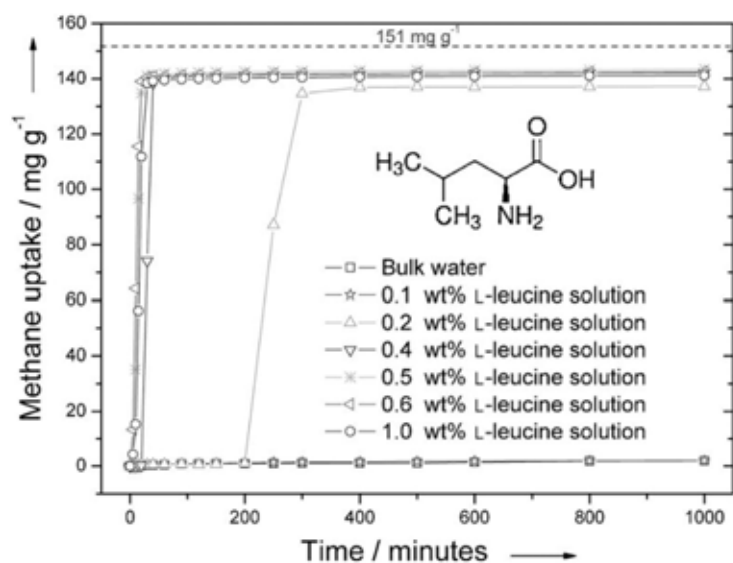


Figure 2.18 Methane uptake of different amino acid concentrations (Liu *et al.*, 2015).

CHAPTER 3

EXPERIMENTAL

3.1 Materials and Equipment

3.1.1 Chemicals

1. Tetrahydrofuran (AR grade from ACL Labscan, Thailand)
2. Leucine (amino acid reagent grade, >98% (HPLC) from Sigma-Aldrich, Singapore)
3. Valine (amino acid reagent grade, >98% (HPLC) from Sigma-Aldrich, Singapore)
4. Methionine (amino acid reagent grade, >98% (HPLC) from Sigma-Aldrich, Singapore)
5. Ultra-high purity methane gas (99.999% purity from Linde Public Company, Thailand)
6. Deionized water

3.1.2 Equipment

Hydrate formation/dissociation apparatus

1. Crystallizer (CR)
2. Reservoir (R)
3. Personal Computer (PC)
4. Pressure transducer (PT)
5. K-type thermocouple
6. Controllable water bath

3.2 Experimental Procedures

3.2.1 Experimental Apparatus

Figure 3.1 presents the schematic of the gas hydrate experimental setup containing an isothermal/isobaric crystallizer. The hydrates was formed in the high-pressure stainless-steel crystallizer and high-pressure sapphire crystallizer (CR) that can withstand a 20-MPa rating and internal volume of 180 mL and 50 mL, shown in Figure 3.2a, b. The supply gas or a reservoir (R) with volume of 150 ml was connected with the hydrate crystallizer. The crystallizer and reservoir were immersed in the temperature-controlled mixed glycol/water bath. The temperature in the mixed glycol/water bath was controlled by an external refrigerator (Model RC-20, Daeyang, Korea) with an accuracy of $\pm 1^\circ\text{C}$. The pressure transmitters (Cole Parmer[®], model 68073-68074, Singapore) with the range of 0-21 MPa and 0.13 % global error were used to measure the pressure. The temperature in the crystallizer was measured by four K-type thermocouples, located at different positions, as seen in Figure 3.2a, b. The pressure and temperature during experiments were recorded by data logger (AI210, Wisco Industrial Instruments, Thailand) that was connected to a personal computer. All experiments were carried out in the constant condition with a fixed amount gas and water in the closed system.

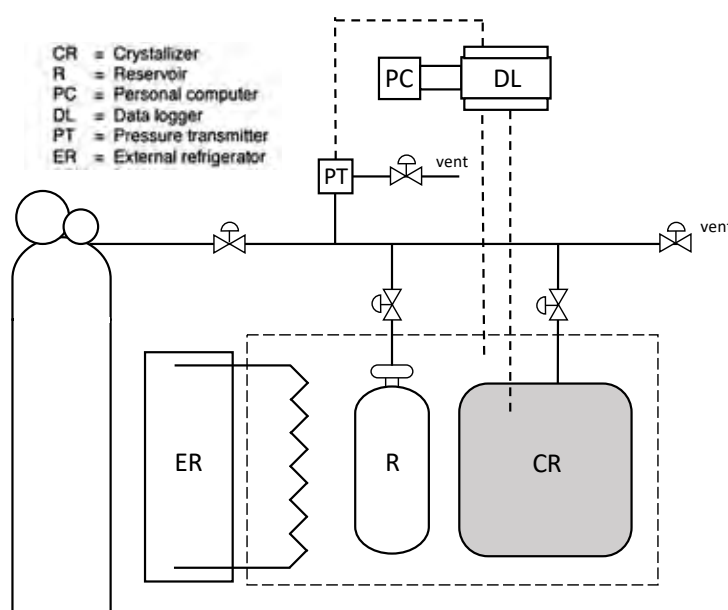


Figure 3.1 Schematic of gas hydrate system.

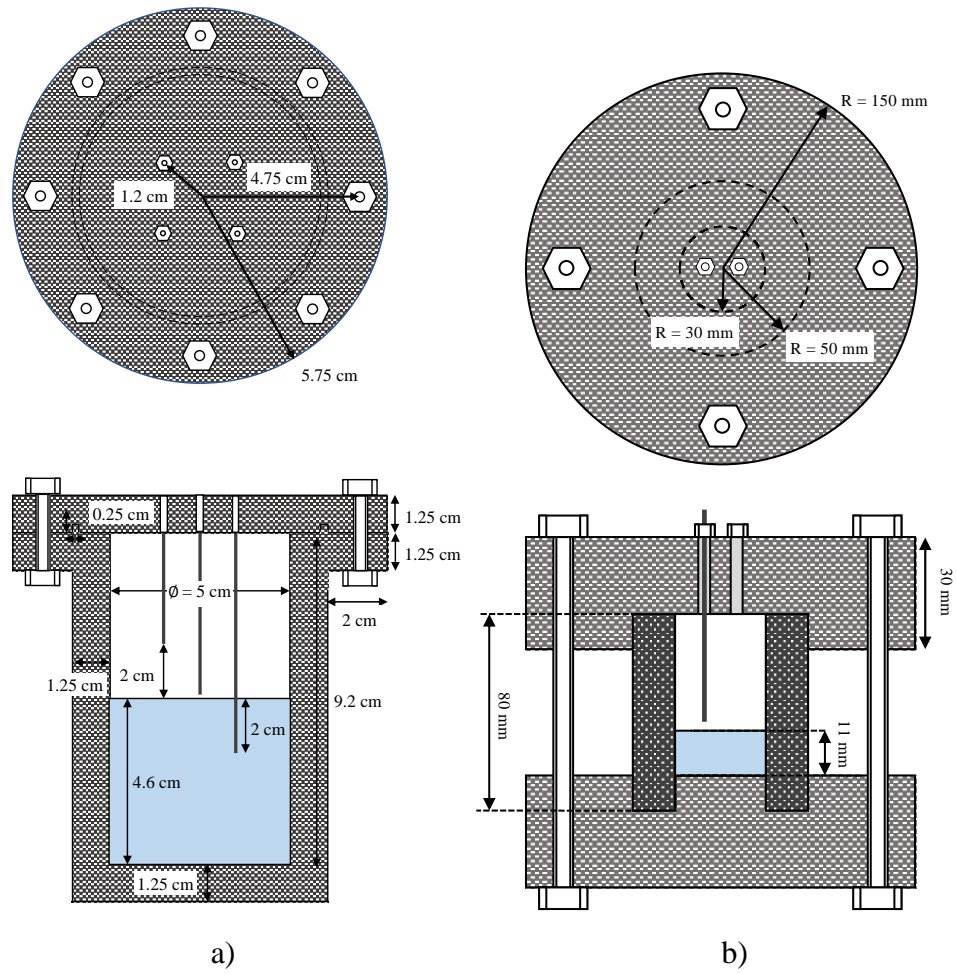


Figure 3.2 a cross-section of a stainless steel crystallizer (a) and a cross-section of a sapphire crystallizer (b) (Inkong *et al.*, 2019a; Siangsai *et al.*, 2015).

3.2.2 Methane Hydrate Formation

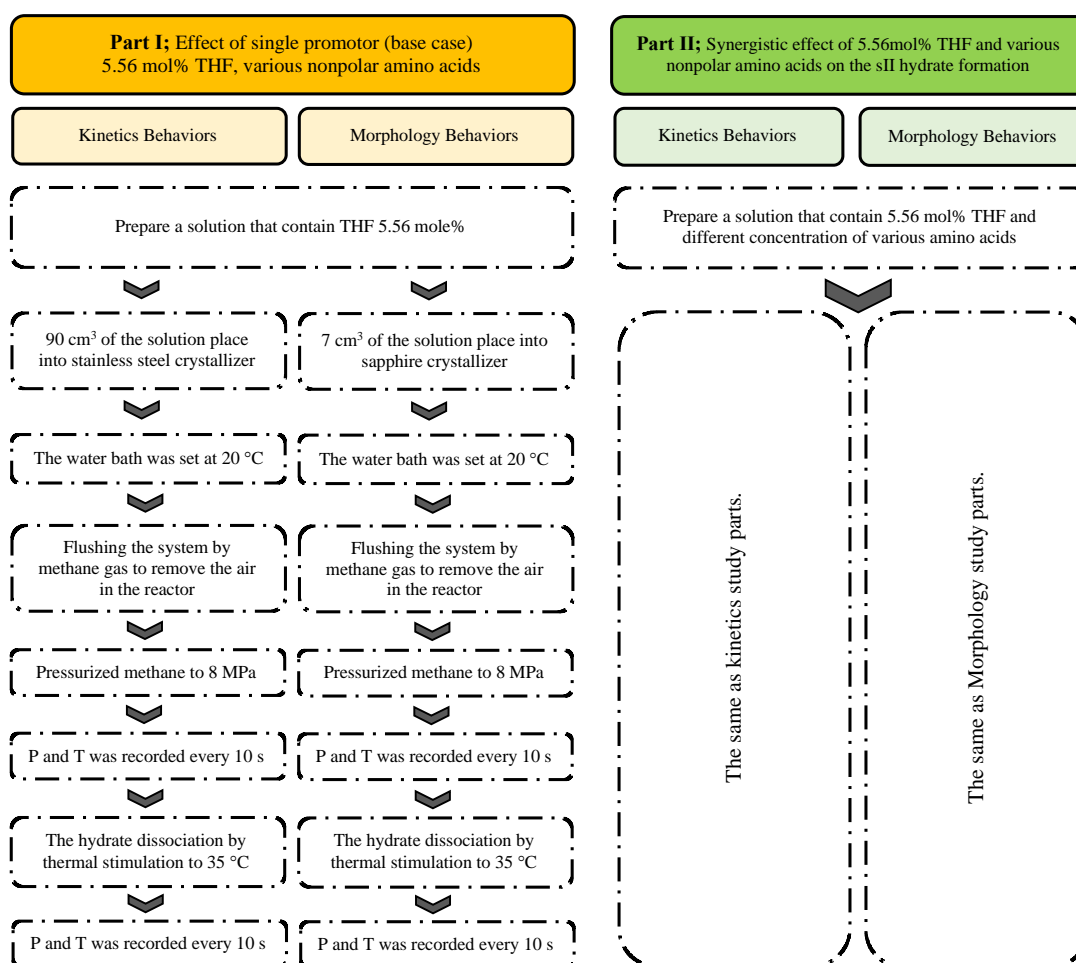


Figure 3.3 Synergistic effect of nonpolar amino acids (leucine, valine and methionine) to 5.56mol% THF on the sII hydrate formation experimental procedures.

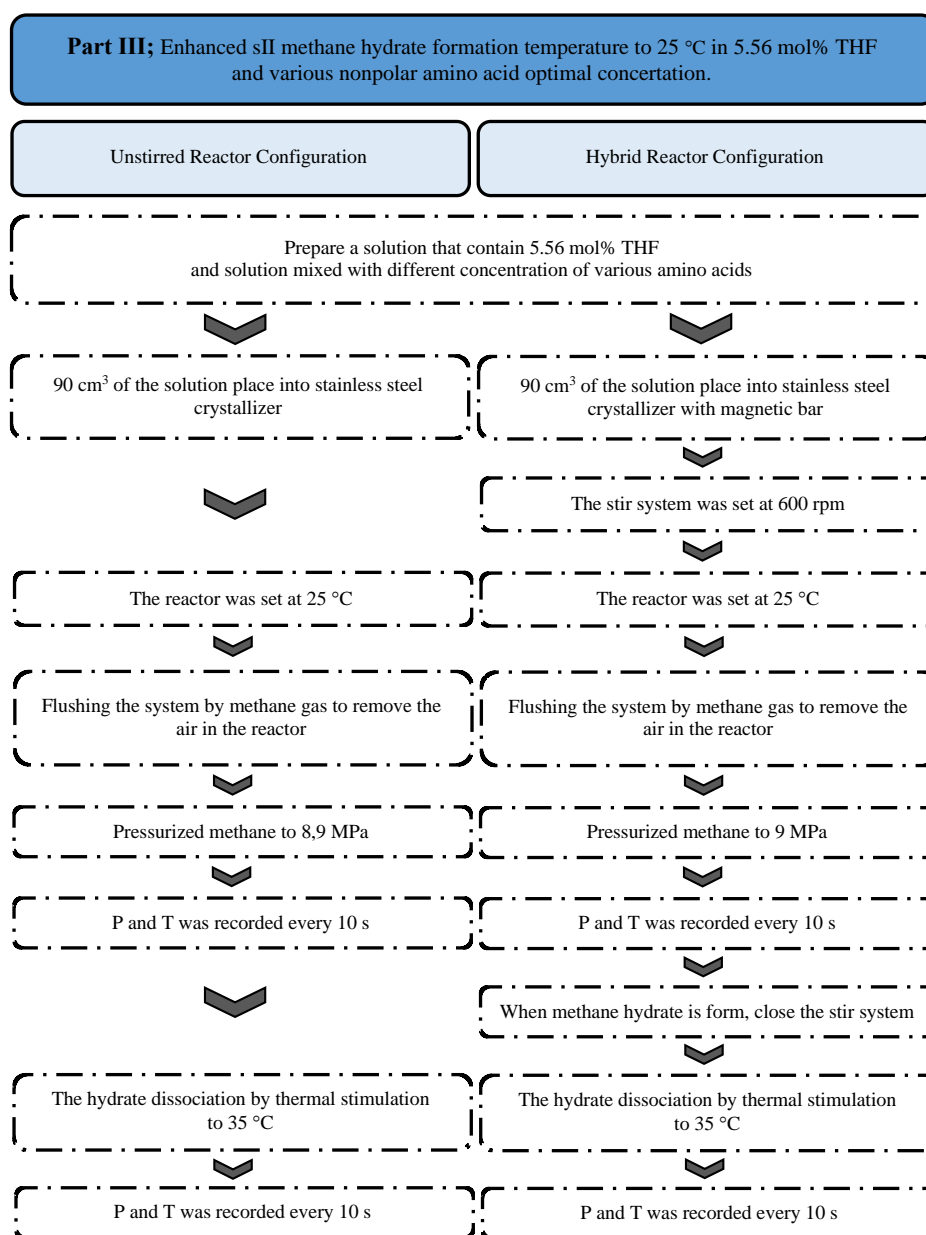


Figure 3.4 Enhanced sII methane hydrate formation temperature in 5.56 mol% THF and various nonpolar amino acid system experimental procedures.

Experimental procedures adopted for synergistic effects of nonpolar amino acids (Reddy *et al.*, 2019) and enhancing methane hydrate formation temperature studies are provided as schematics in Figures 3.3 and 3.4, respectively. Varying types of nonpolar amino acids (valine, leucine, and methionine) were prepared for both kinetic and morphology investigation studies. The experimental apparatus was cleaned using deionized water, purged with methane, to ensure that the

crystallizer was thoroughly clean before each experiment. After that, the crystallizer was cooled until temperature was stabilized. Methane gas was introduced into the system rapidly after the temperature steady until the system pressure reached the desired experimental pressure (8 and 9 MPa). The data was then recorded every 10 s. All experiments were carried out in the constant condition with a fixed of water and gas in the system. While the hydrate formation, the pressure in the CR was reduced due to the gas consumption, and the temperature was increased due to the effect of exothermic reaction. The experiments continued until no significant change in the pressure or until 13 hrs of experiment. All experiments were repeated at least three times to confirm the reproducibility. The pressure and temperature data were used to calculate for the methane consumption (methane uptake) using Equation 3.1 (Babu *et al.*, 2013b; Veluswamy and Linga, 2013).

$$\Delta n_{H,\downarrow} = n_{H,0} - n_{H,t} = \left(\frac{PV}{zRT} \right)_{G,0} - \left(\frac{PV}{zRT} \right)_{G,t} \quad (3.1)$$

where $\Delta n_{H,\downarrow}$ = moles of consumed gas for hydrate formation (mole)

$n_{H,t}$ = moles of hydrate at time t (mole)

$n_{H,0}$ = moles of hydrate at time 0 (mole)

P = pressure of the crystallizer (atm)

T = temperature of the crystallizer (K)

V = the volume of gas phase in the crystallizer (cm³)

Z = compressibility factor Pitzer's correlation (Smith *et al.*, 2005)

R = the universal gas constant 82.06 cm³·atm/mol·K

Subscripts of $G, 0$ and G, t represents the gas phase at time zero and time t respectively. The conversion of water to hydrate was calculated by Equation 3.2 (Babu *et al.*, 2013b).

$$\text{Hydrate yield (\%)} = \frac{\Delta n_{H,\downarrow} \times \text{Hydration number}}{n_{H_2O}} \times 100 \quad (3.2)$$

where n_{H_2O} = moles of water in the system (mole)

$\Delta n_{H,\downarrow}$ = moles of consumed gas for hydrate formation (mole)



411257468

The hydration number is the number of water molecules required per gas molecule to form the hydrate structure. For sII hydrate structure formed in our experiments, this value is considered as 5.67 (Veluswamy *et al.*, 2016c). The normalized initial hydrate formation rate (NR_t) for the first t minutes from the start of hydrate growth was calculated by Equation 3.3 (Veluswamy *et al.*, 2015)

$$NR_t = \frac{R_t}{V_{\text{water}}} \quad (3.3)$$

where V_{water} is the volume of water (m^3) taken in the reactor, and R_t is the rate of hydrate growth (mmol/min) calculated by fitting the average methane uptake due to hydrate growth at each experimental condition versus time for the first t minutes after the induction time, using the least squares method. The time period of t minutes that gives the best fit is selected for rate quantification based on the hydrate methane uptake profiles for all experiments.

3.2.3 Methane Hydrate Dissociation

After methane hydrate formation, the hydrates were dissociated by using thermal stimulation. The temperature was increased from the experimental temperature (20 and 25 °C) to the desired dissociation temperature (35 °C). The extrapolation of equilibrium pressure of the mixed THF-methane hydrate at 35 °C from the report of Lee *et al.* (2012) is 13.0 MPa. Thus, at the dissociation temperature considered (35 °C), all the hydrates formed completely dissociated. The gas released from the hydrates during the dissociation was measured by the pressure transducer. Then, the temperature was increased from the formation temperature to desired dissociation temperature. This point is marked as time zero for the hydrate dissociation experiments. The total moles of gas in the system equal to the moles of gas at time zero. At any given time, the total number of moles ($n_{T,t}$) in the system remains constant and equal to that at time zero ($n_{T,0}$). Therefore, the mole of released methane from the hydrate at any time during the hydrate dissociation was calculated by Equation 3.4 (Siangsai *et al.*, 2015).

$$\Delta n_{H,\uparrow} = n_{H,t} - n_{H,0} = \left(\frac{PV}{zRT} \right)_{G,t} - \left(\frac{PV}{zRT} \right)_{G,0} \quad (3.4)$$

where $\Delta n_{H,\downarrow}$ = moles of consumed gas for hydrate formation (mole)

$n_{H,t}$ = moles of hydrate at time t (mole)

$n_{H,0}$ = moles of hydrate at time 0 (mole)

P = pressure of the crystallizer (atm)

T = temperature of the crystallizer (K)

V = the volume of gas phase in the crystallizer (cm^3)

Z = compressibility factor

R = the universal gas constant $82.06 \text{ cm}^3 \cdot \text{atm} / \text{mol} \cdot \text{K}$

Subscripts of $G,0$ and G,t represent the gas phase at time zero and time t , respectively. The methane recovery was calculated by Equation 3.5 as a function of time for any dissociation experiment based on its information of formation experiment (Siangsai *et al.*, 2015).

$$\% \text{methane recovery} = \frac{(\Delta n_{H,\uparrow})}{(\Delta n_{H,\downarrow})_{\text{End}}} \times 100 \quad (3.5)$$

where $\Delta n_{H,\uparrow}$ = moles of released gas from hydrate during the hydrate dissociation at any given time (mole)

$n_{H,\downarrow}$ = moles of consumed gas for hydrate formation at the end of experiments (mole)

CHAPTER 4

RESULTS AND DISCUSSION

There are previous studies on methane hydrate formation at the Petroleum and Petrochemical College using an anionic surfactant, methyl ester sulfonate (MES), as a co-promoter with THF at a moderate condition, 20 °C and 8 MPa. The result showed that the increase in the hydrate formation rate with almost complete formation at 60 min, and the methane uptake was not significantly different to the solution with pure THF. Although most surfactants are toxic to the environment, some surfactants like MES are biodegradable and less toxic. However, due to the foam formation of surfactant, there is the lost of methane gas during the recovery. Thus, this work investigated the roles of stoichiometric THF and nonpolar amino acids (Reddy *et al.*, 2019) as a co-promoter on the kinetic and morphology of methane hydrate formation at high temperatures to reduce the foam formation and the cooling cost.

4.1 Effects of Single Promoters on Methane Hydrate Formation

4.1.1 Effects of 5.56 mol% THF

THF was reported as the best thermodynamic promoter with 5.56 mol% as the stoichiometric concentration, where all THF molecules are located in the large cage of THF-water hydrates (Beheshtimaal and Haghtalab, 2018; Lin *et al.*, 2018). First, methane hydrate formation was carried out in 5.56mol% THF solution at 20 °C and 8 MPa as the based case to understand its kinetics and morphology in the quiescent system.

4.1.1.1 *Kinetics*

For the kinetics, the experiments were studied inside the stainless steel reactor (Figure 3.2 (a)) with a 90 cm³ solution. Solution without THF (pure water) cannot form hydrates during 10 hours of the experiment at this condition as the experimental condition is in the sI region of the hydrate phase equilibrium (Figure 4.1). The methane hydrate formation driving force to form sII hydrate at this condition is 9 °C and 5.88 MPa temperature (Figure 4.1). With only THF, methane hydrates need at least an hour to start the first crystal nucleation (induction time) and

takes almost four hours to reach 90% of the methane uptake (t_{90}) due to the low normalized rate of hydrate formation for the first 30 min (NR_{30}) as seen in Table 4.1. However, the methane uptake achieved at the end of the experiment is 5.78 kmol of gas/ m^3 of water corresponding with Inkong *et al.* (2019a).

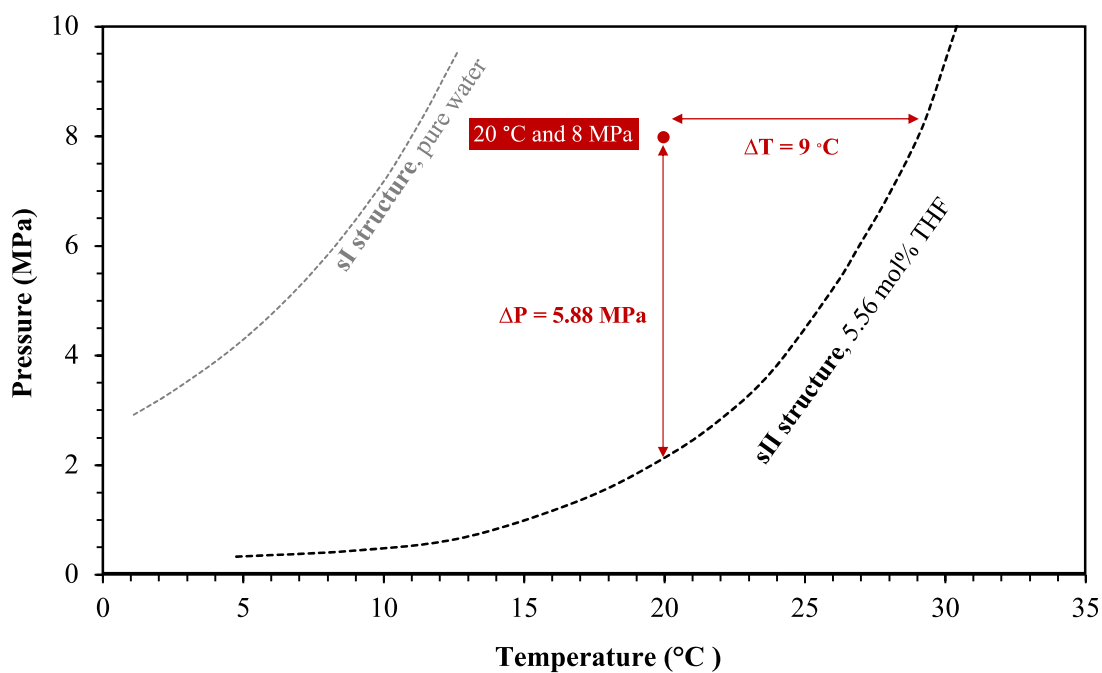


Figure 4.1 Temperature and pressure driving forces of the experiments at 20 °C and 8 MPa (Lee *et al.*, 2012; Nakamura *et al.*, 2003).

Table 4.1 Methane hydrate formation in the 5.56 mol% THF solution at 20 °C and 8 MPa

Experiment	Induction Time (min)	t_{90}^* (min)	Methane Uptake (kmol of gas/ m^3 of water)	NR_{30}^{**} (kmol/hr- m^3)
TH1	59.83	231.33	5.87	0.84
TH2	70.67	231.50	5.78	0.95
TH3	63.33	246.17	5.68	0.95

* t_{90} is the time to reach 90% methane uptake ; $t_{90} = t_i - t_{\text{induction time}}$

** NR_{30} is the normalized rate of hydrate formation 30 min after first nucleation.

Figure 4.2 shows methane uptake profiles during the hydrate growth of three experiments (TH1, TH2, and TH3). The deflection point of the multiple-step methane hydrate formation due to the rapid change of methane hydrate formation rate can be observed. They correspond with the temperature profiles of the hydrate formation, in which two distinct peaks for all trials are present, as shown in Figure 4.3. The temperature spikes in Figure 4.3 indicate the formation of methane hydrates, which is an exothermic reaction. These multiple temperature spikes imply the multiple steps of methane hydrate formation, as reported by Veluswamy *et al.* (2016b) and Inkong *et al.* (2019a). Moreover, the multiple-step methane hydrate formation is present in all three experiments.

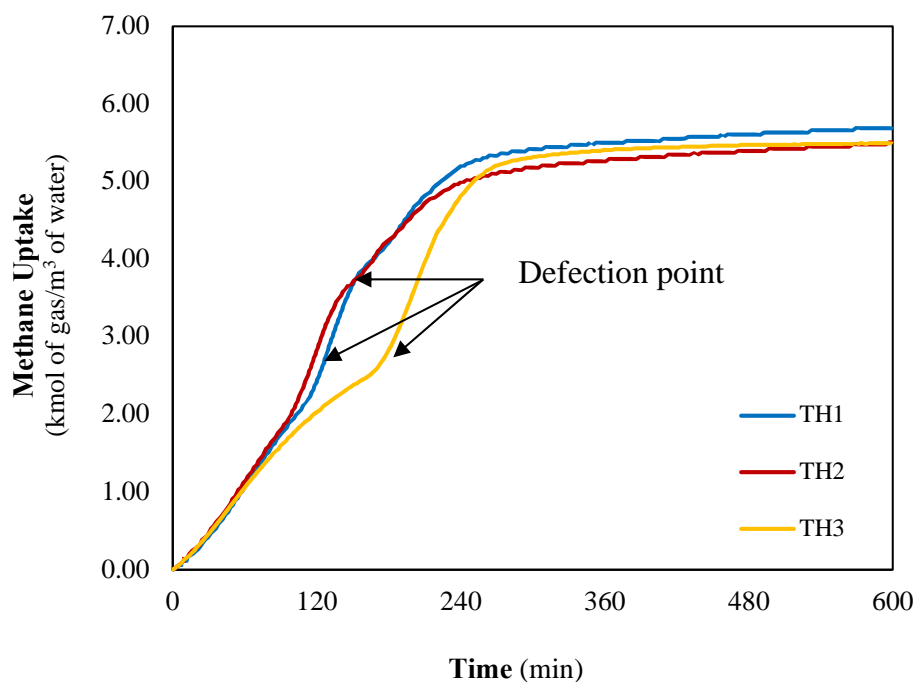


Figure 4.2 Methane uptake profiles from three separate methane hydrate formation experiments in 5.56 mol% THF solution at 20 °C and 8 MPa.

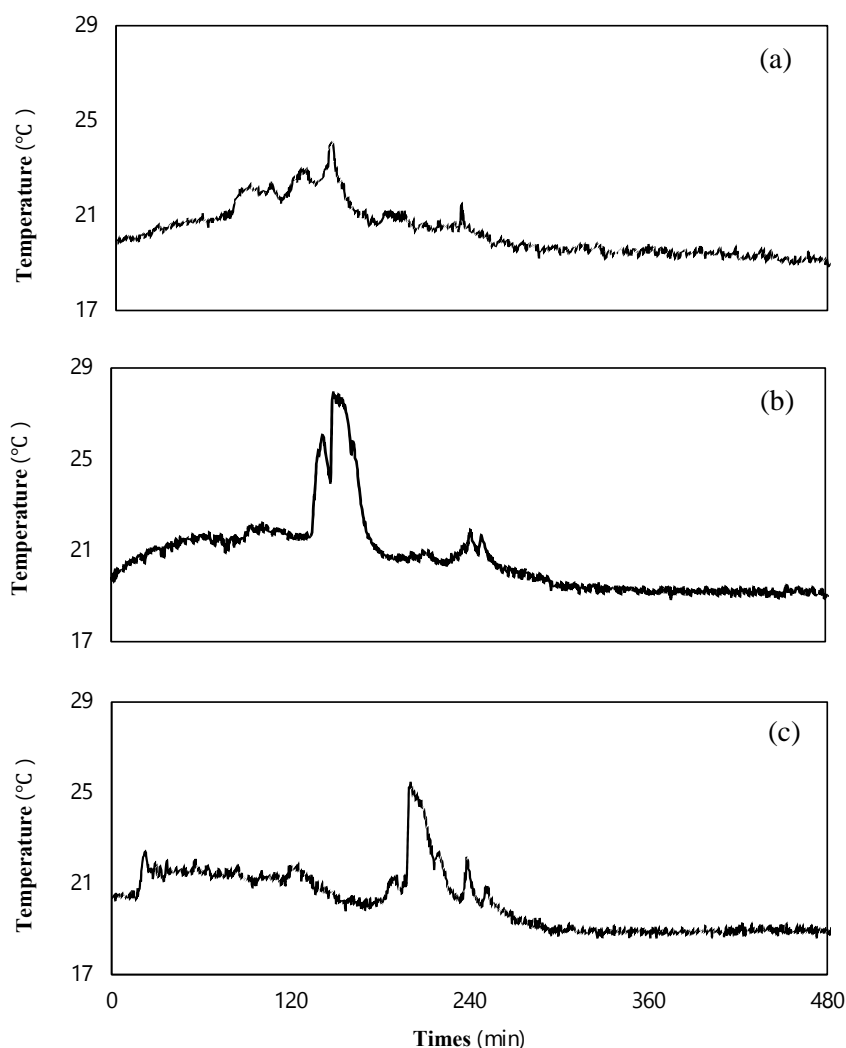


Figure 4.3 Temperature profile of three separate methane hydrate formation experiments of 5.56mol% THF at 20 °C and 8 MPa: (a) TH1, (b) TH2, (c) TH3.

4.1.1.2 Morphology

The morphology during methane hydrate formation was studied in the sapphire crystallizer, Figure 3.2 (b). Figure 4.4 shows morphology during the methane hydrate formation in 7 cm³ of 5.56 mol% THF at 20 °C and 8 MPa. The first nucleation takes place at the gas-liquid interface by forming small crystal of methane hydrates, as shown in Figure 4.4 (b). One minute after the first nucleation, methane hydrates grow in both direction (upward – gas phase, downward – bulk solution) and form a cabbage leaflike layer, Figure 4.4 (c1). The formation continues upwardly as

the leaflike layer stacks up, Figure 4.4 (d). At $t = 10$ min after the first nucleation, Figure 4.4 (g), the methane hydrates stop forming in the upward direction. After that, they continue downwardly, Figure 4.4 (g), until $t = 28$ min, when the methane hydrate formation stops. Methane hydrate nucleation behavior can be better observed in the reduced interfacial area by putting a small diameter vial inside the sapphire crystallizer, Figure S1 in Appendix B.

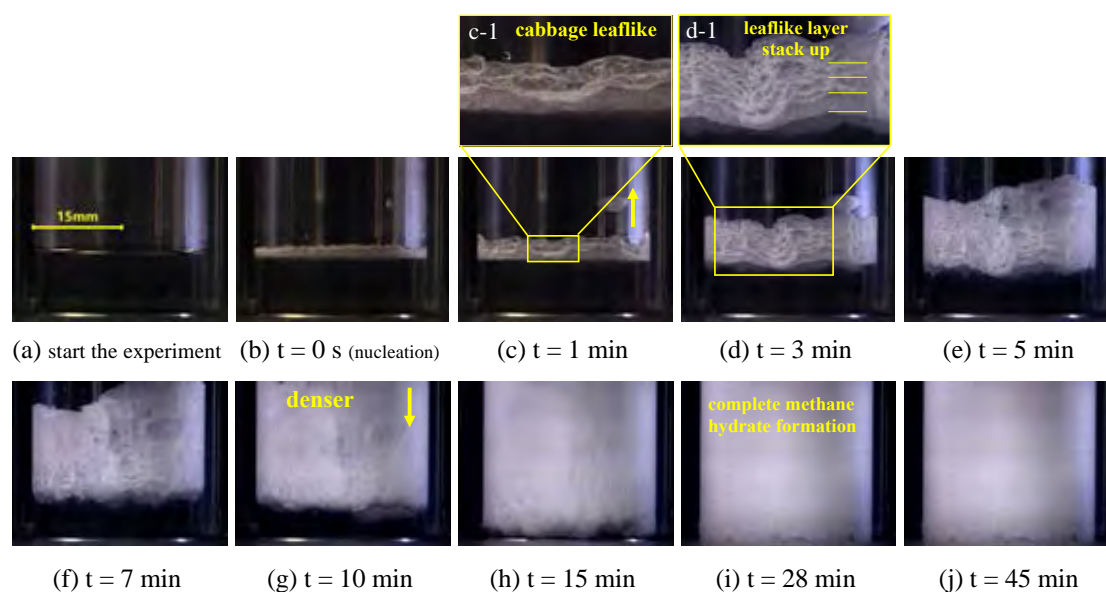


Figure 4.4 Morphology of methane hydrate formation in 5.56 mol% THF solution at 20 °C and 8 MPa.

4.1.2 Effects of Amino Acids

Due to the low rate of methane hydrate formation at 20 °C and 8 MPa, kinetic promoters have to be used. The key factor is to increase the gas dissolution into water (He *et al.*, 2017). As mentioned previously that surfactants have been used to decrease the interfacial tension; however, they shall be replaced because of their toxicity and the foam formation. Amino acids were then selected due to the hydrophobic tails and hydrophilic heads, which has similar structure to surfactants. They are also biodegradable and do not generate foam (Reddy *et al.*, 2019).

However, using an amino acid as a kinetic promoter, by itself, cannot promote methane hydrate formation at at 20 °C and 8 MPa as clearly seen in the phase equilibrium, Figure 4.5 (Bavoh *et al.*, 2018a; Veluswamy *et al.*, 2017a). Note that there are many experiments of amino acids on the sI methane hydrate formation showing that the decrease in the solution interfacial tension resulted in the increase in the hydrate formation rate (Bavoh *et al.*, 2018b; Liu *et al.*, 2015; Veluswamy *et al.*, 2016a).

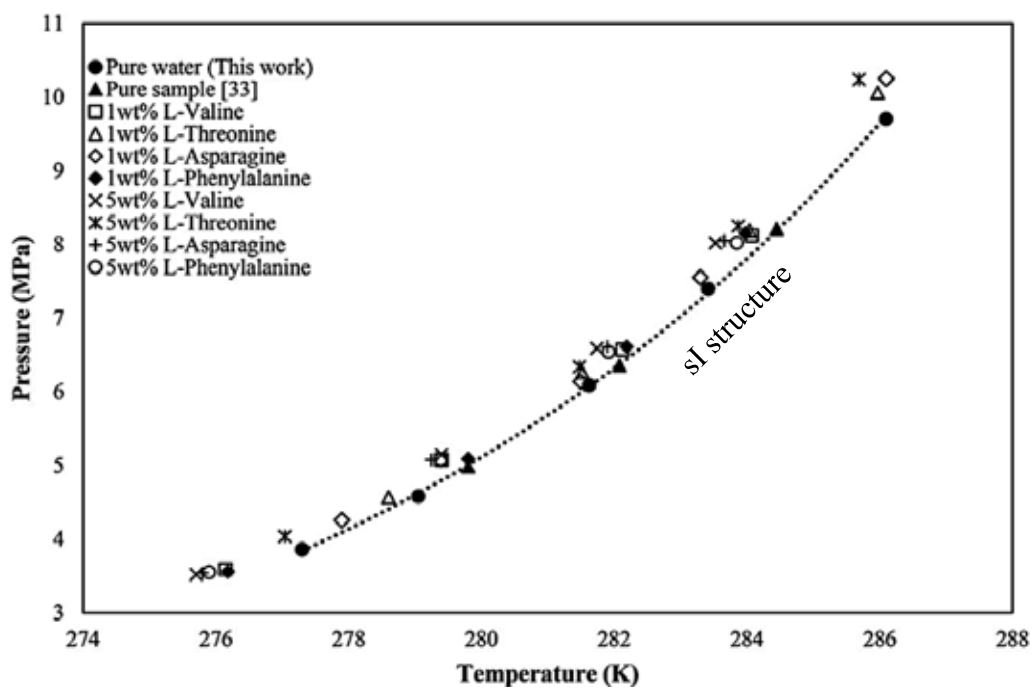


Figure 4.5 Methane hydrate phase equilibrium in the presence of amino acids at different concentrations (Bavoh *et al.*, 2018a).

4.2 Effects of THF and Amino Acids on Methane Hydrate Formation

It is known that THF shifts the methane hydrate formation to the sII region, which extends the hydrate phase equilibrium to a higher formation temperature. However, the induction time is longer, and the rate of methane hydrate formation is slower. The key to increase the formation kinetics is that enough gas must dissolve into water (He *et al.*, 2017). In this work, three different nonpolar amino acids were selected to increase methane solubility, including leucine, valine, and methionine, to co-promote with 5.56 mol% THF at 20 °C and 8 MPa in the quiescent system. These three nonpolar amino acids cover the short and long carbon chains in the molecule. Their different concentrations were also studied and selected from 0.125 wt% to 0.75 wt% to cover its critical micelle concentration (CMC), which shows on the interfacial tension diagram measured by KRUSS Easy Dyne Tensiometer at 20 °C, Figure 4.6. The CMCs leucine, valine, and methionine are 0.25 wt%, 0.75 wt%, and 0.375 wt%, respectively.

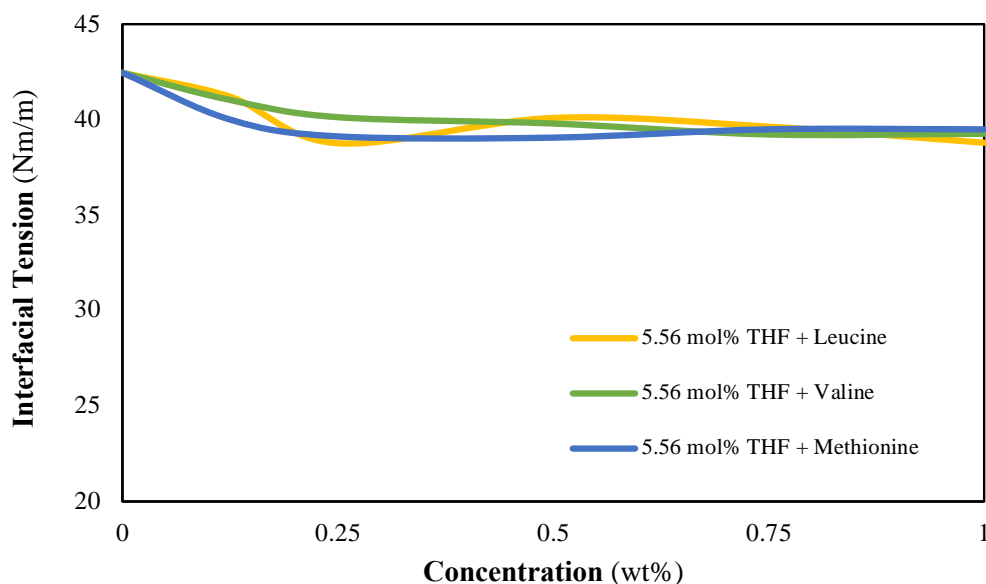


Figure 4.6 Effects of amino acid concentrations on the 5.56 mol% THF solution interfacial tension.

4.2.1 Kinetics

In this part, methane hydrate formation was carried out with 90 cm³ 5.56 mol% THF and amino acids solutions in the stainless-steel crystallizer at 20 °C and 8 MPa. Amino acids alone cannot form methane hydrates at this condition. However, with the amino acids and THF, methane hydrate formation takes place up to 5 times faster than the solution with only THF, as shown in Figure 4.7. Moreover, it seems that there is no significant difference from using different amino acids and different concentrations, which is clearly substantiated from the overlapped slopes of the methane hydrate growth in Figures 4.8 (a1), 4.8 (b1), and 4.8 (c1). Table 4.2 shows THF and all amino acids co-promoted results. In general, it can be noticed that the amino acids increase the rate of hydrate formation and decrease the induction time with almost one hour faster than the THF solution due to the lower solution interfacial tension. The increased formation rate decreases t_{90} resulting in the fast hydrate completion. In addition, the presence of amino acid also affects the methane uptake.

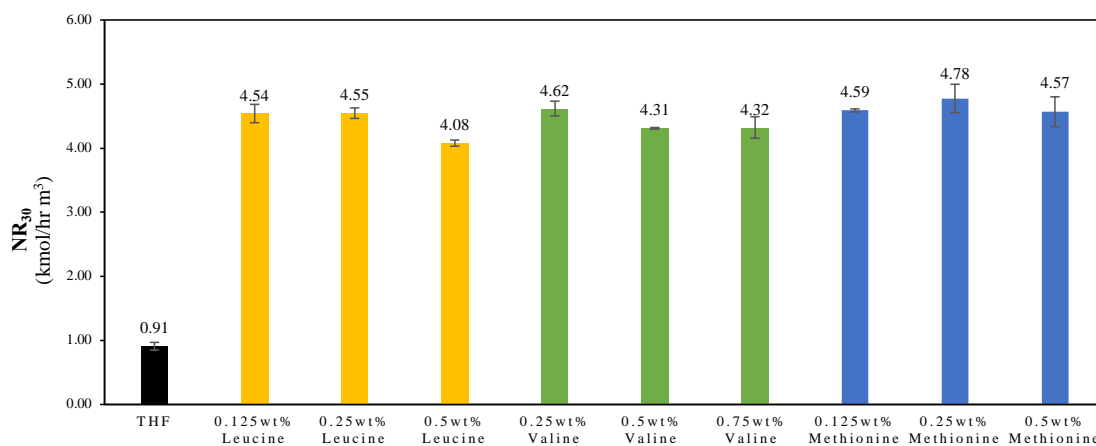


Figure 4.7 Normalized rate of methane hydrate formation (NR_{30}) in 5.56 mol% THF and amino acids at 20 °C and 8 MPa.

Different amino acids affect methane uptake differently. Figures 4.8 (a1), 4.8 (b1), and 4.8 (c1) show methane uptake profiles during the hydrate growth in the 5.56 mol% THF and amino acids, while Figures 4.8 (a2), 4.8 (b2), and 4.8 (c2) display the bar charts of the methane uptake. One distinct observation is the addition of any amino acid accelerates the hydrate formation rate. In addition, methane uptake

profiles of the system with the addition of leucine and methionine show defection points of multi-step hydrate formation. However, the system with valine does not show defection point on the methane uptake profile. The presence of multi-step formation results in the high methane uptake of the system with leucine and methionine as same as the one with only THF, Figures 4.8 (a2) and 4.8 (c2) but the present of valine results in the dramatically decreased methane uptake, Figure 4.8 (b2).

However, not only do different amino acids affect the methane uptake, but also, for leucine, its concentration plays an important role on the gas uptake. The effects of leucine concentrations on the methane uptake are shown in Figures 4.8 (a1) and 4.8 (a2). The increase in the leucine concentration from 0.125 wt% to 0.25 wt% does not affect the methane uptake of the hydrate formation. However, increasing leucine concentration to 0.5 wt%, which is higher than leucine CMC, the methane uptake dramatically decreases to 3.44 kmol of gas/ m³ of water. In addition, the formation does not show any multi-step hydrate formation. Moreover, this behavior can only be observed with the leucine solution, and it is totally different from surfactants, where the methane uptake increases with the increase in the concentration until the concentration reaches its CMC and remains stable (Chaturvedi *et al.*, 2018; Inkong *et al.*, 2019a).

Figure 4.8 (b) shows that the addition of valine decreases the methane uptake. That may be because the hydrates are too stable to be broken for further nucleation, which can be observed from the one-step hydrate formation. The result is as same as the system with 0.5 wt% leucine, Figure 4.8 (b1). Moreover, the change in the valine concentrations (0.25 wt% to 0.75 wt%) does not affect the methane uptake. The methane uptakes are almost the same, 3.88, 3.69, and 3.75 kmol of gas/ m³ of water, Figure 4.8 (b2).

The presence of methionine does not affect the methane uptake, and also shows no significant difference with the change in its concentration, Figures 4.8 (c1) and 4.8 (c2). However, in this case, regardless of methionine concentration, the same multi-step hydrate formation can be observed, and that results are approximately the same, as shown in Figure 4.8 (c2).

Table 4.2 Methane hydrate formation in THF and amino acids at 20 °C and 8 MPa

	Amino Acid (wt%)	Experiment	Induction Time (min)	t ₉₀ (min)	Methane Uptake (kmol of gas/m ³ of water)	NR ₃₀ (kmol/hr·m ³)
5.56 mol% THF	-	TH1	59.83	231.33	5.87	0.84
		TH2	70.67	231.5	5.78	0.95
		TH3	63.33	246.17	5.68	0.95
5.56 mol% THF + Leucine	0.125	L1	12.83	155.84	5.31	4.61
		L2	10.33	145.67	5.39	4.67
		L3	11.67	227.00	5.53	4.34
	0.25	L4	13.83	147.00	5.54	4.60
		L5	9.67	189.17	5.32	4.43
		L6	11.67	146.83	5.82	4.61
	0.5	L7	0.50	309.00	3.43	4.02
		L8	0.33	322.50	3.46	4.14
		L9	1.67	322.66	3.43	4.08
5.56 mol% THF + Valine	0.25	V1	2.83	214.84	3.84	4.73
		V2	1.50	206.33	3.86	4.66
		V3	1.83	154.67	3.61	4.46
	0.5	V4	0.00	159.17	3.52	4.31
		V5	0.67	131.83	3.62	4.30
		V6	0.17	129.33	3.61	4.33
	0.75	V7	14.83	318.34	3.64	4.32
		V8	15.67	257.33	3.50	4.09
		V9	18.67	274.50	3.79	4.56
5.56 mol% THF + Methionine	0.125	M1	3.83	158.84	5.61	4.56
		M2	4.83	138.00	5.68	4.61
		M3	6.83	172.00	5.60	4.61
	0.25	M4	1.50	97.67	5.71	5.07
		M5	1.00	217.16	5.29	4.54
		M6	1.33	108.00	5.78	4.71
	0.5	M7	0.33	114.50	5.63	4.63
		M8	0.17	116.00	5.70	4.41
		M9	0.67	109.83	5.73	4.67

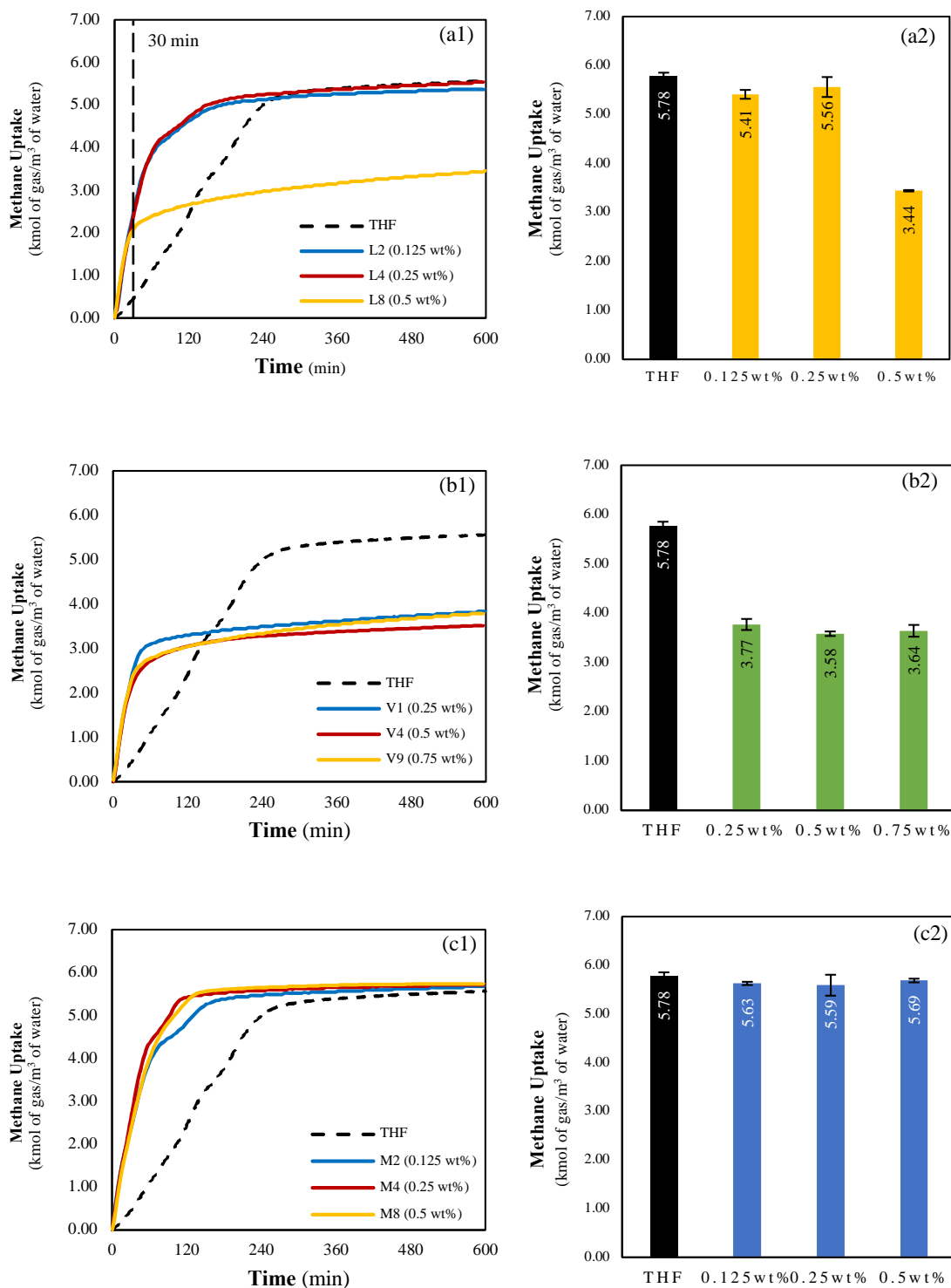


Figure 4.8 Effects of 5.56 mol% THF and 5.56 mol% THF with amino acids on the methane uptake and the normalized rate of methane hydrate formation (NR₃₀): (a) leucine solution, (b) valine solution, and (c) methionine solution at 20 °C and 8 MPa.

Although the presence of amino acids increases the NR_{30} of the methane hydrate formation with 5.56 mol% THF at 20 °C and 8 MPa (Figure 4.7). However, the three amino acids affect the methane hydrate formation at different extents and only leucine shows the concentration effect. Figure 4.9 shows the methane uptake profiles for the hydrate formation with the THF solution and the optimal co-promoter solutions. The figure shows the same multi-step hydrate formation with 5.56 mol% THF and 5.56 mol% THF with 0.25 wt% leucine and 0.125 wt% methionine. The same multi-step hydrate formation behavior can be observed with multiple temperature spikes (red circle) on the formation temperature profiles, Figures 4.10(a), 4.10(b), 4.10(c), and 4.10(d). Figure 4.11 summarizes difference methane hydrate formation behavior in THF and the optimal amino acid solutions at 20 °C and 8 MPa. Clearly, the presence of amino acids increases the NR_{30} significantly, but the amino acids with the specific concentration do not change the NR_{30} , Figure 4.11 (a). The amino acids also decreases the induction time by almost one hour compared to the system with only THF, Figure 4.11 (b). Comparison between the effects of amino acids and surfactant, Figures 4.12 (Inkong *et al.*, 2019a), shows that both increase the formation rate and decrease the induction time. However, in terms of methane uptake, valine does not have the positive effects like the other two amino acids, Figure 4.11 (c).

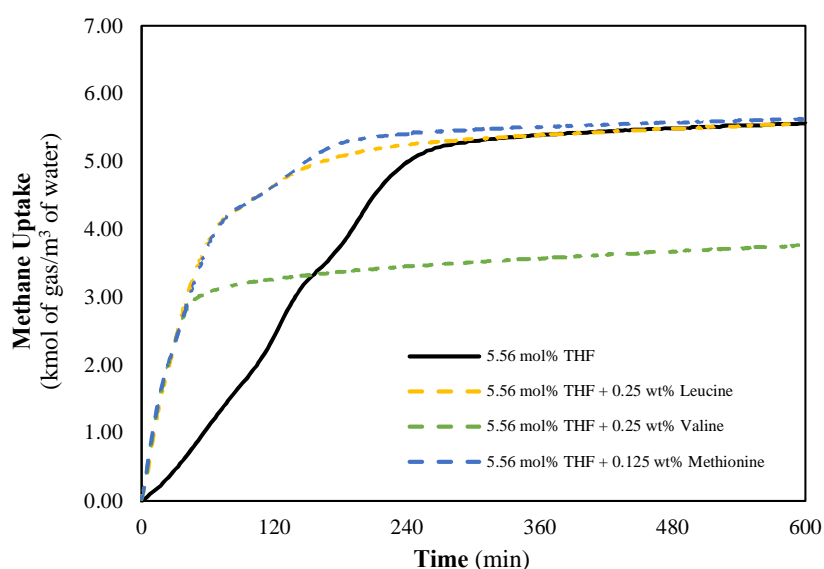


Figure 4.9 Methane uptake profiles from methane hydrate formation with 5.56 mol% THF and 5.56 mol% THF and amino acids at 20 °C and 8 MPa.

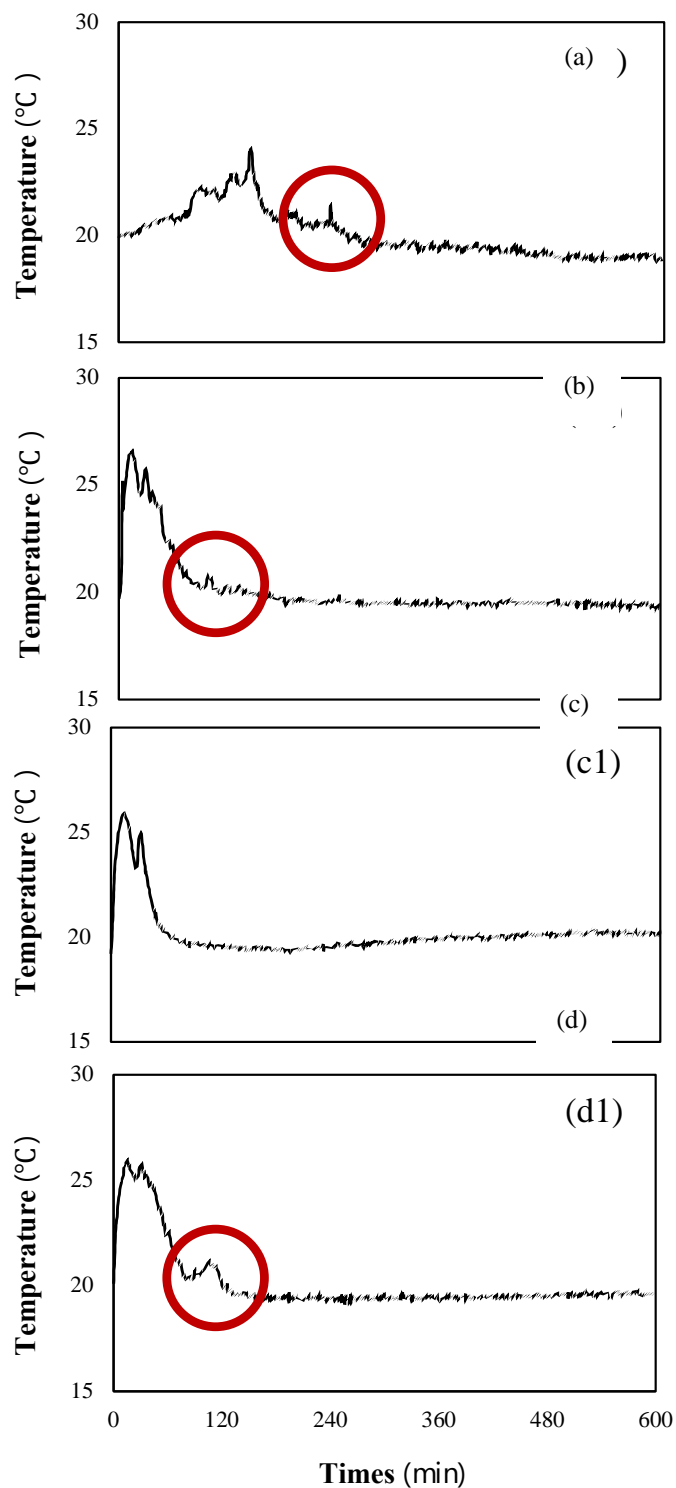


Figure 4.10 Temperature profiles during methane hydrate formation at 20 °C and 8 MPa with (a) 5.56 mol% THF and 5.56 mol% THF with amino acids: (b) 0.25 wt% leucine (c) 0.25 wt% valine (d) 0.125 wt% methionine.

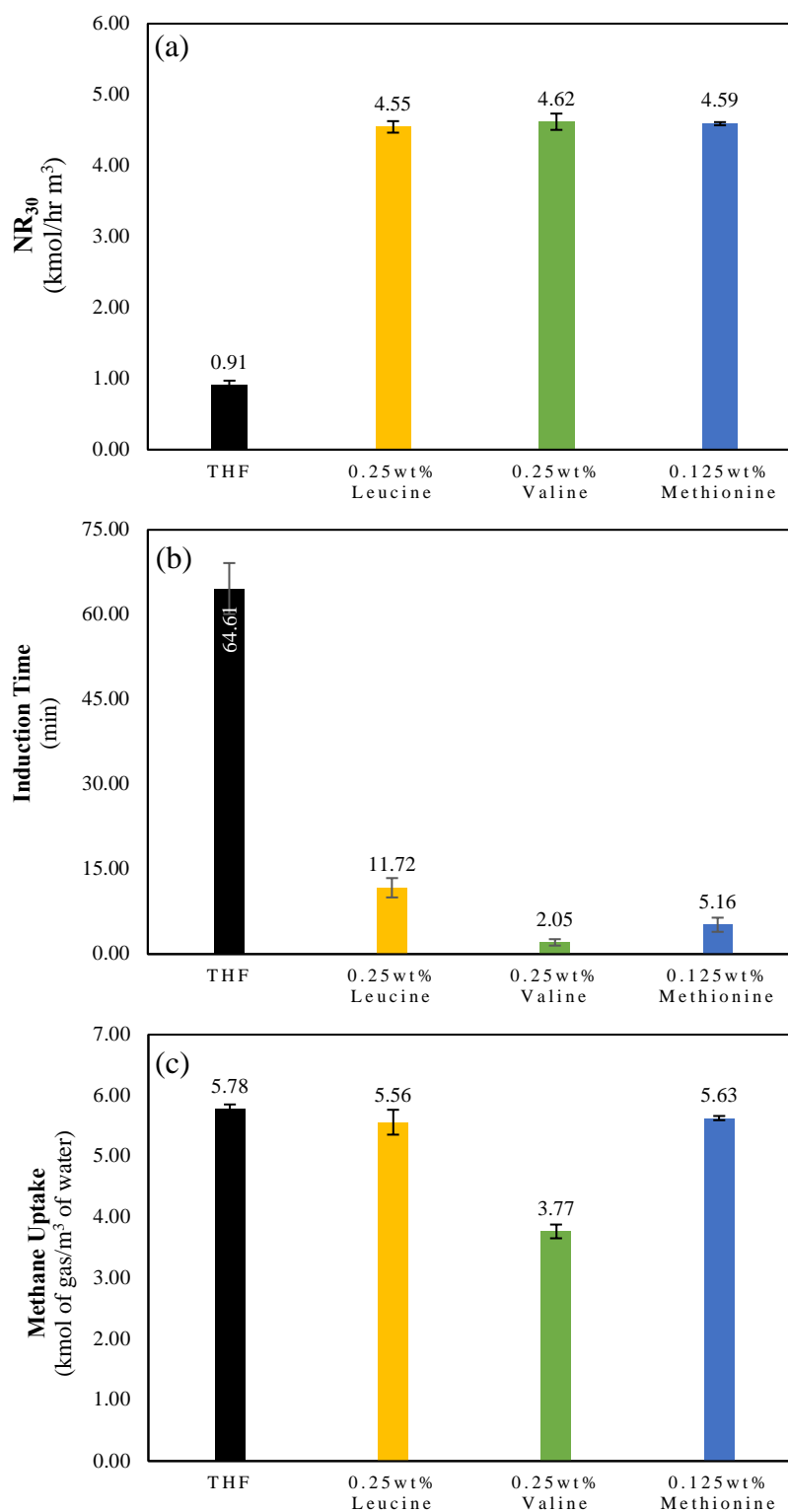


Figure 4.11 Comparison of (a) normalized formation rate (NR_{30}), (b) the induction time of methane hydrate formation, and (c) the methane uptake of THF and amino acids at 20 °C and 8 MPa.



411257468

CU iThesis 6173001063 thesis / rev: 25052563 12:18:23 / seq: 30

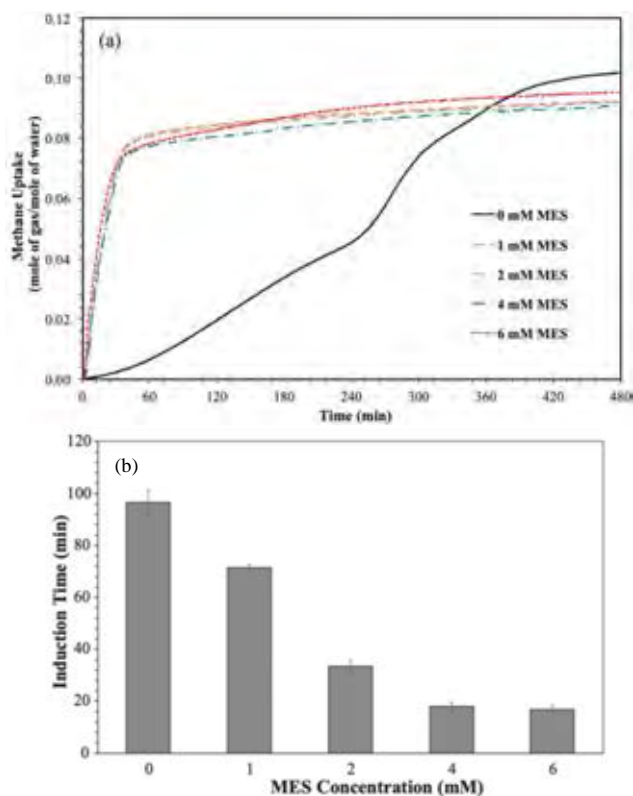


Figure 4.12 Methane uptake profiles (a) and induction times (b) from methane hydrate formation with 5.56 mol% THF and 5.56 mol% THF and methyl ester sulfonate (MES) at 20 °C and 8 MPa (Inkong *et al.*, 2019a).

The difference in amino acid structure may be the reason for their different behavior (Figure 4.13). Leucine and methionine have the same alkyl chain length with five carbon atoms, but methionine has one sulfur atom instead of a second carbon atom. Valine has a shorter alkyl chain length with only four carbon atoms. The structure difference was reported by Cai *et al.* (2017) through the carbon dioxide experiment. They reported that the leading cause of the kinetics enhancement of amino acid was the alkyl chain length. The optimum alkyl chain length that enhanced the carbon dioxide hydrate formation kinetics with the high methane uptake was reported to be leucine and methionine. They also reported that sulfur atom did not have any effect on the kinetics and gave the same result as one carbon atom. For the result of amino acids on methane hydrate formation, similar effects of amino acid are observed. To further understand the exact effects of amino acid structure on methane hydrate formations, effects of shorter and longer carbon chain lengths by using

alanine, glycine (shorter carbon chain), and 2-aminoheptanoic acid (longer carbon chain) should be studied. Moreover, effects of a sulfur atom inside the amino acid structure should be investigated by comparing with cysteine.

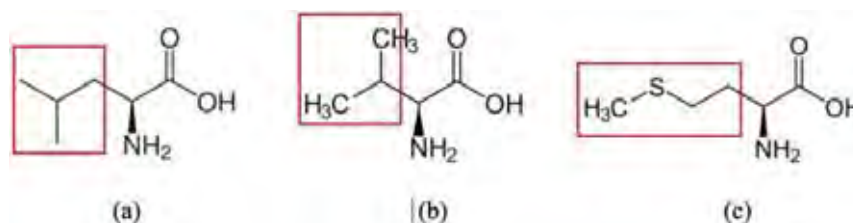


Figure 4.13 Structure of different amino acids (a) leucine, (b) valine, and (c) methionine.

4.2.2 Morphology

The morphology study was carried out in the sapphire crystallizer at the same condition as the kinetic study. Figure 4.14 shows the morphology of methane hydrates during the formation in 5.56 mol% THF and 5.56 mol% THF with 0.25 wt% leucine, 0.25 wt% valine, and 0.125 wt% methionine at 20 °C and 8 MPa. In the presence of only 5.56 mol% THF, the morphology during the hydrate formation indicates that the first nucleation takes place at the gas-liquid interface, Figure 4.14 (a2). After that, the hydrates grow into the gas phase and the bulk solution like a cabbage leaflike layer stacking up, Figures 4.14 (a3) and 4.14 (a4). The hydrate formation continues until $t = 28$ min, where the formation stops.

The morphology during the hydrate formation in 5.56 mol% THF and 0.25wt% leucine is in Figures 4.14 (b1) - 4.14 (b8). The hydrate growth starts at the gas-liquid interface similar to the case with 5.56 mol% THF solution, Figure 4.14 (b2). At $t = 1$ min after the first formation, the methane hydrates form a mushy-like hydrates in the bulk solution. This mushy hydrates contain many fine methane hydrate crystals clumping together, as shown in Figure 4.14 (b3). This figure also shows the curvature of hydrate growth pattern due to the change in the adhesion force between the solution and methane hydrate particles, which results from the lower interfacial tension of leucine solution (Lee *et al.*, 2014; Saito *et al.*, 2011). The hydrates continue to form in the downward direction until they touch the bottom of the reactor. They then start to form in the upward direction, as shown in Figure 4.14 (b4). At $t = 5$ min, the upward methane hydrates only form on the reactor wall, Figure 4.14 (b5),

until $t = 7$ min, when they reach the top of the column and move towards the center of the column, as observed by the dense hydrates, Figures 4.14 (b6) and 4.14 (b7). At 15 min after the first nucleation, the formation is complete, Figure 4.14 (b8).

Figures 4.14 (c1) - 4.14 (c8) show the hydrate formation morphology in the presence of 5.56 mol% THF and 0.25 wt% valine. The hydrate formation also starts at the gas-liquid interface, the same as leucine Figure 4.14 (c2). The hydrates then grow upward into the gas phase by forming on the reactor wall, Figure 4.14 (c3), until they reach the top of the crystallizer at 5 min after the first hydrate nucleation, Figure 4.14 (c4). After that, they turn to form into the bulk solution in the downward direction. During this downward formation, it shows the hydrate curvature growth pattern from the effect of adhesion force the same as leucine, Figures 4.14 (c5). Moreover, the hydrates are broken at $t = 8$ min, Figures 4.14 (c6). The hydrates then continue to form into the bulk solution, as shown by the thickness of the hydrates, Figure 4.14 (c7). The completion is at 12 min after the first hydrate nucleation.

The effects of 0.125wt% methionine are shown in Figures 4.14 (d1) - 4.14 (d8). Similar to the other promoters, the nucleation starts at the gas-liquid interface, Figure 4.14 (d2). Then, the hydrates grow in the upward and downward directions. However, they grow at a different rate. From $t = 0$ s in Figure 4.14 (d2) to $t = 1$ min in Figure 4.14 (d3) shows that the formation grows upwardly to the gas phase faster than in the downward direction until a certain point, where they change into the downward direction at $t = 2.5$ min, Figure 4.14 (d4). The upward methane hydrate formation is not only on the reactor wall similar to the other amino acids but also toward the center of the reactor. It can be noticed by the densified white formation in Figure 4.14 (d3). Methionine solution also shows hydrate curvature growth pattern same as the other amino acids, Figure 4.14 (d5). It also shows the hydrate broken as in the valine case, Figure 4.14 (d6). However, Veluswamy *et al.* (2016a) reported the hydrate bubble formation, which could be the case here except it is broken with the presence of THF and valine or methionine, not leucine. After that, the methane hydrates grow downwardly with a higher hydrate formation rate, Figures 4.14 (d4) - 4.14 (d7), until the formation completes in the downward direction at $t = 3.5$ min. Last, the formation takes place upwardly and completes at $t = 6$ min after the first hydrate nucleation, Figure 4.14 (d8).



411257468

CD IThesis 6173001063 thesis / rev: 25052563 12:18:23 / seq: 30

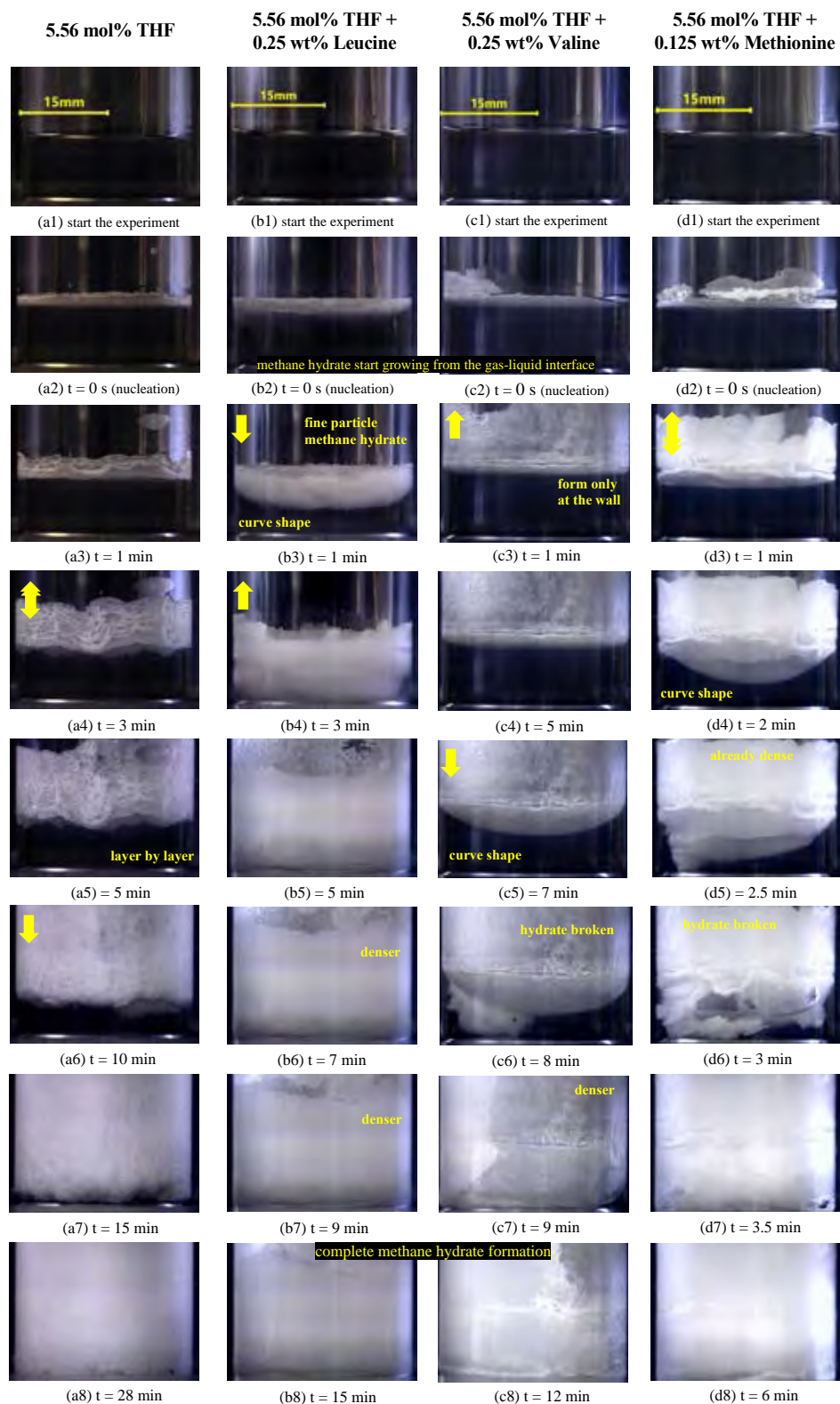


Figure 4.14 Morphology of methane hydrate formation in (a) 5.56 mol% THF and 5.56 mol% THF with amino acids: (b) 0.25wt% leucine, (c) 0.25wt% valine, and (d) 0.125wt% methionine at 20 °C and 8 MPa.

Comparison between the formation morphology of different solutions shows different hydrate growth patterns, as shown in Figure 4.14. They do not have the cabbage leaflike stack up of THF. However, some similarity can be seen in all solutions, hydrates start at the same area, which is at the gas-liquid interface, Figures 4.14 (a2), 4.14 (b2), 4.14 (c2), and 4.14 (d2). All amino acids also show the effects of surfactant-like behavior on the curvature hydrate growth pattern (Veluswamy *et al.*, 2016a). Morphology study could not confirm the multiple-step methane hydrate formation of THF, leucine, and methionine solution or even one-step hydrate formation of valine due to the hydrate growth along the sapphire wall. Nevertheless, these results can confirm the co-promoting ability of amino acids. They show the increase in the NR₃₀ during the hydrate formation. Figures 4.14 (a8), 4.14 (b8), 4.14 (c8), and 4.14 (d8) show the complete methane hydrate formation of THF solution at 28 min, followed by leucine at 15 min, valine at 12 min, and methionine at 6 min.

The hydrate formation pattern difference of THF solution and optimal co-promoter solutions can be seen clearer by adding a dye into the solutions (Figure S2 in Appendix B). It shows the renewal gas-liquid interface of amino acid mixed solutions due to the move up of dye solution along with the methane hydrate layer (Figure S2 insert I,II, and III in Appendix B). It can be deduced that the addition of amino acids results in the porous hydrate layer, which increases the capillary effect and the NR₃₀ (Okutani *et al.*, 2008; Veluswamy *et al.*, 2016a).



To confirm the similarity on the methane hydrate formation in both crystallizers, temperature and pressure during morphology study were recorded and calculated to compare with the results from the kinetic study. Tables 4.3 summarizes the data from the sapphire crystallizer during the morphology study. It shows the increased NR₃₀ due to the amino acids. Figure 4.15 compares the methane uptake between two different crystallizers. They seem to be no significant difference. It can imply that the size of the crystallizer does not have any effect on the methane uptake, which corresponds with the work by Khurana *et al.* (2019).

Table 4.3 Morphology study methane hydrate formation inside sapphire crystallizer at 20 °C and 8 MPa

	Amino Acid (wt%)	Experiment	Methane Uptake (kmol of gas/m ³ of water)	NR₃₀ (kmol/hr·m ³)
5.56 mol% THF	-	TH4	4.83	0.34
		TH5	5.66	0.33
		TH6	5.51	0.34
5.56 mol% THF + Leucine	0.25	L10	5.32	4.62
		L11	5.35	3.70
		L12	5.50	6.34
5.56 mol% THF + Valine	0.25	V10	2.01	7.01
		V11	4.32	5.73
		V12	2.50	7.21
5.56 mol% THF + Methionine	0.125	M10	4.81	7.67
		M11	4.86	7.04
		M12	4.81	7.00

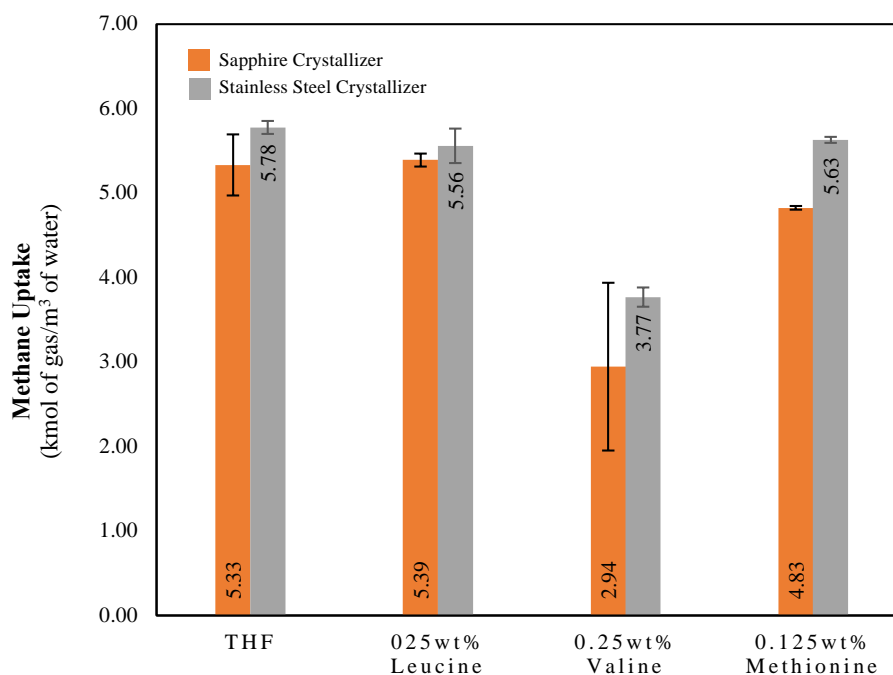


Figure 4.15 Comparison of methane uptakes from methane hydrate formation in the sapphire crystallizer (morphology study) and the stainless-steel crystallizer (kinetic study) at 20 °C and 8 MPa.

4.2.3 Methane Hydrate Dissociation

Gas recovery is another critical factor used to confirm the performance of methane hydrate technology and to ensure that no gas loss during methane hydrate formation. The hydrate dissociation was studied in every experiment after the hydrate formation by increasing the system temperature to 35 °C with the same heating rate as applied in the hydrate formation until there was no significant change in the pressure.

Methane release after the hydrates formed in the 5.56 mol% THF solution and the 5.56 mol% THF with amino acids solutions is shown in Table 4.4. The presence of only 5.56 mol% THF in the formation results in almost 96% methane recovery after the dissociation. Also the hydrates formed in certain leucine concentrations (0.125 and 0.25 wt%) and all methionine concentrations have higher than 95% methane recovery. In addition, the formation in 0.5 wt% leucine and all valine concentrations with the lower gas uptake also results in higher than 95%. The presence of amino acids with different formation behaviors does not affect the hydrate dissociation, and they all show higher than 95% methane recovery.

Morover, the hydrate dissociation morphology study of the hydrate formation in the 5.56 mol% THF solution and the 5.56 mol% THF with amino acids solutions is in Figure 4.16. This figure shows morphology since the start of the hydrate formation until the complete dissociation. This visual images show the same solution level between the start of the formation and the end of dissociation. It shows no foam formation from the use of amino acids in the solution contrary to the results with surfactants (Inkong *et al.*, 2019b; Veluswamy *et al.*, 2016a).

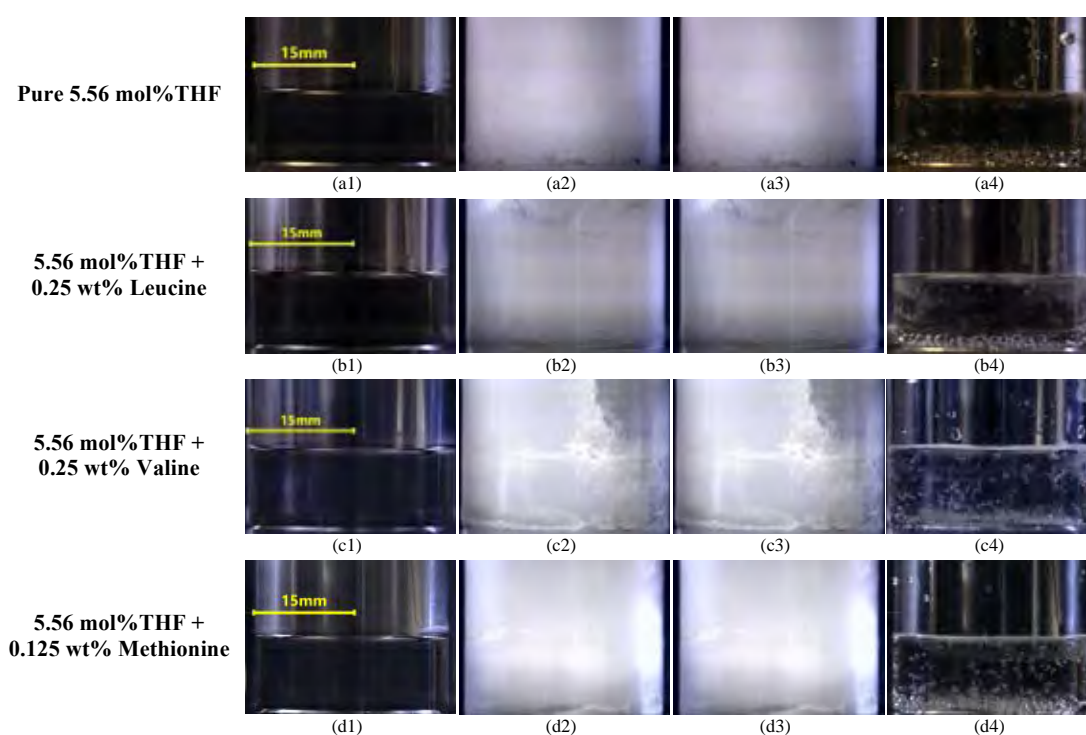


Figure 4.16 Morphology study of methane hydrate dissociation from hydrates formed in different solutions (a) 5.56 mol% THF and 5.56 mol% THF with amino acids: (b) 0.25wt% leucine, (c) 0.25wt% valine, and (d) 0.125wt% methionine monitoring from (1) the start of hydrate formation, (2) the complete of hydrate formation, (3) the start of hydrate dissociation, and (4) the complete of hydrate dissociation.

Table 4.4 Comparison of the methane consumed, the methane release, and the methane recovery from the methane hydrate formation with 5.56 mol% THF and 5.56 mol% THF with amino acids at 20 °C and 8 MPa.

	Amino Acid (wt%)	Experiment	Methane Consumed (mol)	Methane Released (mol)	% Recovery
5.56 mol% THF		TH1	0.427	0.409	95.91
		TH2	0.424	0.407	96.06
		TH3	0.406	0.392	96.50
5.56 mol% THF + Leucine	0.125	L1	0.388	0.375	96.45
		L2	0.399	0.388	97.22
		L3	0.412	0.391	95.02
	0.25	L4	0.409	0.392	95.86
		L5	0.395	0.378	95.52
		L6	0.425	0.409	96.35
	0.5	L7	0.265	0.253	95.39
		L8	0.261	0.248	95.21
		L9	0.261	0.249	95.41
5.56 mol% THF + Valine	0.25	V1	0.290	0.278	95.72
		V2	0.292	0.283	97.05
		V3	0.264	0.252	95.75
	0.5	V4	0.265	0.252	95.21
		V5	0.260	0.248	95.46
		V6	0.267	0.257	95.96
	0.75	V7	0.280	0.272	97.35
		V8	0.270	0.259	96.03
		V9	0.286	0.272	95.04
5.56 mol% THF + Methionine	0.125	M1	0.412	0.396	96.19
		M2	0.413	0.402	97.34
		M3	0.411	0.392	95.31
	0.25	M4	0.410	0.398	97.22
		M5	0.389	0.370	95.19
		M6	0.418	0.408	97.66
	0.5	M7	0.402	0.390	96.84
		M8	0.408	0.388	95.24
		M9	0.411	0.394	95.93

4.3 Enhanced Methane Hydrate Formation at 25 °C with THF and Amino Acids

Methane hydrate formation requires certain amounts of energy to reduce the temperature down to the point, where the nucleation takes place. The formation temperature close to ambient condition is then preferred. This part shows how the formation can be handled so that it can occur at 25 °C with the 5.56 mol% THF and 5.56 mol% THF with amino acids (0.25wt% leucine, 0.25wt% valine, and 0.125wt% methionine).

4.3.1 Methane Hydrate Formation in the Unstirred Reactor Configuration

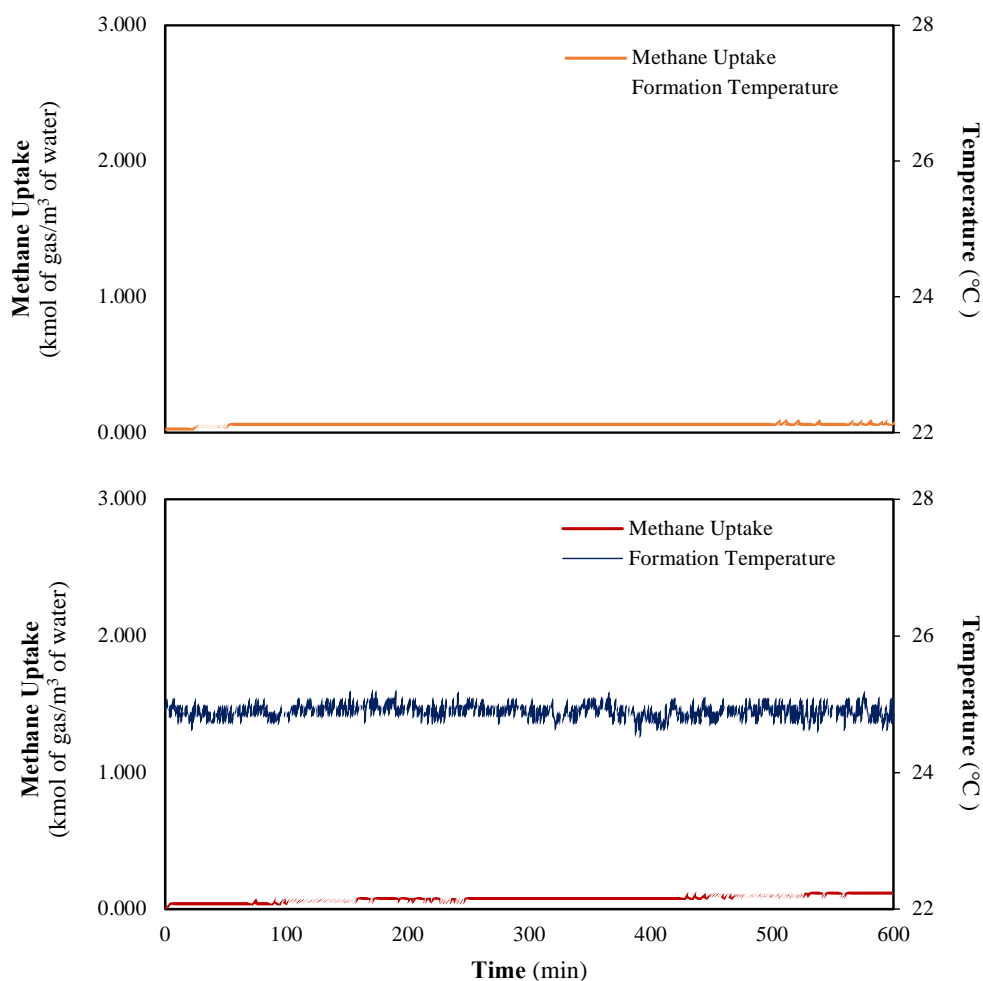


Figure 4.17 Methane uptakes and temperature profiles of (a) 5.56 mol% THF and (b) 5.56 mol% THF and 0.25wt% leucine at 25 °C and 8 MPa.

The experiment was carried out in the quiescent condition to maintain low energy requirement. Figure 4.17 shows the minimal methane uptake and the stable formation temperature in 5.56 mol% THF, and 5.56 mol% THF and 0.25wt% leucine. Table 4.5 summarizes the hydrate formation in the quiescent condition at 25 °C and 8 MPa. The results indicate that there is no hydrate formation during 10 hours of the experiment, which can be described by the decrease in the hydrate formation driving force, which directly affects the hydrate formation. During the hydrate formation at 20 °C and 8 MPa, the temperature and pressure driving forces are $\Delta 9\text{ }^{\circ}\text{C}$ and $\Delta 5.88\text{ MPa}$, respectively, and decreased to $\Delta 4.5\text{ }^{\circ}\text{C}$ and $\Delta 3.5\text{ MPa}$ at 25 °C and 8 MPa, as shown in Figures 4.18 (a) and 4.18 (b). The decrease in the pressure and temperature driving forces results in the dramatic decrease in the gas solubility (Lekvam and Bishnoi, 1997). He *et al.* (2017) reported that enough gas dissolved in water is the main factor of gas hydrate nucleation (form hydrogen bond), which directly influences the increase in the hydrate formation induction time and the decrease in the hydrate formation rate (Inkong *et al.*, 2019a).

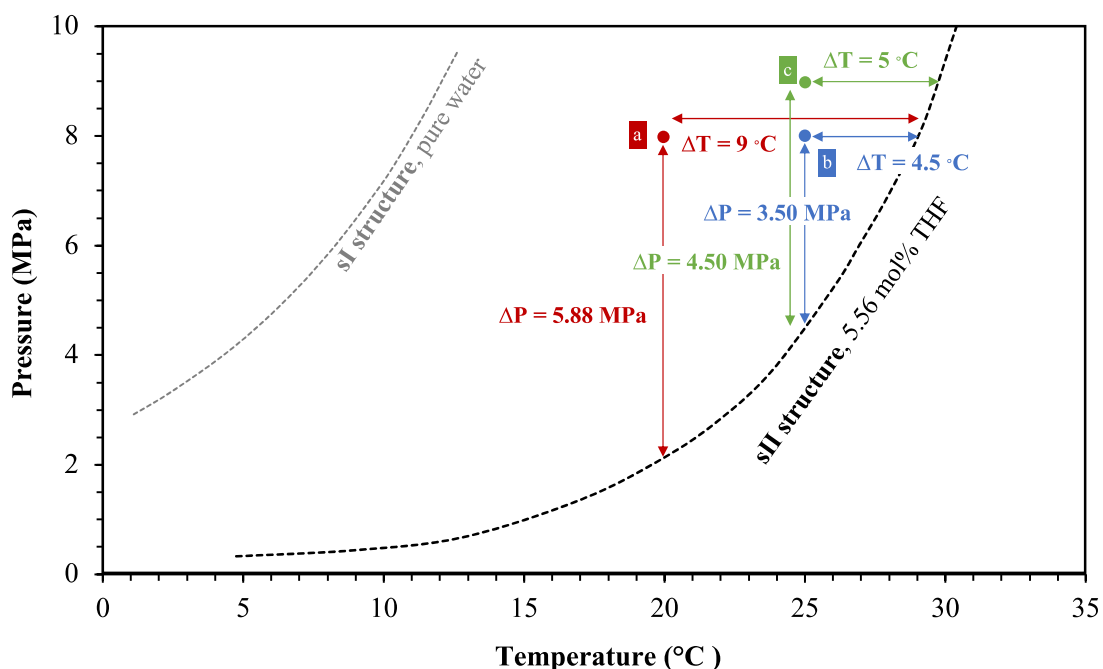


Figure 4.18 Temperature and pressure driving forces of methane hydrate formation at (a) 20 °C 8 MPa, (b) 25 °C 8 MPa and (c) 25 °C 9 MPa (Lee *et al.*, 2012; Nakamura *et al.*, 2003).

Table 4.5 Methane hydrate formation at 25 °C and 8 MPa in the unstirred reactor configuration

	Experiment	Induction Time (min)	Methane Uptake (kmol of gas/m ³ of water)	NR₃₀ (kmol/hr·m ³)
5.56 mol% THF	TH7	a	0.22	a
	TH8	a	0.06	a
5.56 mol% THF + 0.25 wt% Leucine	L13	a	0.12	a
	L14	a	0.10	a
5.56 mol% THF + 0.25 wt% Valine	V13	a	0.03	a
	V14	a	0.07	a
5.56 mol% THF + 0.125 wt% Methionine	M13	a	0.09	a
	M14	a	0.05	a

a = no methane hydrates formed during 10 hours of the experiment

The formation pressure was then increased from 8 MPa to 9 MPa. The pressure and temperature driving forces are then $\Delta 4.5$ MPa and $\Delta 5$ °C, Figure 4.18 (c). However, the increase in the pressure is not enough and the methane hydrates still could not form during 10 hours of the experiment, as shown in Table 4.6.

Table 4.6 Methane hydrate formation at 25 °C and 9 MPa in the unstirred reactor configuration

Amino Acid	Experiment	Induction Time (min)	Methane Uptake (kmol of gas/m ³ of water)	NR₃₀ (kmol/hr·m ³)
5.56 mol% THF	TH9	a	0.11	a
	TH10	a	0.08	a
5.56 mol% THF + 0.25 wt% Leucine	L15	a	0.13	a
	L16	a	0.17	a
5.56 mol% THF + 0.25 wt% Valine	V15	a	0.09	a
	V16	a	0.02	a
5.56 mol% THF + 0.125 wt% Methionine	M15	a	0.08	a
	M16	a	0.06	a

a = no methane hydrates formed during 10 hours of the experiment

4.3.2 Methane Hydrate Formation in the Hybrid Reactor Configuration

The stirred system is another solution to increase the methane hydrate formation possibility, which induces the formation by increasing the gas solubility into the solution, as described by Veluswamy *et al.* (2017a). However, Veluswamy *et al.* (2017a) also reported the decrease in the methane uptake due to the stirred system. In the end, they concluded that the hybrid reactor configuration, which stirred the system for 10 – 30 second after pressurizing the gas, resulted in the high rate of hydrate formation of the stirred system and the high methane uptake of the unstirred reactor configuration.

Hybrid reactor configuration was then selected to enhance the methane hydrate formation in 5.56 mol% THF and 5.56 mol% THF with amino acids at 25 °C and 9 MPa. However, using the hybrid reactor configuration with stirring for 10 – 30 second does not enhance the methane hydrate formation. So, stirring time was increased until the first temperature spike in the temperature profile was observed.

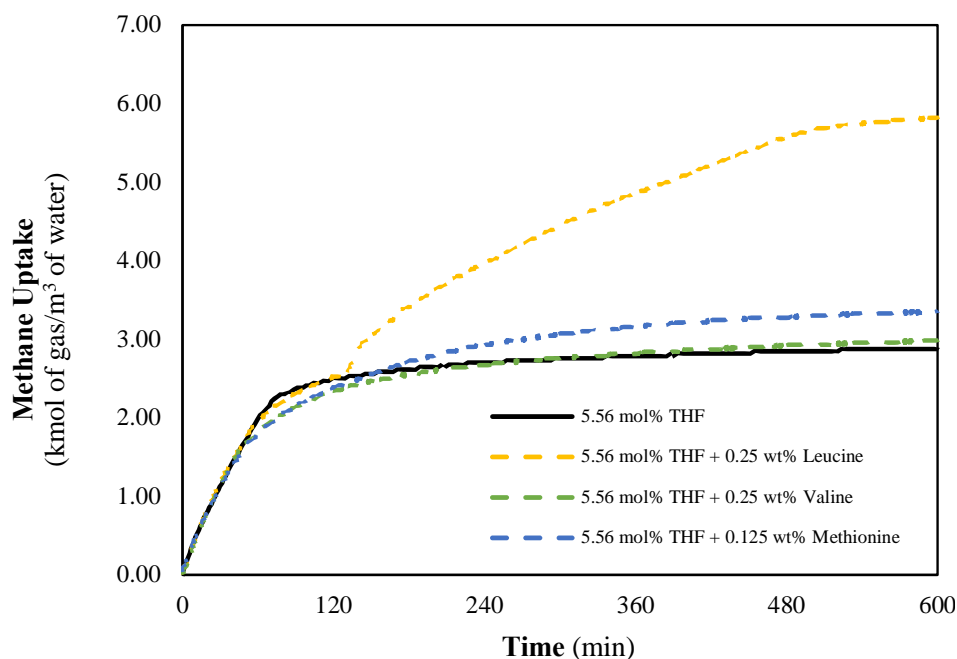


Figure 4.19 Methane uptake profiles from the formation in 5.56 mol% THF and 5.56 mol% THF with amino acids at 25 °C and 9 MPa in the hybrid reactor configuration.

The experiments started with the hydrate formation at 25 °C and 8 MPa with the hybrid reactor configuration; however, the hybrid configuration and the driving force at this condition are not enough for methane hydrate formation. The formation pressure was then increased from 8 MPa to 9 MPa. Figure 4.19 shows the missing multiple-step methane hydrate formation of only 5.56 mol% THF, and 5.56 mol% THF with 0.125 wt% methionine solution in the hydrate formation at 25 °C and 9 MPa in the hybrid reactor configuration. That results in lower the methane uptake than the formation at 20 °C and 8 MPa. It appears to that only the formation in 0.25 wt% leucine solution shows the deflection point on the methane uptake profile and results in the highest methane uptake. This can be confirmed by the comparison between the hydrate formation temperature profile at 25 °C 9 MPa in the hybrid reactor configuration and that at 20 °C 8 and MPa in the unstirred reactor configuration in Figure 4.20. The figure shows the missing multiple-step temperature spikes on the profile from the formation in 5.56 mol% THF and 5.56 mol% THF with 0.125 wt% methionine.

Table 4.7 Methane hydrate formation in 5.56 mol% THF and 5.56 mol% THF with amino acids at 25 °C and 9 MPa in the hybrid reactor configuration.

Amino Acid	Experiment	Induction Time (min)	t_{90} (min)	Methane Uptake (kmol of gas/m ³ of water)	NR ₃₀ (kmol/hr-m ³)
5.56 mol% THF	TH11	14.36	152.00	2.78	2.20
	TH12	30.00	172.83	3.07	2.27
	TH13	10.30	169.17	2.87	2.27
5.56 mol% THF + 0.25 wt% Leucine	L17	5.32	460.50	5.44	2.21
	L18	10.56	461.33	5.18	2.21
	L19	46.00	422.33	5.82	2.33
5.56 mol% THF + 0.25 wt% Valine	V17	18.54	248.00	2.99	2.27
	V18	21.28	273.50	2.78	2.09
	V19	15.27	273.84	2.99	2.27
5.56 mol% THF + 0.125 wt% Methionine	M17	19.15	239.00	3.47	2.33
	M18	25.57	284.66	3.36	2.15
	M19	15.33	205.17	3.50	2.27

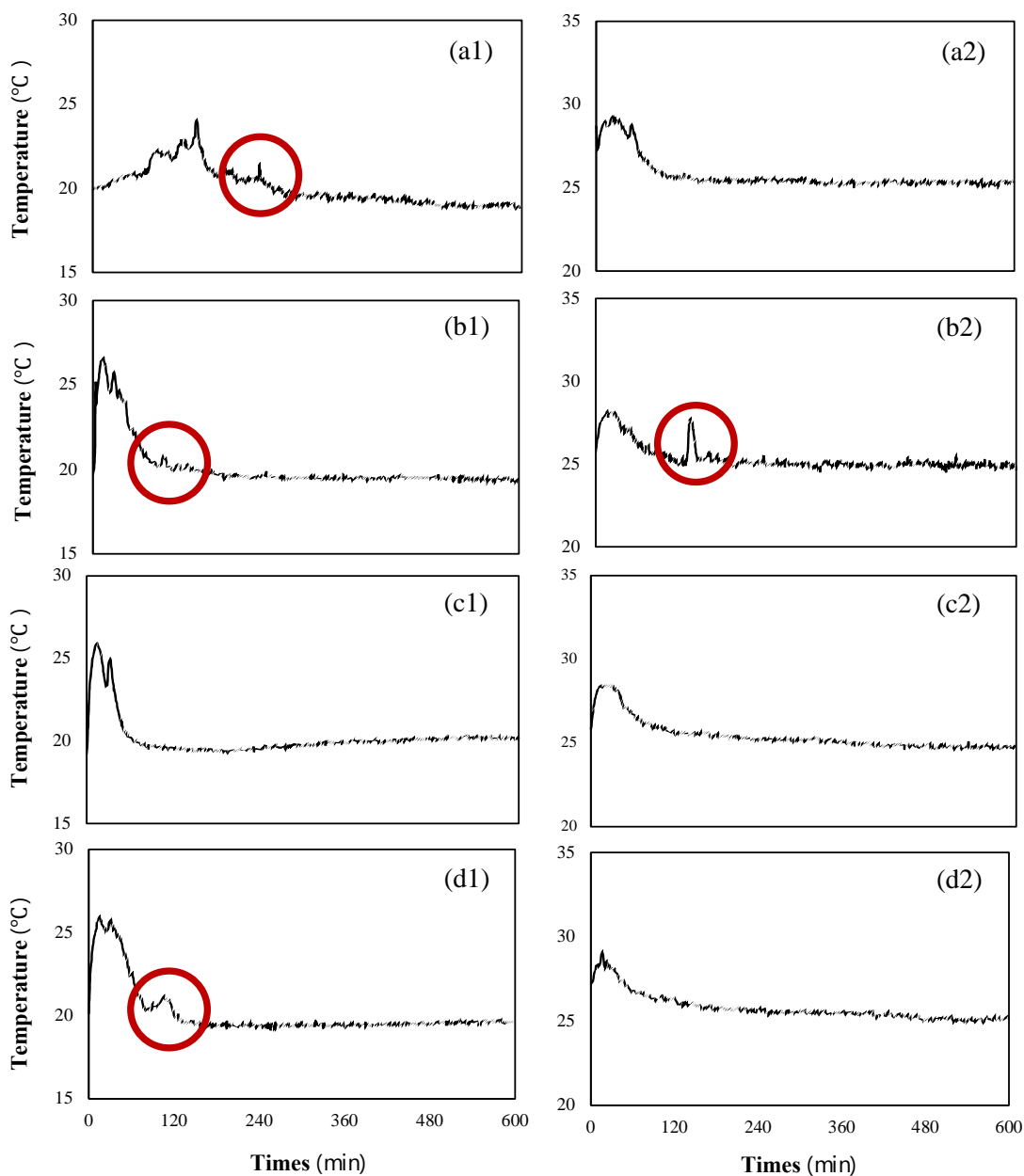


Figure 4.20 Comparison of methane hydrate formation temperature profiles in different solutions (a) 5.56 mol% THF and 5.56 mol% THF with amino acids (b) 0.25wt% leucine (c) 0.25wt% valine (d) 0.125wt% methionine at different hydrate formation conditions (1) 20 °C and 8 MPa in the unstirred reactor configuration, and (2) 25 °C and 9 MPa in the hybrid reactor configuration.

Table 4.7 shows the summary of the experimental data for all experiments conducted with 5.56 mol% THF and 5.56 mol% THF with amino acids at 25 °C and 9 MPa in the hybrid reactor configuration, including the induction time, t_{90} , NR_{30} , and the total methane uptake achieved at the end of the experiment. The NR_{30} at 25 °C and 9 MPa, with or without the amino acids is the same (2.25 kmol/hr·m³). In addition, the NR_{30} remains unchanged regardless of different amino acids in the hybrid reactor, Figure 4.21. This figure also shows the effect of the hydrate formation at 25 °C and 9 MPa in the hybrid reactor configuration (pink) on the NR_{30} . The hydrate formation in 5.56 mol% THF with amino acids at 25 °C and 9 MPa is lower than that in 20 °C and 8 MPa (gray). However, the NR_{30} in 5.56 mol% THF solution has the opposite trend, i.e. the NR_{30} is almost double. This reiterates that the effects of the hybrid reactor configuration are more pronounced than the amino acids on the hydrate formation kinetics at the low hydrate formation driving force.

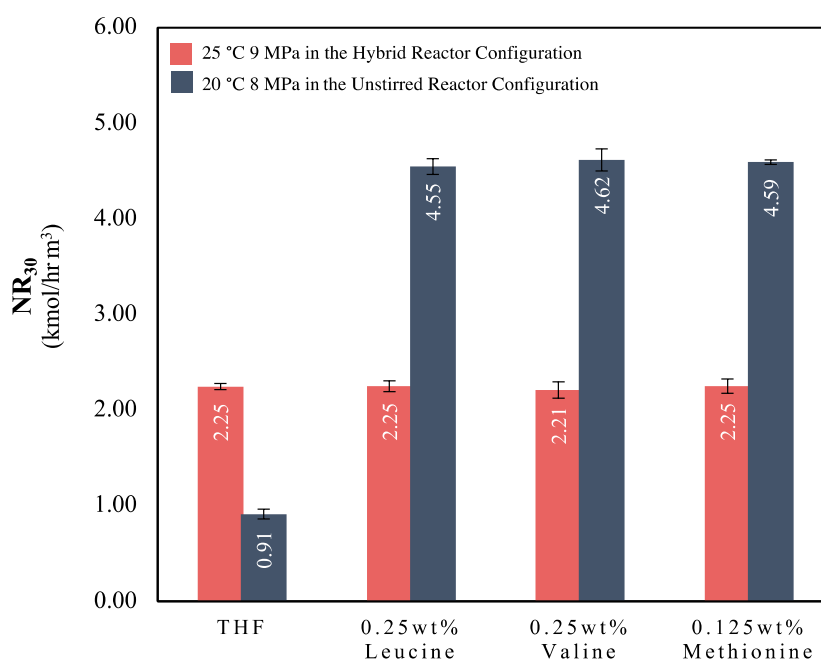


Figure 4.21 Comparison of normalized hydrate formation rate (NR_{30}) between different formation conditions, (pink) at 25 °C and 9 MPa and (gray) at 20 °C and 8 MPa.

The methane uptake from the hydrate formation at 25 °C and 9 MPa in the hybrid reactor configuration, 5.56 mol% THF with 0.25 wt% leucine, reaches the highest methane (5.48 kmol of gas/ m³ of water) followed by with 0.125 wt% methionine (3.44 kmol of gas/ m³ of water), and 0.25 wt% valine and only 5.56 mol% THF with the same methane uptake (2.91 kmol of gas/ m³ of water), Figure 4.22. Comparing the results with the formation at 20 °C and 8 MPa (gray) shows that the methane uptake in 5.56 mol% THF or 5.56 mol% THF with 0.125 wt% methionine is lower with the increase in the formation temperature and pressure (25 °C and 9 MPa) and a small methane uptake decrease in the 0.25 wt% valine solution. Only 0.25 wt% leucine maintains the methane uptake as that at 20 °C and 8 MPa

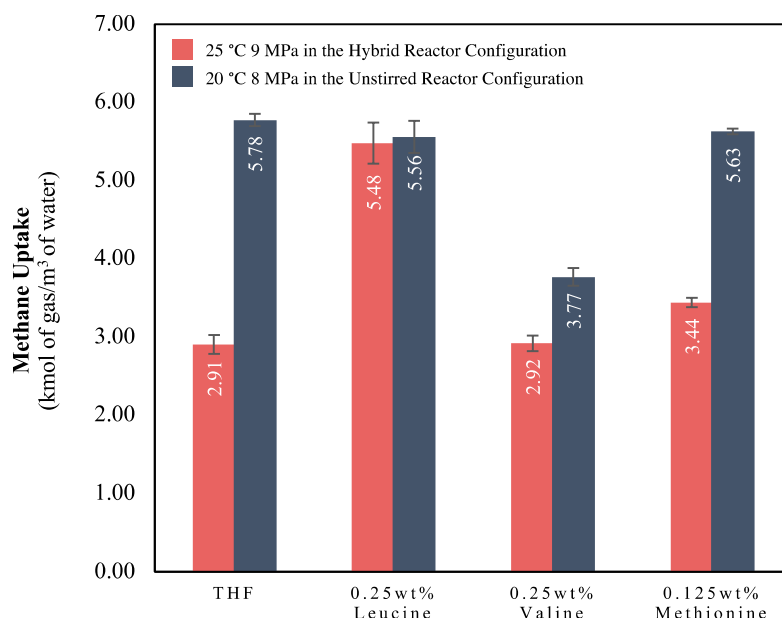


Figure 4.22 Comparison methane uptake between different formation conditions, (pink) at 25 °C and 9 MPa and (gray) at 20 °C and 8 MPa.

The decrease in the methane uptake in the 5.56 mol% THF solution corresponds to the lowering gas dissolved into the solution at the lower formation driving force (Lekvam and Bishnoi, 1997). Moreover, the decrease in the methane uptake in the 0.125 wt% methionine solution and the high methane uptake in the 0.25 wt% leucine solution may be, in part, due to the effects of amino acid concentration that has to reach a certain extent before the amino acid could show any appreciable effects. To ensure this hypothesis, 0.25 wt% and 0.5 wt% methionine was studied.

Figure 4.23 shows the NR_{30} and the methane uptake in 5.56 mol% THF with methionine. The methionine concentration has little effects on the NR_{30} . The effects on the NR_{30} are clearly due to the hybrid reactor configuration than the amino acids on the increased formation rate. However, the concentration affects the methane uptake from the hydrate formation at 25 °C and 9 MPa. That is the increase in the methionine concentration results in the increase in the methane uptake, Figure 4.23. That is because of the increase in the gas solubility and the renewal gas-liquid interface (Okutani *et al.*, 2008; Veluswamy *et al.*, 2016a), which induce the multi-step methane hydrate formation, as shown in the hydrate formation profile, Figure 4.24. Comparing between the results at 25 °C and 9 MPa and 20 °C and 8 MPa indicates that both conditions result in the same methane uptake (5.63 at 20 °C and 5.88 at 25 °C kmol of gas/ m³ of water), as shown in Figures 4.22 and 4.23. Other experimental data for all experiments conducted with different methionine concentrations at 25 °C and 9 MPa are summarized in Table 4.8.

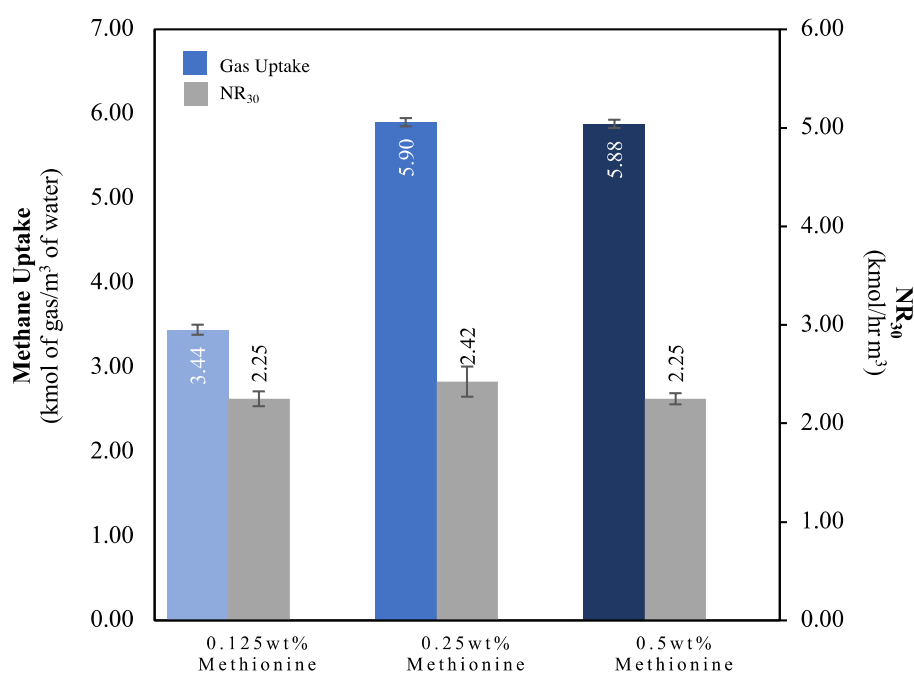


Figure 4.23 Methane uptakes and the normalized methane hydrate formation rate (NR_{30}) between different methionine concentrations at 25 °C and 9 MPa in the hybrid reactor configuration.

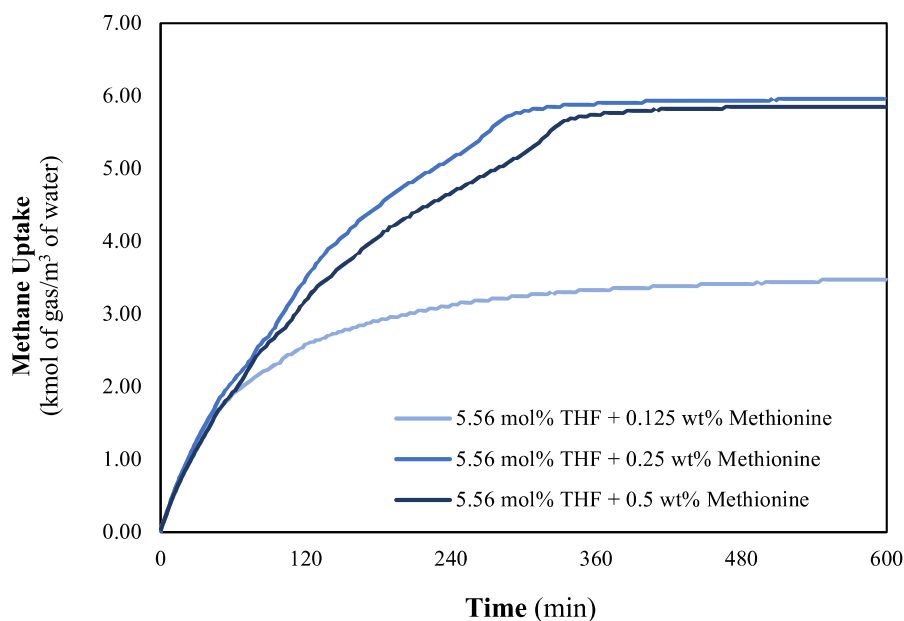


Figure 4.24 Methane uptake profiles from the hydrate formation with 5.56 mol% THF and methionine concentrations at 25 °C and 9 MPa in the hybrid reactor configuration.

Table 4.8 Methane hydrate formation in 5.56 mol% THF and 5.56 mol% THF with methionine concentrations at 25 °C and 9 MPa in the hybrid reactor configuration

	Concentration (wt%)	Experiment	Induction Time (min)	t_{90} (min)	Methane Uptake (kmol of gas/m ³ of water)	NR_{30} (kmol/hr·m ³)
5,56 mol% THF + Methionine	0.125	M17	19.15	239.00	3.47	2.33
		M18	25.57	284.66	3.36	2.15
		M19	15.33	255.17	3.50	2.27
	0.25	M20	17.40	250.50	5.84	2.56
		M21	21.45	261.33	5.96	2.50
		M22	20.00	281.33	5.90	2.21
	0.5	M23	46.00	306.66	5.88	2.21
		M24	33.00	325.66	5.82	2.21
		M25	22.18	285.17	5.94	2.33

4.2.3 Methane Hydrate Dissociation

The hydrate dissociation was also studied in every experiment after the hydrate formation completes by increasing the system temperature from 25 °C to 35 °C. Table 4.9 shows no significant difference in the dissociation, and higher than 99% methane gas can be recovered for all solution. The temperature and pressure also seems to have no effect on the methane hydrate dissociation.

Table 4.9 Methane hydrate dissociation of the hydrates formed with 5.56 mol% THF and 5.56 mol% THF with amino acids at 25 °C and 9 MPa in the hybrid reactor configuration

Amino Acid (wt%)		Experiment	Methane Consumed (mol)	Methane Released (mol)	% Recovery
5.56 mol% THF		TH11	0.204	0.203	99.07
		TH12	0.223	0.223	99.69
		TH13	0.211	0.211	99.67
5.56 mol% THF + Leucine	0.25	L17	0.420	0.417	99.26
		L18	0.418	0.418	99.90
		L19	0.421	0.421	99.88
5.56 mol% THF + Valine	0.25	V17	0.221	0.212	95.89
		V18	0.211	0.210	99.76
		V19	0.226	0.218	96.68
5.56 mol% THF + Methionine	0.125	M17	0.256	0.254	99.37
		M18	0.250	0.239	95.88
		M19	0.254	0.253	99.57
	0.25	M20	0.419	0.419	99.95
		M21	0.429	0.426	99.35
		M22	0.423	0.423	99.98
	0.5	M7	0.421	0.419	99.43
		M8	0.419	0.418	99.81
		M9	0.426	0.423	99.44

CHAPTER 5

CONCLUSIONS AND RECOMMENDATIONS

5.1 Conclusions

In this work, the kinetics and morphology of methane hydrate formation were studied in the presence of nonpolar amino acids with different aliphatic R groups (leucine, valine, and methionine) as a co-promoter with 5.56mol% tetrahydrofuran (THF) at ambient temperature. The hydrate formation first was carried out with single promoter, THF and amino acids in the quiescent system at 20 °C and 8 MPa. The formation with THF resulted in the slow hydrate nucleation and formation and high methane uptake. The morphology showed the leaflike layer stack up formation pattern. Methane hydrates did not form with amino acids in this condition. The co-promoting between THF and amino acids increased the rate of hydrate formation up to 5 times. However, only the addition of leucine and methionine resulted in the methane uptake as high as adding THF. The amino acid concentration showed different effects from surfactant behavior, and the optimal concentration were 0.25wt% leucine, 0.25wt% valine, and 0.125wt% methionine. The hydrate formation patterns were not only different with or without amino acids but also different among the amino acids. Moreover, the morphology study also showed the increased methane hydrate formation rate by the addition of amino acids. Every solution showed the same solution level and no foam formation after hydrate dissociation. The experiment was further studied to increase the hydrate formation temperature to 25 °C. To induce methane hydrate formation, 9 MPa formation pressure and hybrid reactor configuration were needed. At this formation condition (25 °C and 9 MPa), amino acids were needed to increase the methane solubility. The addition of 0.25 wt% leucine was able to increase the methane solubility resulting in the high methane uptake. However, 0.125 wt% methionine was not enough, and the addition of 0.25% and 0.5 wt% methionine was needed. In addition, using the hybrid reactor configuration at this low driving force condition reiterated that the hybrid reactor was the one that promoted the formation kinetics.

5.2 Recommendations

Based on the experimental results, the recommendation is to investigate roles of amino acids with a shorter and longer carbon chain lengths. Another recommendation is to construct the co-promoter hydrate phase equilibrium.



411257468

CU Theses 6173001063 thesis / recv: 25052563 12:18:23 / seq: 30

APPENDICES

Appendix A Calculation

- Methane gas consumption

From;
$$\Delta n_{H,\downarrow} = n_{H,0} - n_{H,t} = \left(\frac{PV}{zRT}\right)_{G,0} - \left(\frac{PV}{zRT}\right)_{G,t}$$

where $\Delta n_{H,\downarrow}$ = moles of consumed gas for hydrate formation, (mole)

$n_{H,t}$ = moles of hydrate at time t, (mole)

$n_{H,0}$ = moles of hydrate at time 0, (mole)

P = pressure of the crystallizer, (atm)

T = temperature of the crystallizer, (K)

V = the volume of gas phase in the crystallizer, (cm³)

Z = compressibility factor Pitzer's correlation (Smith et al., 2005)

R = the universal gas constant 82.06 cm³·atm/mol·K

Properties of methane

Critical Temperature (T_c) = 190.45 K

Critical Pressure (P_c) = 4596 kPa

Acentric Factor (ω) = 0.0115

Properties of additive

Density of tetrahydrofuran (THF) in pure water = 0.889 g/cm³

Molecular weight of THF = 72.11 g/mol

Density of leucine in pure water = 1.17 g/cm³

Molecular weight of leucine = 131.17 g/mol

Density of valine in pure water = 1.32 g/cm³

Molecular weight of valine = 117.15 g/mol

Density of methionine in pure water = 1.34 g/cm³

Molecular weight of methionine = 149.21 g/mol



411257468

Step 1: To find pressure reduced (P_r) and temperature reduced (T_r)

Data: Experiment No. TH1

At time 0,	Pressure (P)	=	8265.75 kPa	=	80.16 atm
	Temperature (T)	=	293.15 K		
At time t,	Pressure (P)	=	5562.00 kPa	=	54.89 atm
	Temperature (T)	=	293.15 K		

Solution:

$$T_r = \frac{T}{T_c} = \frac{293.15 \text{ K}}{190.45 \text{ K}} = 1.54$$

$$\text{At time 0, } P_r = \frac{P}{P_c} = \frac{8265.75 \text{ kPa}}{4596 \text{ kPa}} = 1.80$$

$$\text{At time t, } P_r = \frac{P}{P_c} = \frac{5562.00 \text{ kPa}}{4596 \text{ kPa}} = 1.21$$

Step 2: To find volume of gas phase (V_{cr}) and volume of additive (V_{add})

<u>Data:</u>	Volume of reactor with reservoir ($V_{reactor}$)	=	384.53 cm ³
	Volume of solution (V_{sol})	=	90 cm ³
	Volume of gas phase ($V_{reactor} - V_{sol}$)	=	294.53 cm ³
	Volume of additive (V_{add})		

$$V_{add} = \frac{5.56 \text{ mol THF}}{94.44 \text{ mol H}_2\text{O}} \times \frac{1 \text{ mol H}_2\text{O}}{18 \text{ g H}_2\text{O}} \times \frac{1 \text{ g H}_2\text{O}}{1 \text{ mL H}_2\text{O}} \times \frac{72.11 \text{ g THF}}{1 \text{ mol THF}} \times \frac{1 \text{ mL THF}}{0.89 \text{ THF}} \times 100$$

$$= 26.5 \text{ mL in 100 mL of water}$$

Therefore,	solution	126.5 mL	have THF	26.5 mL
	solution	90 mL	have THF =	$\frac{90 \times 26.5}{126.5} = 18.85 \text{ mL}$
	solution	90 mL	have H ₂ O =	$90 - 18.85 = 71.15 \text{ mL}$



Step 3: To find compressibility factor (z)

$$\beta^0 = \frac{0.083-0.422}{T_r^{1.6}} = \frac{0.083-0.422}{1.54^{1.6}} = -0.13$$

$$\beta^1 = \frac{0.139-0.172}{T_r^{4.2}} = \frac{0.139-0.172}{1.54^{4.2}} = 0.11$$

$$\text{time 0, } z = 1 + \beta^0 \frac{P_r}{T_r} + \omega \beta^1 \frac{P_r}{T_r} = 1 + (-0.13) \left(\frac{1.80}{1.54} \right) + (0.0115)(0.11) \left(\frac{1.80}{1.54} \right) = 0.851$$

$$\text{time t, } z = 1 + \beta^0 \frac{P_r}{T_r} + \omega \beta^1 \frac{P_r}{T_r} = 1 + (-0.13) \left(\frac{1.21}{1.54} \right) + (0.0115)(0.11) \left(\frac{1.21}{1.54} \right) = 0.900$$

Step 4: To fine the methane consumption

$$\begin{aligned} \Delta n_{H,\downarrow} &= \left(\frac{PV}{zRT} \right)_{G,0} - \left(\frac{PV}{zRT} \right)_{G,t} \\ &= \left(\frac{80.16 \text{ atm} \times 294.53 \text{ cm}^3}{0.851 \times 82.06 \text{ cm}^3 \text{ atm/mol K} \times 293.15 \text{ K}} \right)_{G,0} - \left(\frac{54.89 \text{ atm} \times 294.53 \text{ cm}^3}{0.900 \times 82.06 \text{ cm}^3 \text{ atm/mol K} \times 293.15 \text{ K}} \right)_{G,t} \\ &= 0.4266 \text{ mol} \end{aligned}$$

Therefore, the methane consumption is 0.4266 mol

$$\begin{aligned} \text{methane consumption} &= \frac{0.4266 \text{ mol CH}_4}{71.15 \text{ mL H}_2\text{O}} \times \frac{18 \text{ mL H}_2\text{O}}{1 \text{ mol H}_2\text{O}} = 0.108 \text{ mol CH}_4/\text{mol H}_2\text{O} \\ &= \frac{0.108 \text{ mol CH}_4}{1 \text{ mol H}_2\text{O}} \times \frac{1 \text{ kmol CH}_4}{1000 \text{ mol CH}_4} \times \frac{1 \text{ mol H}_2\text{O}}{18 \text{ g H}_2\text{O}} \times \frac{1 \text{ g H}_2\text{O}}{1 \text{ cm}^3 \text{ H}_2\text{O}} \times \frac{10^6 \text{ cm}^3 \text{ H}_2\text{O}}{1 \text{ m}^3 \text{ H}_2\text{O}} \\ &= 6 \text{ kmol CH}_4/\text{m}^3 \text{ H}_2\text{O} \end{aligned}$$

- The percentage of methane recovery

$$\text{From; } \% \text{methane recovery} = \frac{(\Delta n_{H,\uparrow})}{(\Delta n_{H,\downarrow})_{\text{End}}} \times 100$$

where $\Delta n_{H,\uparrow}$ = moles of released gas from hydrate during the hydrate dissociation at any given time, (mole)

$\Delta n_{H,\downarrow}$ = moles of consumed gas for hydrate formation at the end of experiments, (mole)

$$\text{Thus } \% \text{methane recovery} = \frac{(0.409)}{(0.427)} \times 100 = 95.91\%$$

Step 5: To find the normalized rate of hydrate formation 30 minutes after first nucleation (NR₃₀)

The methane consumption at 30 minutes after first nucleation is 0.0427 mol

$$\text{methane consumption} = \frac{0.0427 \text{ mol CH}_4}{71.15 \text{ mL H}_2\text{O}} \times \frac{18 \text{ mL H}_2\text{O}}{1 \text{ mol H}_2\text{O}} = 0.0108 \text{ mol CH}_4/\text{mol H}_2\text{O}$$

$$= \frac{0.0108 \text{ mol CH}_4}{1 \text{ mol H}_2\text{O} \cdot 30 \text{ min}} \times \frac{1 \text{ kmol CH}_4}{1000 \text{ mol CH}_4} \times \frac{60 \text{ min}}{1 \text{ hr}} \times \frac{1 \text{ mol H}_2\text{O}}{18 \text{ g H}_2\text{O}} \times \frac{1 \text{ g H}_2\text{O}}{1 \text{ cm}^3 \text{ H}_2\text{O}} \times \frac{10^6 \text{ cm}^3 \text{ H}_2\text{O}}{1 \text{ m}^3 \text{ H}_2\text{O}}$$

$$= 0.84 \text{ kmol CH}_4/\text{m}^3 \text{ H}_2\text{O} \cdot \text{hr}$$



411257468

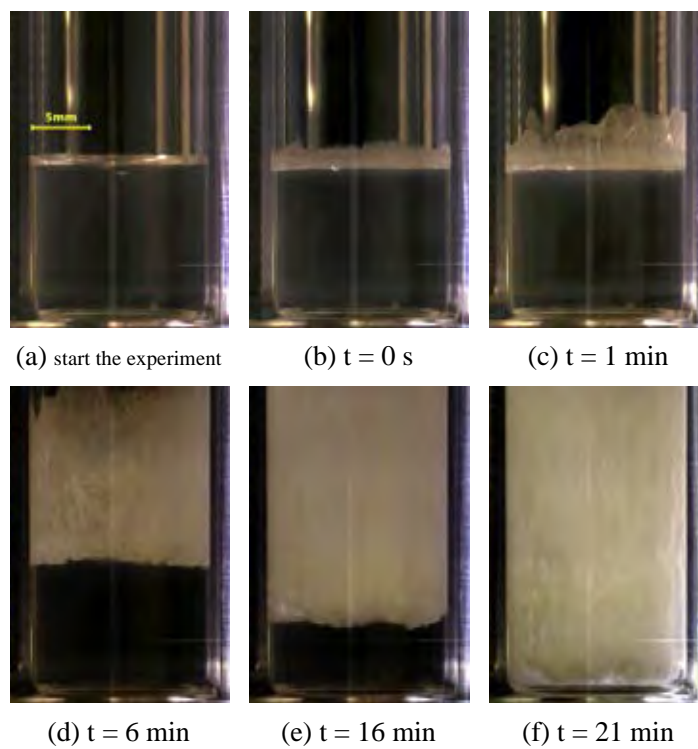
Appendix B Supporting information

Figure S1 Morphology methane hydrate formation of 5.56 mol% THF solution in a small glass vial.



411257468

CD IThesis 6173001063 thesis / rev: 25052563 12:18:23 / seq: 30

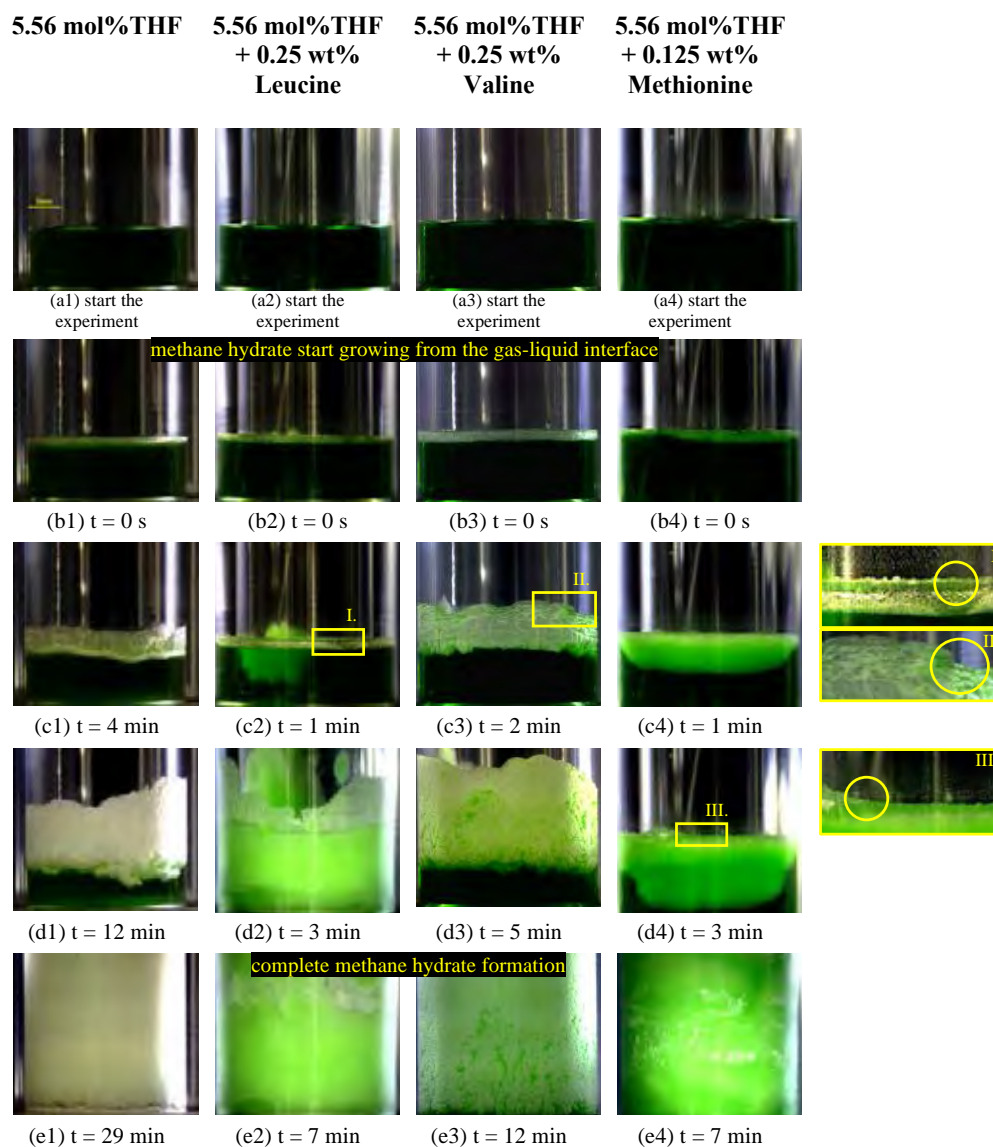


Figure S2 Dye morphology methane hydrate formation of (a) THF solution and optimal co-promoter solutions: (b) 0.25wt% leucine (c) 0.25wt% valine (d) 0.125wt% methionine.

REFERENCES

- Afewerk, B., Bodn, A., Stenhouse, K., and Donev, J. (2018). Natural gas vehicle fuel storage. from Energy Education
- Archer, D. (2007). Methane hydrate stability and anthropogenic climate change. Biogeosciences Discuss., 4(2), 993-1057.
- Babu, P., Ho, C. Y., Kumar, R., and Linga, P. (2014). Enhanced kinetics for the clathrate process in a fixed bed reactor in the presence of liquid promoters for pre-combustion carbon dioxide capture. Energy, 70, 664-673.
- Babu, P., Kumar, R., and Linga, P. (2013a). Medium pressure hydrate based gas separation (HBGS) process for pre-combustion capture of carbon dioxide employing a novel fixed bed reactor. International Journal of Greenhouse Gas Control, 17, 206-214.
- Babu, P., Kumar, R., and Linga, P. (2013b). Pre-combustion capture of carbon dioxide in a fixed bed reactor using the clathrate hydrate process. Energy, 50, 364-373.
- Babu, P., Nambiar, A., He, T., Karimi, I. A., Lee, J. D., Englezos, P., and Linga, P. (2018). A review of clathrate hydrate based desalination to strengthen energy–water nexus. ACS Sustainable Chemistry & Engineering, 6(7), 8093-8107.
- Bavoh, C. B., Khan, M. S., Lal, B., Bt Abdul Ghaniri, N. I., and Sabil, K. M. (2018a). New methane hydrate phase boundary data in the presence of aqueous amino acids. Fluid Phase Equilibria, 478, 129-133.
- Bavoh, C. B., Nashed, O., Khan, M. S., Partoon, B., Lal, B., and Sharif, A. M. (2018b). The impact of amino acids on methane hydrate phase boundary and formation kinetics. The Journal of Chemical Thermodynamics, 117, 48-53.
- Beheshtimaal, A., and Haghtalab, A. (2018). Thermodynamic modeling of hydrate formation conditions using different activity coefficient models in the presence of tetrahydrofuran (THF). Chemical Engineering Research and Design, 129, 150-159.
- Bohrmann, G., and Torres, M. E. (2006). Gas hydrates in marine sediments. In *Marine Geochemistry* (pp. 481-512).
- BP. (2019). bp-energy-outlook-2019. <https://www.bp.com/content/dam/bp/business-sites/en/global/corporate/pdfs/energy-economics/energy-outlook/bp-energy->

outlook-2019.pdf

- Cai, Y., Chen, Y., Li, Q., Li, L., Huang, H., Wang, S., and Wang, W. (2017). CO₂ Hydrate formation promoted by a natural amino acid l-methionine for possible application to CO₂ capture and storage. Energy Technology, 5(8), 1195-1199.
- Chaturvedi, E., Prasad, N., and Mandal, A. (2018). Enhanced formation of methane hydrate using a novel synthesized anionic surfactant for application in storage and transportation of natural gas. Journal of Natural Gas Science and Engineering, 56, 246-257.
- Dashti, H., Zhehao Yew, L., and Lou, X. (2015). Recent advances in gas hydrate-based CO₂ capture. Journal of Natural Gas Science and Engineering, 23, 195-207.
- de Deugd, R. M., Jager, M. D., and de Swaan Arons, J. (2001). Mixed hydrates of methane and water-soluble hydrocarbons modeling of empirical results. AIChE Journal, 47(3), 693-704.
- Du, J., Li, H., and Wang, L. (2014). Effects of ionic surfactants on methane hydrate formation kinetics in a static system. Advanced Powder Technology, 25(4), 1227-1233.
- EIA. (2018). Natural Gas - Energy Explained. from U.S. Energy Information Administration
https://www.eia.gov/energyexplained/print.php?page=natural_gas_home
- Englezos, P., and Lee, J. D. (2005). Gas hydrates: A cleaner source of energy and opportunity for innovative technologies. Korean Journal of Chemical Engineering, 22(5), 671-681.
- Gabitto, J. F., and Tsouris, C. (2010). Physical properties of gas hydrates: A Review. Journal of Thermodynamics, 2010, 1-12.
- Gudmundsson, J. S., Parlaktuna, M., and Khokhar, A. A. (1994). Storage of natural gas as frozen hydrate. SPE Production & Facilities, 9(01), 69-73.
- Harrison, S. E. (2010). Natural gas hydrates. from Stanford University
- He, Z., Linga, P., and Jiang, J. (2017). What are the key factors governing the nucleation of CO₂ hydrate? Physical Chemistry Chemical Physics, 19(24), 15657-15661.
- Inkong, K., Rangsunvigit, P., Kulprathipanja, S., and Linga, P. (2019a). Effects of temperature and pressure on the methane hydrate formation with the presence of

- tetrahydrofuran (THF) as a promoter in an unstirred tank reactor. Fuel, 255.
- Inkong, K., Veluswamy, H. P., Rangsunvigit, P., Kulprathipanja, S., and Linga, P. (2019b). Investigation on the kinetics of methane hydrate formation in the presence of methyl ester sulfonate. Journal of Natural Gas Science and Engineering, 71.
- Jager, M. D., de Deugd, R. M., Peters, C. J., de Swaan Arons, J., and Sloan, E. D. (1999). Experimental determination and modeling of structure II hydrates in mixtures of methane+water+1,4-dioxane. Fluid Phase Equilibria, 165(2), 209-223.
- Kang, K. C., Linga, P., Park, K.-n., Choi, S.-J., and Lee, J. D. (2014). Seawater desalination by gas hydrate process and removal characteristics of dissolved ions (Na⁺, K⁺, Mg²⁺, Ca²⁺, B³⁺, Cl⁻, SO₄²⁻). Desalination, 353, 84-90.
- Khokhar, A. A., Gudmundsson, J. S., and Sloan, E. D. (1998). Gas storage in structure H hydrates. Fluid Phase Equilibria, 150-151, 383-392.
- Khurana, M., and Veluswamy, H. (2019). SNG Technology. from New Gen Gas
- Khurana, M., Veluswamy, H. P., Daraboina, N., and Linga, P. (2019). Thermodynamic and kinetic modelling of mixed CH₄-THF hydrate for methane storage application. Chemical Engineering Journal, 370, 760-771.
- Khurana, M., Yin, Z., and Linga, P. (2017). A Review of clathrate hydrate nucleation. ACS Sustainable Chemistry & Engineering, 5(12), 11176-11203.
- Kumar, A., Sakpal, T., Linga, P., and Kumar, R. (2015). Enhanced carbon dioxide hydrate formation kinetics in a fixed bed reactor filled with metallic packing. Chemical Engineering Science, 122, 78-85.
- Kumar, A., Veluswamy, H. P., Kumar, R., and Linga, P. (2019). Kinetic promotion of mixed methane-THF hydrate by additives: Opportune to energy storage. Energy Procedia, 158, 5287-5292.
- Lang, X., Fan, S., and Wang, Y. (2010). Intensification of methane and hydrogen storage in clathrate hydrate and future prospect. Journal of Natural Gas Chemistry, 19(3), 203-209.
- Lee, S. Y., Kim, H. C., and Lee, J. D. (2014). Morphology study of methane–propane clathrate hydrates on the bubble surface in the presence of SDS or PVCap.



411257468

CU Theses 6173001063 thesis / recv: 25052563 12:18:23 / seq: 30

Journal of Crystal Growth, 402, 249-259.

- Lee, Y.-J., Kawamura, T., Yamamoto, Y., and Yoon, J.-H. (2012). Phase equilibrium studies of tetrahydrofuran (THF) + CH₄, THF + CO₂, CH₄ + CO₂, and THF + CO₂ + CH₄ Hydrates. Journal of Chemical & Engineering Data, 57(12), 3543-3548.
- Lekvam, K., and Bishnoi, P. R. (1997). Dissolution of methane in water at low temperatures and intermediate pressures. Fluid Phase Equilibria, 131(1), 297-309.
- Lenz, A., and Ojamae, L. (2011). Structures of the I-, II- and H-methane clathrates and the ice-methane clathrate phase transition from quantum-chemical modeling with force-field thermal corrections. Journal of Physical Chemistry, 115(23), 6169-6176.
- Lin, Y., Veluswamy, H. P., and Linga, P. (2018). Effect of eco-friendly cyclodextrin on the kinetics of mixed methane–tetrahydrofuran hydrate formation. Industrial & Engineering Chemistry Research, 57(17), 5944-5950.
- Liu, Y., Chen, B., Chen, Y., Zhang, S., Guo, W., Cai, Y., Tan, B., and Wang, W. (2015). Methane storage in a hydrated form as promoted by leucines for possible application to natural gas transportation and storage. Energy Technology, 3(8), 815-819.
- Lonero, A. (2008). How are methane hydrates formed, reserved, and released? Geology 340 Term Paper.
- Lozano-Castelló, D., Alcañiz-Monge, J., de la Casa-Lillo, M. A., Cazorla-Amorós, D., and Linares-Solano, A. (2002). Advances in the study of methane storage in porous carbonaceous materials. Fuel, 81(14), 1777-1803.
- Luo, Y. T., Zhu, J. H., Fan, S. S., and Chen, G. J. (2007). Study on the kinetics of hydrate formation in a bubble column. Chemical Engineering Science, 62(4), 1000-1009.
- Mainusch, S., Peters, C. J., de Swaan Arons, J., Javanmardi, J., and Moshfeghian, M. (1997). Experimental determination and modeling of methane hydrates in mixtures of acetone and water. Journal of Chemical & Engineering Data, 42(5), 948-950.

- Makogon, Y. F. (2007). Hydrate of natural gas. Petroleum Engineering – Upstream.
- Mech, D., Gupta, P., and Sangwai, J. S. (2016). Kinetics of methane hydrate formation in an aqueous solution of thermodynamic promoters (THF and TBAB) with and without kinetic promoter (SDS). Journal of Natural Gas Science and Engineering, 35, 1519-1534.
- Nakamura, T., Makino, T., Sugahara, T., and Ohgaki, K. (2003). Stability boundaries of gas hydrates helped by methane—structure-H hydrates of methylcyclohexane and cis-1,2-dimethylcyclohexane. Chemical Engineering Science, 58(2), 269-273.
- Okutani, K., Kuwabara, Y., and Mori, Y. H. (2008). Surfactant effects on hydrate formation in an unstirred gas/liquid system: An experimental study using methane and sodium alkyl sulfates. Chemical Engineering Science, 63(1), 183-194.
- Partoon, B., Sabil, K. M., Lau, K. K., Lal, B., and Nasrifar, K. (2018). Production of gas hydrate in a semi-batch spray reactor process as a means for separation of carbon dioxide from methane. Chemical Engineering Research and Design, 138, 168-175.
- Reddy, M. K., Nikita Desai, Y. C., Gregersen, E., Lotha, G., Promeet, D., Rogers, K., Setia, V., Singh, S., Sinha, S., and Britannica, T. E. o. E. (2019). Amino acid. Encyclopaedia Britannica Retrieved May 22, 2020 <https://www.britannica.com/science/amino-acid>
- Rodger, P. M. (1989). Cavity potential in type I gas hydrates. Journal of Physical Chemistry, 93(18), 6850-6855.
- Saito, K., Kishimoto, M., Tanaka, R., and Ohmura, R. (2011). Crystal growth of clathrate hydrate at the interface between hydrocarbon gas mixture and liquid water. Crystal Growth & Design, 11(1), 295-301.
- Seo, S. D., Hong, S. Y., Sum, A. K., Lee, K.-H., Lee, J. D., and Lee, B. R. (2019). Thermodynamic and kinetic analysis of gas hydrates for desalination of saturated salinity water. Chemical Engineering Journal, 370, 980-987.
- Seo, Y. T., Kang, S. P., and Lee, H. (2001). Experimental determination and thermodynamic modeling of methane and nitrogen hydrates in the presence of



411257468

CU Theses 6173001063 thesis / recv: 25052563 12:18:23 / seq: 30

- THF, propylene oxide, 1,4-dioxane and acetone. Fluid Phase Equilibria, 189(1), 99-110.
- Shi, B.-H., Yang, L., Fan, S.-S., and Lou, X. (2017). An investigation on repeated methane hydrates formation in porous hydrogel particles. Fuel, 194, 395-405.
- Siangsai, A., Rangsunvigit, P., Kitiyanan, B., Kulprathipanja, S., and Linga, P. (2015). Investigation on the roles of activated carbon particle sizes on methane hydrate formation and dissociation. Chemical Engineering Science, 126, 383-389.
- Siažik, J., and Malcho, M. (2017). Accumulation of primary energy into natural gas hydrates. Procedia Engineering, 192, 782-787.
- Sloan, E. D. (2003). Fundamental principles and applications of natural gas hydrates. <https://www.nature.com/articles/nature02135.pdf>
- Sloan, E. D., and Koh, C. A. (2008). *Clathrate Hydrates of Natural Gases*. New York: CRC Press.
- Smith, J. M., Van Ness, H. C., and Abbott, M. M. (2005). *Introduction to Chemical Engineering Thermodynamics*. Singapore: McGraw-Hill.
- Sun, Q., Chen, G., Guo, X., and Liu, A. (2014). Experiments on the continuous separation of gas mixtures via dissolution and hydrate formation in the presence of THF. Fluid Phase Equilibria, 361, 250-256.
- Tang, L.-G., Li, X.-S., Feng, Z.-P., Lin, Y.-L., and Fan, S.-S. (2006). Natural gas hydrate formation in an ejector loop reactor: Preliminary Study. Industrial & Engineering Chemistry Research, 45(23), 7934-7940.
- Veluswamy, H. P., Ang, W. J., Zhao, D., and Linga, P. (2015). Influence of cationic and non-ionic surfactants on the kinetics of mixed hydrogen/tetrahydrofuran hydrates. Chemical Engineering Science, 132, 186-199.
- Veluswamy, H. P., Hong, Q. W., and Linga, P. (2016a). Morphology study of methane hydrate formation and dissociation in the presence of amino acid. Crystal Growth & Design, 16(10), 5932-5945.
- Veluswamy, H. P., Kumar, A., Kumar, R., and Linga, P. (2017a). An innovative approach to enhance methane hydrate formation kinetics with leucine for energy storage application. Applied Energy, 188, 190-199.
- Veluswamy, H. P., Kumar, A., Seo, Y., Lee, J. D., and Linga, P. (2018). A review of



411257468

CU Theses 6173001063 thesis / revv: 25052563 12:18:23 / seq: 30

- solidified natural gas (SNG) technology for gas storage via clathrate hydrates. Applied Energy, 216, 262-285.
- Veluswamy, H. P., Kumar, S., Kumar, R., Rangsunvigit, P., and Linga, P. (2016b). Enhanced clathrate hydrate formation kinetics at near ambient temperatures and moderate pressures: Application to natural gas storage. Fuel, 182, 907-919.
- Veluswamy, H. P., Lee, P. Y., Premasinghe, K., and Linga, P. (2017b). Effect of biofriendly amino acids on the kinetics of methane hydrate formation and dissociation. Industrial & Engineering Chemistry Research, 56(21), 6145-6154.
- Veluswamy, H. P., and Linga, P. (2013). Macroscopic kinetics of hydrate formation of mixed hydrates of hydrogen/tetrahydrofuran for hydrogen storage. International Journal of Hydrogen Energy, 38(11), 4587-4596.
- Veluswamy, H. P., Wong, A. J. H., Babu, P., Kumar, R., Kulprathipanja, S., Rangsunvigit, P., and Linga, P. (2016c). Rapid methane hydrate formation to develop a cost effective large scale energy storage system. Chemical Engineering Journal, 290, 161-173.
- Verrett, J., Posteraro, D., and Servio, P. (2012). Surfactant effects on methane solubility and mole fraction during hydrate growth. Chemical Engineering Science, 84, 80-84.
- Vysniauskas, A., and Bishnoi, P. R. (1983). A kinetic study of methane hydrate formation. Chemical Engineering Science, 38(7), 1061-1072.
- Wang, X., French, J., Kandadai, S., and Chua, H. T. (2010). Adsorption measurements of methane on activated carbon in the temperature range (281 to 343) K and pressures to 1.2 MPa. Journal of Chemical & Engineering Data, 55(8), 2700-2706.
- Yin, Z., Chong, Z. R., Tan, H. K., and Linga, P. (2016). Review of gas hydrate dissociation kinetic models for energy recovery. Journal of Natural Gas Science and Engineering, 35, 1362-1387.
- Zhang, J. S., Lee, S., and Lee, J. W. (2007). Does SDS micellize under methane hydrate-forming conditions below the normal Krafft point? Journal of Colloid and Interface Science, 315(1), 313-318.
- Zhao, J., Tian, Y., Zhao, Y., and Cheng, W. (2015). Experimental investigation of effect



411257468

CU Theses 6173001063 thesis / recv: 25052563 12:18:23 / seq: 30

on hydrate formation in spray reactor. Journal of Chemistry, 2015, 1-5.

Zhong, D.-L., Lu, Y.-Y., Sun, D.-J., Zhao, W.-L., and Li, Z. (2015). Performance evaluation of methane separation from coal mine gas by gas hydrate formation in a stirred reactor and in a fixed bed of silica sand. Fuel, 143, 586-594.



411257468

CU Theses 6173001063 thesis / recv: 25052563 12:18:23 / seq: 30

VITA

NAME	Kan Jeenuang
DATE OF BIRTH	27 October 1995
PLACE OF BIRTH	Bangkok
INSTITUTIONS ATTENDED	Department of Chemical Technology Faculty of Science, Chulalongkorn University
HOME ADDRESS	11 Soi Rat Burana 26 District/Subdistrict Rat Burana Bangkok 10140



411257468

CU ThesIs 6173001063 thesis / recv: 25052563 12:18:23 / seq: 30